Topics in Magnetism

Maxwell's Equations

Demagnetizing Factors

DC Permeability and Hysteresis

Toroidal Coil and Solenoid

Origin of Ferro and Ferri Magnetism

Landau-Lifshitz-Gilbert Equation

RF Permeability of Ferrites

Ferrite-Tuned RF Cavity Resonators

Shane Rupert Koscielniak

TRIUMF Beam Note: TRI-BN-25-13 (June)

Contents

1 Magnetism **7**

1.1 Electricity and Magnetism . . . 7
1.1.1 Notation . . . 7
1.1.2 Nomenclature . . . 8
1.2 Maxwell's Equations . . . 9
1.2.1 Equations in matter . . . 9
1.3 Magnetisation . . . 10
1.3.1 Potential and Green's functions . . . 11
1.3.2 Boundary conditions . . . 11
1.3.3 Field directions for bar magnet . . . 11
1.3.4 Scalar potential for magnetized cylinder . . . 12
1.4 Demagnetization Factor . . . 12
1.4.1 Spherical magnet in external field . . . 13
1.4.2 Recursive relation between H and M . . . 14
1.4.3 Consequences of symmetry . . . 15
1.4.4 Other geometries . . . 16
1.4.5 Properties of the demagnetizing tensor . . . 17
1.4.6 Brown's Theorem . . . 18
1.5 Permeability and Hysteresis (DC) . . . 20
1.5.1 Measurement of permeability . . . 20
1.5.2 Hysteresis curves . . . 21
1.5.3 Hard versus soft magnetic materials . . . 22
1.5.4 Using a B-H curve . . . 23
1.5.5 Toy models for B-H branches . . . 23

2 Magnetic Field of Toroidal Coil **25**

2.1 Introduction . . . 25
2.2 Field Within Cylindrical Can . . . 26
2.2.1 Confined radial currents . . . 27
2.3 Field With n-Fold Symmetry . . . 28
2.4 Ampère's Circuit Law . . . 29
2.4.1 Fields from short straight wires . . . 30
2.5 Cylindrical Harmonics . . . 30
2.6 Vector Potential . . . 31
2.7 Complex Analysis . . . 33
2.7.1 Two-dimensional electric fields . . . 34
2.8 Conclusion . . . 34

3 Ferro- and Ferri-Magnetism **35**
3.1 Introduction . . . 35
3.2 Exchange Interaction . . . 35
3.3 Theory of Ferro-magnetism . . . 36
3.3.1 Free Energy of Magnetic Material . . . 37
3.3.2 Weiss domains . . . 37
3.4 Theory of Ferri-magnetism . . . 38
3.5 Magnetic Resonance in Ferrites . . . 39
3.5.1 Gyromagnetic ratio . . . 39
3.5.2 Motion of spin magnetic moment . . . 39
3.5.3 Conditions for FMR . . . 40
3.5.4 Demagnetizing factor . . . 40
3.5.5 Importance of damping . . . 41
3.5.6 Ferri-magnetic resonance . . . 41
3.6 Simple Ferrite Structures . . . 41
3.6.1 Spinel structure . . . 41
3.6.2 Garnet structure . . . 42

4 Landau-Lifshitz-Gilbert Equation **43**
4.1 History . . . 43
4.2 Effective magnetic field . . . 43
4.3 Spin-Magnetization Equation of Motion . . . 44
4.4 RF Parallel to Bias . . . 45
4.4.1 Linearized solution . . . 45
4.4.2 Near-linear solution . . . 46
4.4.3 Nonlinear solution . . . 46
4.4.4 Magnetization equations for cylinder . . . 47
4.5 RF Perpendicular to Bias . . . 47
4.5.1 Linearized solution . . . 47
4.5.2 Magnetized cylinder . . . 48
4.5.3 Polder tensor . . . 49
4.6 Sphere with RF perpendicular to bias . . . 50
4.6.1 Nonlinear solution for sphere . . . 50
4.6.2 Equations for Fourier harmonics . . . 53

5 RF Permeability of Ferrites **57**
5.1 Incremental permeability . . . 58
5.1.1 Naming and notation . . . 58
5.2 Magnetic-bias dependence . . . 58
5.3 Major-loop dependence . . . 59
5.4 Frequency dependence . . . 60
5.4.1 Snoek's law . . . 62
5.5 Orientation dependence . . . 63
5.5.1 Approximate dual dependence $\mu_r(H, \nu)$ . . . 63
5.6 Measurement of RF permeability . . . 64
5.6.1 Network permeability . . . 64
5.6.2 Ferrite data tables . . . 65

6 Magnetically Biased Ferrites for RF Cavity Tuning **67**
6.1 Prologue . . . 67
6.2 Article structure . . . 67
6.3 Introduction . . . 68
6.3.1 Motivation . . . 68
6.3.2 Narrow versus wide band resonator . . . 68
6.3.3 Transit time factor . . . 68
6.3.4 Ferrites in a nutshell . . . 69
6.3.5 Tuning and shrinking . . . 69
6.3.6 FMR in a nutshell . . . 70
6.3.7 RF waves in media . . . 70
6.3.8 Relation of permeability to tuning range . . . 70
6.3.9 Practicalities . . . 71
6.3.10 Measured dual dependence $\mu_\Delta(H,\nu)$ . . . 71
6.3.11 Calculating bias field from frequency . . . 71
6.4 Magnetic biasing . . . 72
6.4.1 Bipolar versus unipolar bias current supply . . . 72
6.5 Theory of parallel bias tuning . . . 73
6.5.1 Example . . . 74
6.6 Theory of perpendicular bias tuning . . . 75
6.6.1 Magnetic quality factor . . . 76
6.6.2 Example . . . 76
6.7 Geometry of ferrite and bias current conductors . . . 77
6.7.1 Parallel bias of concentric core . . . 77
6.7.2 Perpendicular bias of concentric core . . . 78
6.8 Parallel or perpendicular, Ni-Zn or YIG? . . . 79
6.9 Parallel biased Ni-Zn ferrite . . . 79
6.9.1 Literature Survey . . . 79
6.10 Perpendicular biased YIG ferrite . . . 81
6.10.1 Influence of bias orientation on tuning . . . 81
6.10.2 Literature survey . . . 82
6.11 RF hardening resonator . . . 84
6.12 Conclusion . . . 86
6.12.1 Pedagogy . . . 87
6.12.2 Research . . . 87
6.12.3 Unresolved . . . 87

Chapter 1

Magnetism

1.1 Electricity and Magnetism

Electric charges experience a force in an electric vector field **E**. Charge currents and magnetized objects experience force in a magnetic vector field **B**. These definitions of *electric* and *magnetic* appear almost tautologies. The circularity is broken by experience: loadstones[1] (lodestones) and terrestrial magnetism exist; rubbing together amber and fur cause them to be mutually attracted. Both observations[2] need explanation, and each a name. Naming typically follows the first *recorded* historical use. The Greek words for the minerals amber and magnetite, elektron and magnètis [lithos][3], respectively, are the roots of the modern day names. But concepts evolve, names change in response; and this leads to inconsistency - as noted in Sec. 1.1.2. The word electro-magnetism, with the terms conjoined, usually denotes the study of the second two expressions in Eq. 1.1 wherein a changing magnetic field can create an electric field, and vice versa.

1.1.1 Notation

Maxwell (1831-1879) constructed the classical (mathematical) theory of electro-magnetism from the experiments, observations and physical laws deduced by others[4]. Bevis, Cavendish, Coulomb and Poisson founded static electricity. Ampere, Oersted, Biot and Faraday founded electric current and magnetism. In his treatise[1], Maxwell Vol. II Chap. IX General Equations of the Electromagnetic Field, Article 618, introduced/defined the vector quantities in Table 1.1.

Maxwell[5] also introduced the line, surface and volume density of electric charge λ, σ, ρ respectively. Maxwell's treatise predates modern vector notation. Rather than bold face type he used German Fraktur script; for example $\mathfrak{A} \equiv \mathbf{A}$ and $\mathfrak{B} \equiv \mathbf{B}$. Balanis (1989) continues the Fraktur script convention. There is no distinct Fraktur letter representing J, so Maxwell moved on to the next letter K. Modern sources, using Roman letters, restored the alphabetic logic using **J** for volume current density and **K** for surface current density.

Vector calculus operators were introduced by Englishman Oliver Heaviside (1850-1925); his notation for the operators is still in use. In 1884 he recast Maxwell's 12 explicit component equations as 4 of vector equations. Vector analysis and notation was introduced by Josiah Willard Gibbs in 1888 and promulgated by him in 1902[2]. Gibbs standardized vector notation, as it is used today.

[1] Naturally occurring magnetite. The chinese word is "motherly stone" because magnetite attracts iron like babies are attracted to their mothers. The french word for magnet is "aimant", which has a similar logic.

[2] Often first credited to Greek polymath Thales of Miletus (624–546 BCE).

[3] Stone from a geographic location called Magnesia, in the region of Anatolia (now in Turkey).

[4] John Bevis, 1695-1771. Henry Cavendish, 1731-1810. Charles-Augustine de Coulomb, 1736-1806. Jean-Baptiste Biot, 1774-1862. André-Marie Ampère, 1775-1836. Hans Oersted 1777-1851. Michael Faraday, 1791-1867.

[5] Vol. I, Chap. II, Elementary Mathematical Theory of Statical Electricity, Article 64.

Maxwell	Modern symbol	Name or Definition	Modern name
$\boldsymbol{\rho}$	$\mathbf{r}$	radius vector of a point	same
$\mathbf{A}$	$\mathbf{A}$	electromagnetic momentum[6]	magnetic vector potential (function)
$\mathbf{B}$	$\mathbf{B}$	magnetic induction	varies
$\mathbf{C}$	$\mathbf{J}$	(total) electric current density	total current density
$\mathbf{D}$	$\mathbf{D}$	electric displacement	same
$\mathbf{E}$	$\mathbf{E}$	electromotive intensity[7]	electric field
$\mathbf{F}$	$\mathbf{F}$	force (on an object)	same
$d\boldsymbol{\rho}/dt$	$d\mathbf{r}/dt$	velocity of a point[8]	same
$\mathbf{H}$	$\mathbf{H}$	magnetic force	varies
$\mathbf{I}$	$\mathbf{M}$	magnetization	same
$\mathbf{K}$	$\mathbf{J}_c$	(conduction) current density	same

Table 1.1: Notation for vector quantities in electro-magnetism.

Notes [6] [7] [8]

1.1.2 Nomenclature

Most of the symbols introduced by Maxwell are still in use. Modern authors are uniform in the usage of the symbols **A**, **B**, **D**, **E**, **F**, **H**, **J**, **M** and **P** (polarization); but not in the naming they attach to those symbols. Table 1.2 compares naming conventions.

Symbol	Naming	Authority
$\mathbf{B}$	magnetic induction	[1, 4, 5, 6]
$\mathbf{B}$	magnetic flux density	[7, 9, 10, 12]
$\mathbf{B}$	magnetic field	[11, 13]
$\mathbf{H}$	magnetic field or field intensity	[4, 5, 6, 7, 8, 12]
$\mathbf{H}$	magnetic field strength	[9, 10]
$\mathbf{M}$	magnetization	[4, 5, 6, 9, 7, 10, 12, 13]
$\mathbf{J}$	(volume) current density	[4, 5, 6, 7, 9, 10, 11, 12, 13]
$\mathbf{J}_s$	surface current density	[9, 12]
$\mathbf{K}$	surface current density	[7, 11, 13]
$\mathbf{P}$	(electric) polarization	[4, 5, 6, 7, 9, 8, 10, 11, 12, 13]
$\mathbf{D}$	(electric) displacement	[1, 4, 5, 6, 7, 9, 10, 11]
$\mathbf{D}$	electric flux density	[12]
$\partial\mathbf{E}/\partial t$	displacement current	[8, 11, 12, 13]
$\partial\mathbf{D}/\partial t$	displacement current	[4, 5, 6, 7, 9]
Φ	vector flux through surface	[5, 6, 9, 8, 10, 11, 13]
ρ	(volume) charge density	[4, 5, 6, 7, 9, 8, 11, 13]

Table 1.2: Nomenclature for vector quantities in electro-magnetism.

Some of this variation is historical, and some philosophical. The fundamental fields are **E** and **B**. If there were no magnetization or dielectric polarization, there would be no need for the auxiliary fields **H** and **D**. As it is, they are useful constructs. Griffiths[11] states the case well:

> H plays a role in magnetostatics analogous to D in electrostatics; Just as D allowed us to write Gauss's law in terms of the free charge alone, H permits us to express Ampere's law

[6] Maxwell specifies the vector line integral $\oint \mathbf{A} \cdot d\mathbf{l} = \Phi$ the total magnetic flux through the surface contained by the path **l**.

[7] Maxwell also uses the phrase "electric field".

[8] Maxwell also uses the symbol **G**, maintaining the alphabetic order.

> in terms of the free current alone—and free current is what we control directly. Bound current, like bound charge, comes along for the ride—the material gets magnetized, and this results in bound currents; we cannot turn them on or off independently, as we can free currents.

Contrastingly, Zangwill states:

> In this book, only the electric field E and the magnetic field B are fundamental. We give no special names to the auxiliary fields D and H.

Sometimes it is necessary to make the distinction between electric and magnetic flux $\Phi_E = \oint \mathbf{E} \cdot d\mathbf{S}$ and $\Phi_B = \oint \mathbf{B} \cdot d\mathbf{S}$. Evidently, it is legitimate to call the integrands flux density. Maxwell is singular in calling $\mathbf{H}$ magnetic force and using the symbol $\mathbf{I}$ for magnetization. But his idea is modern, because the "force" $\mathbf{H}$ is under our control. Panofsky[5] calls dE/dt the vacuum displacement current. Balanis[12] naming of $\mathbf{D}$ echoes that of $\mathbf{B}$ flux density. Griffiths[11] and Zangwill[13] are almost singular in calling $\mathbf{B}$ magnetic field. Zangwill does not introduce $\mathbf{H}$ and Griffith simply calls it H (no name). We shall resort to the names B-field, H-field; or equivalently magnetic induction and magnetic field, respectively. Induction is short and is clearly different to field.

1.2 Maxwell's Equations

The equations of electricity and magnetism are Maxwell's equations. The equations in vacuum:

$$\nabla \cdot \mathbf{E} = \rho_f/\epsilon_0\,, \quad \nabla \cdot \mathbf{B} = 0\,, \quad \nabla \times \mathbf{E} = -(\partial \mathbf{B}/\partial t)\,, \quad \nabla \times \mathbf{B}/\mu_0 = \mathbf{J}_f + (\partial \mathbf{E}/\partial t)/\epsilon_0\,. \tag{1.1}$$

Here the subscript f denotes free charges and currents; the latter may include conduction currents. The values ϵ_0 and μ_0 are the permittivity and permeability of free space, respectively.

1.2.1 Equations in matter

We begin by drawing an anlogy between dielectrics and magnetics. Dielectric[9] materials are insulators; they contain no free electrons for conduction. However, they do contain electric charges bound to atoms or molecules. Dielectrics are electrically neutral, but an externally applied electric field can produce a slight separation of the positive and negative charges leading to an electric dipole density throughout the volume of the material; a phenomenon called electric polarization. There is an analogous effect in magnetic materials: they contain atomic-scale magnetic dipoles bound to the atoms or molecules of which the material is composed. An externally applied magnetic field can align these magnetic dipoles. If the alignment persists after the field is withdrawn, the phenomenon is called magnetization. Each of these dipoles can be considered as a sub-atomic current loop. They are in fact the electron intrinsic spins. A smaller contribution is also made by the electron orbital rotation. These spin currents do not participate in electrical conduction. The magnetization vector $\mathbf{M}$ measures the density of magnetic dipoles per unit volume, just as the polarization vector $\mathbf{P}$ measures the density of electric dipoles. The spin currents are necessarily present whenever we have a magnetized medium.

Electric polarization is due to bound charges, ρ_b such that $\rho_b = -\nabla \cdot \mathbf{P}$. Magnetization is due to bound currents, $\mathbf{J}_b$, such that $\mathbf{J}_b = \nabla \times \mathbf{M}$. The bound-currents do not flow, but they do have a magnetic effect. When electric fields are time-varying, the concept of current is extended to include them. The total current becomes $\mathbf{J} = \mathbf{J}_f + \mathbf{J}_b + \mathbf{J}_p + \epsilon_0 \partial \mathbf{E}/\partial t$ where $\mathbf{J}_p = \partial \mathbf{P}/\partial t$ is called the

[9]The Encyclopaedia Britannica tells us the pioneers of dielectrics are the Prussian scientist Ewald Georg von Kleist (1700-1748), Dutch physicist Pieter van Musschenbroek (1692-1761) – both of whom made Leyden jars – and English astronomer John Bevis (1695-1771) who made the first capacitor in 1747. The history of dielectrics is tied to that of capacitors. At the time of Maxwell, capacitors were called condensers or accumulators (of charge).

polarization current. The system of relations between fields and multiple types of sources $(\rho, \mathbf{J})$ is simplified conceptually if we introduce the *auxillary fields*

$$\mathbf{D} = \epsilon_0 \mathbf{E} + \mathbf{P} \quad (\text{such that} \quad \nabla \cdot \mathbf{D} = \rho_f) \quad \text{and} \quad \mathbf{H} = -\mathbf{M} + \mathbf{B}/\mu_0 \,. \tag{1.2}$$

The equations in matter (or media) are

$$\nabla \cdot \mathbf{D} = \rho_f \,, \quad \nabla \cdot \mathbf{B} = 0 \,, \quad \nabla \times \mathbf{E} = -\partial \mathbf{B}/\partial t \,, \quad \nabla \times \mathbf{H} = \mathbf{J}_f + \partial \mathbf{D}/\partial t \,. \tag{1.3}$$

The electric field $\mathbf{E}$ and magnetic induction $\mathbf{B}$ remain the fundamental physical quantities. In M.K.S. units the ratios E/B and H/D are both equal to the speed of light. The units of D are Coulomb/m^2 and of H are Ampere/m.

1.3 Magnetisation

The sources of magnetic field are currents, which are of three types: free or bound or displacement. The associated effects, respectively, are: field around current-carrying conductors, magnets and magnetization, electro-magnetic waves.

Magnetisation has a classical description in terms of Ampèrian currents, which act as sub-microscopic magnetic diples; but those currents/dipoles can only be explained by quantum mechanics. Nevertheless, the *macroscopic* Eqs. 1.1-1.3 are perfectly adequate to predict a wide variety of fascinating phenomena. (We sketch a quantum-based description of magnetism in Chap. 3.) These sub-atomic dipoles come from two sources: the electron intrinsic spin (the dominant contribution) and electron orbital angular momentum in an atom. The spin property was predicted by Dirac[14]. The intrinsic spin is an inevitable feature of writing the quantum wave function as the components of a 4-vector, such that the wave function is Lorentz invariant (i.e. consistent with special relativity).

In the Ampèrian description, the magnetization consists of a vast 3D array of tiny current loops; and which constitute magnetic dipoles. We may think of the loops as occupying sub-microscopic 3D cells. If the current loops are equal, then they cancel on shared faces of adjacent cells. If the density of loops is uniform, the residual is a shell of current loops only at the exterior surface of the material; and we recognize this as uniform magnetization. If the currents are not equal, there is a net variation of bound-current density throughout the material; which we recognize as non-uniform magnetization. All of this may seem abstract, but it can be made tangible: the lines of magnetic force around a magnetized object can be rendered visible with iron filings. Moreover, the iron filings will float perpendicular to the pole surfaces; and if we snap/break the object in two, the iron filings will cling perpendicular to the newly exposed pole faces that were previously within the body of the object.

The classical physics description of magnetization goes back to Ampere, Poisson and Maxwell[3]. However, we follow the pedagogic example of Slater and Frank[4] - with one change in notation: we replace Slater's $\mathbf{J}_m$ by $\mathbf{J}_b$. When the magnetization *varies* continuously from point to point, the spatial variation of the (non-conduction) magnetization current density $\mathbf{J}_b$ is proportional to the curl (rotation density) of $\mathbf{M}$. The vectors are related thus:

$$\mathbf{J}_b = \nabla \times \mathbf{M} \,. \tag{1.4}$$

The magnetization current is just as effective in producing magnetic induction $\mathbf{B}$ as a real current $\mathbf{J}_f$ of free charged particles. Ampere's circuital law is updated thus:

$$\nabla \times \mathbf{B} = \mu_0(\mathbf{J}_f + \mathbf{J}_b) = \mu_0(\mathbf{J}_f + \nabla \times \mathbf{M}) \,. \tag{1.5}$$

Evidently, curl$(\mathbf{B}/\mu_0 - \mathbf{M}) = \mathbf{J}_f$. It makes no difference if $\mathbf{J}_f$ is a flow of free charges or a conduction current inside a metal. The quantity $\mathbf{H} = (\mathbf{B}/\mu_0 - \mathbf{M})$ is called the magnetic field; and its source is free current such that $\mathbf{J}_f = \nabla \times \mathbf{H}$.

For magnetostatic problems in magnetic media, and no free currents, there are three equations that determine the fields:

$$\nabla \cdot \mathbf{B} = 0\,, \quad \nabla \times \mathbf{H} = \mathbf{0}\,, \quad \mathbf{B} = \mu_0(\mathbf{H} + \mathbf{M})\,. \tag{1.6}$$

The last equation states that the magnetic induction is the sum of a field $\mathbf{H}$ due to free currents and a contribution $\mathbf{M}$ from the magnetization (alignment) of (sub)-microscopic magnetic dipoles. The state of the latter depends on prior magnetizations or spontaneous alignments, and so will contribute depending on the history of the magnetic medium (an effect called hysteresis).

1.3.1 Potential and Green's functions

For given magnetization, the general solution of Eq. 1.6 can be expressed as the gradient of a scalar potential: $\mathbf{H} = -\nabla U$. Inside the magnetic body, $\nabla \cdot (\mathbf{H} + \mathbf{M}) = 0$ implies that the potential satisfies Poisson's equation $\nabla^2 U = \nabla \cdot \mathbf{M}$. Outside the body, where magnetization is zero, U satisfies Laplace's equation $\nabla^2 U = 0$.

There is a formal Green's function[10] solution for the potential:

$$4\pi U(\mathbf{r}') \;=\; \int_{\rm Vol} \frac{\rho_m(\mathbf{r})}{|\mathbf{r}' - \mathbf{r}|} dV \;+\; \int_{\rm Surf} \frac{\sigma_m(\mathbf{r})}{|\mathbf{r}' - \mathbf{r}|} dS\,. \tag{1.7}$$

Here $\rho_m = \nabla \cdot \mathbf{M}(\mathbf{r})$ and $\sigma_m = \mathbf{n} \cdot \mathbf{M}(\mathbf{r})$ are the volume density and surface density, respectively, of magnetic dipoles. If the magnetization is uniform, the first term is zero. $\mathbf{n}$ is the unit normal outward from the surface.

Note that U enables us to find the magnetic field H and induction B for *given* magnetization, but $\mathbf{M}$ itself must be found by other means[20, 31]. It transpires that the internal magnetic forces between the sub-microscopic dipoles will minimize the volume density and surface density of dipoles.

1.3.2 Boundary conditions

In addition to Eqs. 1.6, there are boundary conditions at the surface of the magnet. The component of $\mathbf{H}$ parallel to the surface must be continuous. The component of $\mathbf{B}$ normal to the surface must be continuous. To be more precise, the tangential component of $\mathbf{H}$ is continuous across a surface carrying no free current $\mathbf{J}_f$. If there is a surface current, its value is $\mathbf{J}_f = \Delta\mathbf{H} \times \mathbf{n}$ where $\Delta\mathbf{H}$ is the discontinuity across the surface and $\mathbf{n}$ is the unit normal vector to the surface. There are similar statements to be made for $\mathbf{M}$ and $\mathbf{J}_b$.

1.3.3 Field directions for bar magnet

We take a moment to consider the directions of the quantities $\mathbf{M}$, $\mathbf{H}$, $\mathbf{B}$ for the simple case of a magnetized iron bar. The situation is sketched in Fig. 1.1 for a short cylindrical bar magnet aligned with the vertical axis z. The fields are derived from the scalar potential, as in Sec. 1.3.4. Which end of the bar is a north (N) or south pole (S) depends on the polarity of the magnetic field that drove the bar into saturation. Let us suppose the external magnetizing field has been removed. Inside the bar, by definition, the magnetization points from the south to the north pole. Inside the bar, H points directly from N to S (and is entirely the demagnetization field). Outside the bar, H points outward away from the N pole, follows a return path outside the magnet, and then points inward to the S pole. The magnetic induction B points directly from S to N within the magnet; and follows the same direction as H outside the magnet. Note, there is a discontinuity in H at the surface of the poles; this is attributable to a surface density of magnetic dipoles.

[10] George Green (1793-1841): An Essay on the Application of Mathematical Analysis to the Theories of Electricity and Magnetism, 1828.

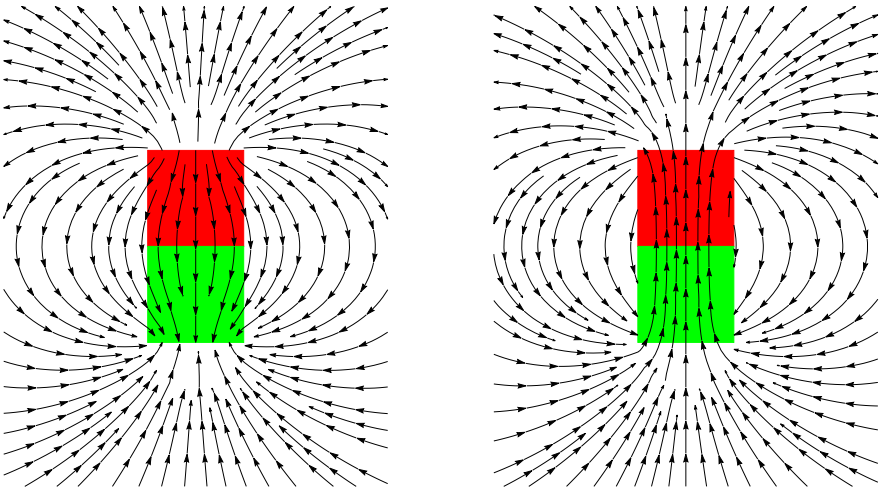

Figure 1.1: Fields around and within a bar magnet. Left: magnetic field **H**. Right: magnetic induction **B**. The bar is shown with a red coloured north pole and green south pole.

1.3.4 Scalar potential for magnetized cylinder

The magnetic field of a uniformly magnetized cylindrical bar may be found from the magnetic scalar potential. Corson[6] Chap. 9.8 points out that the H-field of such a cylinder is identical (in shape) to the electric field of an electret (described in [6] Chap. 3.7) whose field is equivalent to that of two oppositely charged circular discs with their faces parallel. The scalar (electric) potential for a charged disc is given in spherical polar coordinates $[r, \theta, \phi]$ by Morse[37] Chap. 10.3 pg. 1267 Eq. 10.3.29. Let the discs have radius a, and set $\rho \equiv r/a$ and $c \equiv \cos\theta$. The axial coordinate is $z = r\cos\theta$. The potential due to one disc is

$$V_a = (2Q/a)[1 - \rho|P_1(c)| + (1/2)\rho^2 P_2(c) - (1/8)\rho^4 P_4(c) + \ldots] \quad \rho < 1 \tag{1.8}$$

$$V_b = (2Q/a)[(1/2)\rho^{-1} - (1/8)\rho^{-3} P_2(c) + (1/16)\rho^{-5} P_4(c) + \ldots] \quad \rho > 1 \tag{1.9}$$

Here P_n are the Legendre polynomials. $P_1(c) = c$ and so $\rho|P_1(c)| = (r/a)|\cos\theta| = |z|/a$. The potential is independent of ϕ and reduces to Q/r at large distances, as it should. There is a discontinuity in gradient at the surface of the disc equal to $4Q/a^2$.

Suppose the electret or bar magnet is of length $\Delta z = 2L$. We find the field of the electret as follows: (1) Form the gradient vector of the potential; (2) convert from spherical to Cartesian coordinates; (3) for the positive-charged disc move the origin to $z = +L$, and for the negative-charged disc move the origin to $z = -L$; (4) sum the two vector fields to give **E**; (5) sum the field and polarization vector $\mathbf{P} = P\mathbf{u}_z$ to obtain the displacement $\mathbf{D} = \mathbf{E} + \mathbf{P}$. Due to the "region of applicability" conditions in V_a, V_b care must be taken to sum the correct fields in the relevant regions; assuming $L > a$ there are six regions. The construction for magnetic fields is analogous: V_a, V_b become the scalar potential whose (negative) gradient is **H**. The magnetic induction inside the bar is $\mathbf{B} = \mu_0(\mathbf{H} + \mathbf{M})$ where $\mathbf{M} = \mathbf{u}_z M$ and $M = 4Q/a^2$.

1.4 Demagnetization Factor

The purpose of this article is to de-mystify an effect called the de-magnetizing field. We shall begin with the result, and follow with the explanation. Suppose there is an 3D object of arbitrary shape, with internal uniform magnetization **M**. With respect to a Cartesian coordinate system, **M** has the components $[M_x, M_y, M_z]$. Further suppose there is no external field **H** due to free current; to be clear, we mean there is no externally applied H-field. Inside the magnetized material, the induction

is $\mathbf{B} = \mu_0(\mathbf{H}_{\rm int} + \mathbf{M})$. Outside the material, the induction is $\mathbf{B} = \mu_0(\mathbf{H}_{\rm ext})$. The demagnetization tensor (or matrix) $\bar{\mathbf{N}}$ tells us what is the internal H-field for a given magnetization $\mathbf{M}$ of the object:

$$\mathbf{H}_{\rm int} \;=\; -\bar{\mathbf{N}}\mathbf{M}\,. \tag{1.10}$$

This internal field[11] is attributable to the density of magnetic dipoles at the surface of the object. The external field $\mathbf{H}_{\rm ext}$ is given by the field equations (with no source currents $\mathbf{J}_f$) and the boundary conditions at the surface of the object. The orientation of the Cartesian unit vectors could be arbitrary, but if the object has a symmetry axis it is customary to align one of the unit vectors, say $\mathbf{u}_z$, with that axis. If in addition to the fields already mentioned, we introduce an external field (due to free currents), then it is customary to orient this field either parallel or transverse to the object's symmetry axis.

Each of the matrix elements $N_{i,j}$ is a demagnetization factor. In the situation that there is a single non-zero magnetization component, and that we are interested solely in the parallel H-field component, there is a tendency for authors to notate the demagnetization factor $\gamma \equiv N_{i,i}$.

We now enter the explanation. We follow a pedagogic path from a single component magnetization and scalar relationship between M and $H_{\rm int}$, ending in the tensor form above. We start with the confounding result that for an infinite[12] block with uniform magnetization $\mathbf{M}$, the magnetic induction is $\mathbf{B} = \mu_0\mathbf{M}$ – whereas for an isolated magnetized sphere in vacuuo the induction is $\mathbf{B} = \mu_0(2/3)\mathbf{M}$. The effect is explained by topology: there can be no *outside* field for an infinite block, whereas there are inside and outside fields for the sphere. The equations for the magnetic induction $\mathbf{B}$ have to be satisfied inside, outside and at the boundary between. There is a near field (related to the magnetization inside the specimen), and a far field varying as the inverse square of distance from the source; and they have to be married at the boundary which has bound currents at its surface; this is the origin of the so-called demagnetizing field. The value of the demagnetization factor γ depends on the 3D shape of the magnetized material. The auxiliary function $\mathbf{H}$, which has different (mathematical) forms inside versus outside, will resolve the mystery of the missing one third magnetic induction (in the case of the sphere).

Suppose we have a sample of magnetized material, and that the interior is filled with a vector field $\mathbf{M}$ which we call the magnetization. $\mathbf{M}$ is confined to the magnetic material, and does not extend outside. We may know $\mathbf{M}$, but not necessarily the distribution of bound magnetic dipoles on its surface. What is the magnetic induction $\mathbf{B}$ inside the sample? The answer is $\mathbf{B} = \mu_0(\mathbf{H} + \mathbf{M})$; in which we must find $\mathbf{H}$ in a region where there may be bound currents (in/on the magnetized sample) but no free currents. We gave the equations of magneto-statics in Sec. 1.3. In general, the equations for the potential must be solved numerically for a particular geometry of the magnetic material. But in the case of very high symmetry, such as the sphere, analytic methods are possible.

1.4.1 Spherical magnet in external field

Let $\mathbf{u}_z$ be a unit vector along the axis z. Consider a sphere (radius a) with uniform magnetization $\mathbf{M} = M\mathbf{u}_z$. Suppose the sphere is subject to a uniform external magnetic field. (For example, it is placed between the iron poles of a large dipole electromagnet whose gap-field points along z.) We adopt spherical polar coordinates r, θ, ϕ. Let the radius vector r make an angle θ with the axis z. $\nabla \cdot \mathbf{M} = 0$ inside the sphere. We take trial forms for the potentials inside and outside the sphere:

$$U_1(r < a) \;=\; -H_1 r\cos\theta \tag{1.11}$$

$$U_2(r > a) \;=\; -H_2 r\cos\theta + (A/r^2)\cos\theta \tag{1.12}$$

$$\mathbf{H}(r < a) \;=\; [H_r, H_\theta, H_\phi] \;=\; [H_1\cos\theta, -H_1\sin\theta,\ 0] \tag{1.13}$$

$$\mathbf{H}(r > a) \;=\; [(H_2 + 2A/r^3)\cos\theta, (-H_2 + A/r^3)\sin\theta,\ 0] \tag{1.14}$$

[11] If the magnetization is non-uniform, then there is also a contribution from bound current density within the body.

[12] In all spatial directions.

The third component H_ϕ is zero. H_1, H_2, A are adjustable constants. The subscripts $1, 2$ indicate inside and outside, respectively. The normal and tangential components of $\mathbf{M}$ are $M_r = +M\cos\theta$ and $M_\theta = -M\sin\theta$. It is a peculiarity of the coordinate system that the axial component is $M_z = M_r\cos\theta - M_\theta\sin\theta = M$. Continuity of the tangential component of $\mathbf{H}$ H_θ at $r = a$ implies $H_1 = H_2 - A/a^3$. Continuity of the normal component of $\mathbf{B}$ $B_{r<a} = \mu_0(H_r + M_r)$ and $B_{r>a} = \mu_0 H_r$ implies $(H_1 + M) = (H_2 + 2A/a^3)$. Two simultaneous equations may be solved for $H_1 = H_2 - M/3$ and $A = a^3M/3$. Hence the fields.

$$\text{Inside the sphere} \quad \mathbf{H} = \mathbf{H}_2 - \mathbf{M}/3 \quad \text{and} \quad \mathbf{B} = \mu_0(\mathbf{H} + \mathbf{M}) = \mu_0(\mathbf{H}_2 + 2\mathbf{M}/3) \tag{1.15}$$

$$\text{Outside the sphere} \quad \mathbf{H} = \mathbf{H}_2 + (a/r)^3 M[(2/3)\cos\theta, (1/3)\sin\theta, 0] \,, \quad \mathbf{B} = \mu_0\mathbf{H} \,. \tag{1.16}$$

The import of Eqs. 1.15 and 1.16 is as follows. If there is no externally applied field[13] $\mathbf{H}_2 = \mathbf{0}$, the H-field and magnetic induction inside the sphere are $\mathbf{H} = -(1/3)\mathbf{M}$ and $\mathbf{B} = \mu_0(2/3)\mathbf{M}$ respectively. Inside a magnetized sphere placed in an external field $\mathbf{H}_2$, the H-field is only $\mathbf{H}_2 - \mathbf{M}/3$. The geometry-dependent scale factor N_z, which happens to be $\frac{1}{3}$ for a sphere, is called the demagnetizing factor. The quantity $\mathbf{H} = -N_z\mathbf{M}$ is called the demagnetizing H-field, and it arises from the exterior surface density of magnetic dipoles on the sphere. The Eqs. 1.15 and 1.16 are illustrated in Fig. 1.2 which show a section of the sphere in the y, z plane. The particular values used are $a = 2, M = 4$ and applied H-field equal 0 or 2.

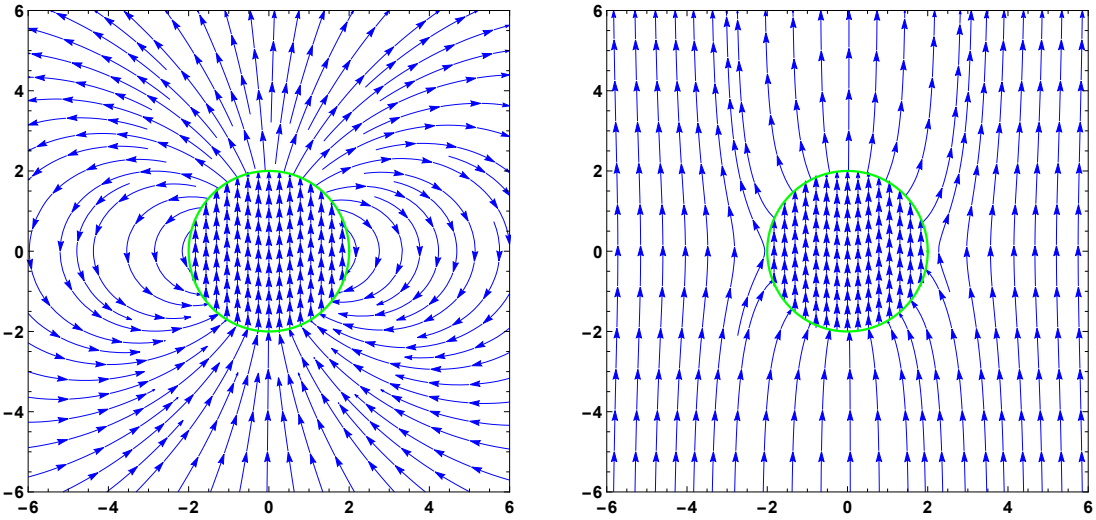

Figure 1.2: Magnetic field $\mathbf{B}$ lines in a planar section of the sphere. In Cartesian coordinates (x, y, z), the plane could be $x = 0$ or $y = 0$, with the z-axis vertical. Left: no external applied H-field, but upward magnetization. Right: with applied upward H-field and magnetization. The sphere circumference is shown green.

1.4.2 Recursive relation between H and M

The name "demagnetizing field" is strongly suggestive that it opposes the externally applied field $\mathbf{H}_2$. And yet, the demagnetizing field is present even when there is no applied field; in which case there is nothing to oppose. So, how does the effect come by its name? The answer is that the magnetization $\mathbf{M}$ usually depends on the magnetic force $\mathbf{H}$ inside the material. This is recursive: M depends on H, and M contributes an H-field which is oppositely directed to M. This is how $-N_z\,M$ gets the name demagnetizing field. If the relation between M and H (called permeability)

[13] That is no electromagnet present to provide a uniform bias field.

is near-linear, the recursion may be solved for the magnetization and B-field as a function of H_2; as in Sec. 1.5.1. The recursive nature of $M(H)$, recognized since the early 1900's, has the implication that the shape of lines (and surfaces) of constant magnetization value depend on the permeability of the material. For example, in the case of the cylinder with axial applied field, the internal field lines become increasingly parallel at larger values of material permeability. This, in turn, implies that the spatial-average demagnetization factor also varies with material permeability. Hence, it is necessary to tabulate γ as functions both of aspect ratio (diameter/length) and permeability. Chen[22] gives an overview of the literature for the cylinder.

The demagnetizing fields has consequences for two practical scenarios. Suppose that we take a magnetized block and that we move it into the field of an electro-magnet. When the move is complete, what is the shape of the **B**-field? Again, we must find **H**. A variant would be to keep the block still, and change the field of the electromagnet. In both situations, there is a slight re-adjustment of the interior volume density and the exterior surface density of magnetic dipoles in/on the block - so as to (partially) oppose the applied H-field. The final configuration is consistent with minimizing the self-interaction energy of all the sub-microscopic dipoles. However, we shall not need that condition to find the **H**-field. We simply assume that an equilibrium is reached, and that magneto-statics applies.

1.4.3 Consequences of symmetry

Symmetry is important. In the case of the sphere with applied field H_z, plots of the field lines Fig. 1.2 are identical in the planes $x = 0$ and $y = 0$. Likewise if the applied field is H_y, field plots are identical in the planes $x = 0$ and $z = 0$; and so on for applied field H_x. It follows that the demagnetizing factors $N_x = N_y = N_z$ are all equal, and their sum equal to 1.

Symmetry is important. An infinite medium has only an *inside*, there is no *outside*; so there is no surface upon which to place magnetic dipoles. Another way to think of this is that the surface dipoles (along with the surface) have been moved away to infinity, and therefore can have no effect. Therefore the demagnetization factor is zero in every direction. Yet another description is that the infinite medium has complete translational invariance, so there can be no geometry-dependent effects.

A magnetic medium that is infinite in one direction only, and has finite extent in the other two, will have demagnetization factor zero in that one direction – irrespective of the cross-section shape in the other two directions. Thus, for example, the infinite prism aligned with the z-axis has demagnetizing factors $N_z = 0$ and $N_x + N_y = 1$. In the case of an infinite cylinder, with rotational symmetry, the factors are $N_z = 0$ and $N_x = N_y = \frac{1}{2}$.

An ellipsoid, is a closed surface of which all plane cross sections are either ellipses or circles. An ellipsoid is symmetrical about three mutually perpendicular axes (called principal axes) that intersect at the centre; but has lower symmetry than the sphere. If the (uniform) H-field is applied parallel to one of the principal axes, the reactive (demagnetizing) field is also parallel to the axis. The lower symmetry implies the demagnetizing factors N_x, N_y, N_z are unequal; but they still sum to 1. If the (uniform) H-field is applied in a general direction, not along a principal axis, the relation between the demagnetization field and the magnetization **M**, is given by a matrix (tensor of rank 2) with elements $N_{i,j}$ such that $\mathbf{u}_i \cdot \mathbf{H}_{\text{demag}} = -N_{i,j}\mathbf{M} \cdot \mathbf{u}_j$ where $\mathbf{u}_k$ is a unit vector in direction k.

Consider a solid cylinder like the one in Fig. 1.1. The reader may notice that even when the magnetization is uniform (aligned with the vertical z-axis), the H-field and B-field inside the bar are not uniform and not aligned with the magnetization. In this case, the relation between the demagnetization field and the magnetization **M**, is given by a tensor of rank 3 whose elements vary both with direction and position. This complication is usually evaded by averaging[14] over the sample (to eliminate the spatial dependence) leaving a matrix. Nevertheless, the rotational symmetry

[14]The mid-plane average is called the fluxmetric (or ballistic) value, while the volume average is called the magnetometric value.

implies that special relationships exist between the matrix elements when uniform external fields are applied along x or y or z.

The toroid is a surface of revolution with a hole in the middle. Take Cartesian coordinates with z aligned with the rotation axis. We may apply uniform fields along x or y or z, and find $N_x = N_y$ and $N_x + N_y + N_z = 1$. The same body may be described in cylindrical polars $[r, \theta, z]$. Suppose there is a method to create an azimuthal magnetization. The toroid has single-axis rotational invariance. This implies there is no (cross-sectional) plane perpendicular to the azimuth (θ) upon which to deposit surface magnetic dipoles; and therefore the azimuthal demagnetization factor N_θ is zero. Does this imply that $N_r + N_z = 1$ or $N_r = N_z$? Not necessarily so. We have to consider how the individual fields H_r or H_θ or H_z would be created and applied to the sample. The axial field H_z could be created, for example, by a Helmholtz coil[15] or large aperture H-frame dipole magnet. The azimuthal field H_θ could be created by many helical turns around the circular limb of the torus. But there is no way to create a field H_r, because it would require the presence of a magnetic monopole. So in magnetostatics, N_r is meaningless. However, if we consider time varying fields (AC or RF), the second pair of Maxwell equations in Eq. 1.3 are consistent with TM cavity modes that have H_θ or TE cavity modes that have H_r. But only if the cylindrical symmetry of the normal mode is broken, is it possible to find modes with both H_θ and H_r non-zero.

Note, a single-turn current-carrying winding about the circular limb of the torus leads to a situation in which there is both an inside and outside field, and so there is a demagnetizing field. However, in this configuration neither the magnetization nor the internal H-field is uniform. Contrastingly, if there are a large number of equally spaced turns in the winding, the outside field drops toward zero; and the azimuthal factor N_θ tends to zero. Note how N_z of a very long cylinder behaves like N_θ of the torus. We may think of bending a long straight cylinder into a torus, such that the end faces of the cylinder touch and become lost within the body of the torus. The equal in size and oppositely directed, North versus South, surface density on (what were) the end faces become united into a cross-sectional sheet of magnetic dipole density (within the torus) just like any other cross-section of the original magnetized rod. Evidently the end-face dipole density (which is a source of demagnetizing field) disappears, and so the factor N_θ must become zero.

1.4.4 Other geometries

Only in the case of the uniformly magnetized ellipsoid, is the demagnetizing H-field uniform and parallel to the magnetization. For other geometries, even if $\mathbf{M}$ is uniform, the internal H-field $\mathbf{H}$ is neither uniform nor everywhere parallel to $\mathbf{M}$. In such a situation we make the projection of $\mathbf{H}$ onto $\mathbf{M}$, and integrate the vector scalar product $\mathbf{M} \cdot \mathbf{H}$ over the volume to obtain the average demagnetizing factor. Under that procedure, by symmetry, the demagnetization factors of the cube are all equal $\frac{1}{3}$.

The demagnetizing factor arises from the surface magnetic dipole density. Thus we should expect the internal H-field to be proportional to the area of the exposed face, and stronger if the interior is close to the surfaces (poles). Thus we should expect that a thin circular disc or a square lamina to have $\gamma \to 1$ in the direction perpendicular to the large flat surfaces. Similar reasoning tell us that if an object has aspect ratios $a : b : c$ in orthogonal directions, the demagnetization factors will be approximately in the ratio: $1/a, 1/b, 1/c$, that is smallest in the direction in which the object is longest.

In the case of a magnetized ellipsoid[18, 19], and the external field aligned with one of the principal axes, there are different demagnetizing factors for each orthogonal direction; and they sum to unity when S.I. units are employed. In c.g.s units the individual direction-dependent factors sum to 4π. Demagnetization factors are known, or have been numerically calculated, for the following geometries:

[15] Two current-carrying turns of cable each of radius R placed a distance $\Delta z = R$ apart.

- Ellipsoids[3, 18, 19]
- Cylinders[21, 22, 23, 24, 25, 26, 27] and square rods[26]
- Cylindrical cores[29] and related shapes.
- Toroids[30] and related shapes
- Cuboids (a.k.a rectangular bricks)[31, 32, 33] and cylinder tiles[34]. These works are intended for finite element analysis (FEA) wherein an object is subdivided into a 3D grid of 3D cells.

A cylindrical core is a solid cylinder with an inner coaxial cylindrical hole. Typically, the authors assume uniform magnetization. Chen[22] gives an excellent historical account of work on the solid cylinder, with many references. With the exception of the cuboids, most authors consider axial magnetization. Chen[28] attempts to calculate a radial demagnetization factor; but the work is misleading.

The annular torus is an excellent geometry for magnetic permeability measurements. In the limit of a large number of winding turns about the annular core, H and B are confined entirely within the winding. In this case, there is no outside field; and there can be no demagnetization factor in the azimuthal direction. In fact, such is the high degree of symmetry that remarkably few turns are needed to confine the fields within the annular solenoid. In a configuration known as the Rowland[16] ring, one winding creates the H-field and a second winding can be used to measure the B-field from the electromotive force (known as back e.m.f) when the current in the windings is varied.

The condition of uniform magnetization $\nabla \cdot \mathbf{M} = 0$ is unusual and/or artificial. In the general case, for arbitrary geometry, numerical methods must be employed. The calculation of magnetization is a specialized topic with its own literature. One important tool is finite element analysis: subdividing the geometry into cells and summing the (Greens function) contribution of each cell. The book by Wei[20] provides an introduction to this method.

Horseshoe magnet

Over a long period of time, the internal demagnetizing field has a tendency to demagnetize a short iron bar. The demagnetization factor is much reduced in long, thin bars, but the shape is unwieldy. However, if the long bar is bent into a horseshoe or U-shape, the magnet becomes more compact and retains its long-form magnetic longevity. The horseshoe magnet was invented by Englishman William Sturgeon in 1821. The external B-field appears between the (N and S) pole tips, which can be quite close together. The magnetization can be retained for many years if an iron *keeper* is placed across the poles when the magnet is not in use. With the keeper in place, the geometry becomes that of an annular solenoid - which has a zero-value demagnetization factor along the azimuth. Sturgeon (1783-1850) was a founder of electrical engineering, amateur physicist, and inventor of the worlds first electro-magnet in 1824.

1.4.5 Properties of the demagnetizing tensor

Brown[35] uses the long-range classical dipole interaction energy to explore the ferromagnetic properties of single-domain particles; and *en-passant* deduces two properties of the tensor $\bar{\mathbf{N}}$. The reasoning is elaborate and reprised and explained in Sec. 1.4.6. Here we state the results:

$$\sum_i N_{ii} = 1 \qquad \text{and} \qquad N_{ij} = N_{ji} \; . \tag{1.17}$$

[16] Named for American physicist Henry Augustus Rowland (1848-1901).

Thus the trace, equal to the sum of the eigenvalues, is unity. Further, the matrix is symmetric, equal to its transpose. The general 3×3 matrix has nine unequal elements; but the symmetry condition implies only six distinct elements.

We consider now the influence of the geometry of the magnetized object; in particular cylindrical symmetry. We may write the magnetization and the H-field either in Cartesian (x, y, z) or cylindrical polar coordinates (r, θ, z). The physical system does not change, but the elements of the tensor must be transformed. Suppose the tensor is written $\bar{\mathbf{N}}$ in the Cartesian system, and $\tilde{\mathbf{N}}$ in the polar system; they are related by a similarity transform: $\tilde{\mathbf{N}} = \mathbf{R}\bar{\mathbf{N}}\mathbf{R}^{-1}$. The coordinate transform has the property that the inverse is equal the transpose $\mathbf{R}^{-1} = \mathbf{R}^T$. The matrices are

$$\bar{\mathbf{N}} = \begin{bmatrix} N_{11} & N_{12} & N_{13} \\ N_{21} & N_{22} & N_{23} \\ N_{31} & N_{32} & N_{33} \end{bmatrix} \qquad \text{and} \qquad \mathbf{R} = \begin{bmatrix} \cos\theta & \sin\theta & 0 \\ -\sin\theta & \cos\theta & 0 \\ 0 & 0 & 1 \end{bmatrix} .$$

In general, the matrix elements of $\tilde{\mathbf{N}}$ will contain terms in $\cos\theta$ and $\sin\theta$. However, we may insist that $\tilde{\mathbf{N}}$ is independent of azimuthal angle θ, and this will lead to conditions on the elements of $\bar{\mathbf{N}}$. The conditions are

$$N_{22} = N_{11}, \quad N_{21} = -N_{12}, \quad N_{31} = N_{13} = N_{32} = N_{23} = 0 \, . \tag{1.18}$$

The symmetry $N_{ij} = N_{ji}$ further implies $N_{21} = N_{12} = 0$. Hence cylindrical symmetry implies $\bar{\mathbf{N}}$ must be a diagonal matrix with two elements equal $N_{xx} = N_{yy}$. Thinking of the annulus, the reader may be wondering why we did not find (and cannot generate) a condition such as $N_{22} = N_{\theta\theta} = 0$. The answer is simple: $N_{\theta\theta}$ is zero when there is no outside field; but the whole apparatus of $\bar{\mathbf{N}}$ assumes there *is* an outside field. To summarise, we have found that when the magentized sample is immersed in its own external H-field, the components inside the sample are $H_r = N_{xx}M_r$, $H_\theta = N_{xx}M_\theta$ and $H_z = N_{zz}M_z$. However, there is no guarantee that it is possible to make a radial or azimuthal magnetization unless the fields are time varying (AC or RF), or there is no outside field.

1.4.6 Brown's Theorem

Brown's theorem is Eq. 1.17. The following derivation uses results deduced by Poisson, Maxwell and Brown[35]. Poisson tells us how to imagine an electric or magnetic (or gravitational) dipole moment. Take a 3D body of arbitrary shape and density ρ. In suitable units, the potential inside satisfies $\nabla^2\Phi = \rho$; and outside $\nabla^2\Phi = 0$. Superpose an equal body of negative density, but displaced a small (or infinitesimal distance) dx from its positive twin. The result is an empty shell with equal positive and negative halves separated by a contour of zero potential. The density on the shell is not uniform. For example, if the body is a solid sphere of radius $r = a$ and the radius vector makes an angle θ with the displacement vector $\mathbf{dx}$, the density varies as $\delta(r - a)\cos\theta$. This surface density gives rise to a field inside the shell. The potential due to the shell is $\Psi = \Phi(\mathbf{r}) - \Phi(\mathbf{r} + \mathbf{dx}) = -\nabla\Phi(\mathbf{r}) \cdot \mathbf{dx}$. The force on a test charge or particle is $\mathbf{F} = -\nabla\Psi$ or in component form:

$$F_j = -\frac{\partial\Psi}{\partial x_j} = -\frac{\partial}{\partial x_j}\sum_i \frac{\partial\Phi}{\partial x_i}dx_i = -\sum_i \frac{\partial^2\Phi}{\partial x_j \partial x_i}dx_i \, .$$

Maxwell[17] re-interprets these results for a 3D body with constant density ρ of magnetizable dipoles. This density is the analog of mass density for the gravitational case. Positive and negative density bodies are offset by a displacement dx to give a shell with equal and opposite magnetic dipole (surface) density on its two halves, giving rise to a a uniform magnetization (parallel to the displacement dx) within the interior. Accompanying the surface dipole distribution is an internal

[17] Ref. [1], Vol. II, Article 437.

H-field, which is given by the gradient of the scalar magnetic potential thus $\mathbf{H} = -\nabla\Psi$. Maxwell goes on to find explicit expressions for Φ and Ψ in the case of an ellipsoid of uniform density. Φ is a quadratic function and Ψ is a linear function of the coordinates (x, y, z). Maxwell then writes the matrix relation between the components of the magnetization $\mathbf{M}$ and the magnetic force $\mathbf{H}$; and notes (i) that all $N_{ij} > 0$, and (ii) that energy conservation demands the elements $N_{ij} = N_{ji}$ be equal.

The short-range exchange interaction aligns spins locally, whereas the Weiss domains owe their existence to the long-range classical dipole interaction energy. Brown[35] uses the latter to explore the ferromagnetic properties of single-domain particles; and *en-passant* deduces two properties of the tensor $\bar{\mathbf{N}}$. Let $\mathbf{u}_i$ be the vector magnetic moment of an atom (or spin-lattice) site i. In a field $\mathbf{H}$, the moment is subject to a couple $C = \mathbf{u}_i \times \mathbf{H} = |\mathbf{u}_i||\mathbf{H}| \sin\phi$ where ϕ is the angle between the two vectors. This couple can be found by differentiation with respect to angle of the potential energy $W_i = -\mathbf{u}_i \cdot \mathbf{H} = -|\mathbf{u}_i||\mathbf{H}| \cos\phi$; so $-dW_i/d\phi = C$.

The mutual potential energy of two individual dipole moments $\mathbf{u}_i$ and $\mathbf{u}_j$ is

$$W_{ij} = \frac{1}{r_{ij}^3}\left[\mathbf{u}_i \cdot \mathbf{u}_j - 3\frac{(\mathbf{r}_{ij} \cdot \mathbf{u}_i)(\mathbf{r}_{ij} \cdot \mathbf{u}_j)}{r_{ij}^2}\right] \equiv -\mathbf{u}_i \cdot \mathbf{h}_{ij} \equiv -\mathbf{u}_j \cdot \mathbf{h}_{ji} \; . \tag{1.19}$$

Here $\mathbf{r}_{ij}$ is the position vector from i to j. The total internal magnetic energy $W_{\rm int}$ within the material is the sum of W_{ij} over all individual moments i. Thus $W_{\rm int} = -\frac{1}{2}\sum_i \mathbf{u}_i \cdot \mathbf{h}_i$ where $\mathbf{h}_i = \sum_{j\neq i} \mathbf{h}_{ij}$. Following Lorentz[36], Brown proposes that $\mathbf{h}_i = \mathbf{H}' + \frac{1}{3}\mathbf{M}$ where $\mathbf{H}'$ is the demagnetizing field due to surface σ_m and volume ρ_m dipole density. The sum over individual dipoles is replaced by a volume integral over the density of magnetic dipoles (also known as the magnetization $\mathbf{M}$) within the body.

$$2W_{\rm int} = -\sum_i \mathbf{u}_i \cdot [\mathbf{H}' + \mathbf{M}/3] \equiv -\int \mathbf{M} \cdot [\mathbf{H}' + \mathbf{M}/3] dV \; .$$

Brown advances arguments that this integral may be written

$$2W_{\rm int} = \int |\mathbf{H}'|^2 dV \; + W_0 \quad \text{where} \quad W_0 = -\frac{1}{3}\int |\mathbf{M}|^2 dV \; . \tag{1.20}$$

W_0 is a constant, and has no influence on orientation. From Eq. 1.20 follows the principle of pole avoidance: the internal magnetic energy is least when $\mathbf{H}' = \mathbf{0}$ everywhere; that is when the magnetization varies in such a way that there are no poles (as occcurs in the annular solenoid). If there is an external applied field $\mathbf{H}_2$, there is additional magnetic energy within the body equal to $W_{\rm ext} = \sum_i \mathbf{u}_i \cdot \mathbf{H}_2 = \int \mathbf{M} \cdot \mathbf{H}_2 dV$. Let V be the volume of the body. For an ellipsoidal single-domain particle, the components $H_i' = -N_i M_i$ and the internal magnetic energy is

$$W_{\rm int} = W_0 - \frac{V}{2}\sum_i M_i H_i' = W_0 + \frac{V}{2}\sum N_i M_i^2 \tag{1.21}$$

In zero external field, equilibrium demands that $\mathbf{M}$ lie along the direction that minimizes $W_{\rm int}$; this is the principal ellipsoid axis corresponding to the smallest N_i, namely the longest axis. An external field $\mathbf{H}_2$ can rotate $\mathbf{M}$ out of this direction. Later, Brown re-writes Eq. 1.21 in a form that demonstrates greater generality:

$$W_{\rm int} - W_0 = -\frac{1}{2}\sum_i M_i \int H_i' dV = \frac{V}{2}\sum_i M_i \sum_j M_j \int \frac{\partial^2 \Phi}{\partial x_i \partial x_j} dV = \frac{V}{2}\sum_i \sum_j N_{ij} M_i M_j \; . \tag{1.22}$$

This leads to the identification

$$N_{ij} = \frac{1}{V}\int \frac{\partial^2 \Phi}{\partial x_i \partial x_j} dV = N_{ji} \tag{1.23}$$

Independence of the order in which the partial derivatives are formed leads to $N_{ij} = N_{ji}$. Φ is the solution of $\nabla^2\Phi = \rho = 1$ within the magnetizable body. The quadratic form $\sum_i \sum_j N_{ij} M_i M_j$ may be written $\mathbf{M}^T \bar{\mathbf{N}} \mathbf{M}$. If we transform to a new vector basis, the matrix $\bar{\mathbf{N}}$ may be diagonalised. The diagonal matrix is generated by a similarity transform: $\mathbf{N}^* = \mathbf{P}^{-1}\bar{\mathbf{N}}\mathbf{P}$ where the columns of the matrix $\mathbf{P}$ are the eigenvectors of $\bar{\mathbf{N}}$. In the new basis, the magnetization vector becomes $\mathbf{M}^* = \mathbf{P}^{-1}\mathbf{M}$, and the quadratic form becomes $\sum_i N^*_{ii}(M^*_i)^2$. Further, the coordinate system is transformed: $\mathbf{r}^* = \mathbf{P}^{-1}\mathbf{r}$. When the potential Φ is written in these new coordinates, we find

$$\sum_j N_{jj} = \sum_i N^*_{ii} = \frac{1}{V}\int \sum_i \frac{\partial^2 \Phi}{\partial (x^*_i)^2} dV = \frac{1}{V}\int \nabla^2 \Phi dV = 1 \,. \tag{1.24}$$

Evidently, the trace of $\bar{\mathbf{N}}$ is equal to unity. Further, we may conclude that as far as W_{int} is concerned, the single-domain particle of arbitary shape is equivalent to an ellipsoid. A case in point: the sphere and (spatial average of) the cube have equal demagnetization factors

1.5 Permeability and Hysteresis (DC)

It is customary to begin a description of magnetic materials with their properties in the quasi-static or near-DC regime. Permeability is a measure of magnetization produced in a material in response to an applied magnetic H-field. Susceptibility, notated χ, gives the relation between magnetization M and H-field. Permeability, notated μ, expresses the relationship between the magnetic induction B and the magnetic field H *inside* the magnetic material. Defined that way, the permeability depends only upon the material properties but not on its shape/geometry. Trivially, $\mu = 1 + \chi$.

1.5.1 Measurement of permeability

Suppose for the moment that the relation between magnetization M and (interal) magnetic field H is near linear; and we may write $B = \mu_0 \mu_r H$ where the relative permeability μ_r is constant. Let H_2 be the applied external field. B and H_2 may be measured, but not H. Inside the material $H = H_2 - \gamma M$ where γ is the demagnetization factor for a particular orientation of the specimen with respect to the applied field.

Hence inside $B = \mu_0(H + M) = \mu_0(H_2 - \gamma M \ + M)$. B may be eliminated in favour of the magnetization M, and this substituted back into B, yielding a relation between B and H_2.

$$M = \frac{H_2(\mu_r - 1)}{1 + \gamma(\mu_r - 1)} \,, \qquad \mu_r = \frac{B(\gamma - 1)}{(\gamma B - \mu_0 H_2)} \,. \tag{1.25}$$

If B and H_2 are measured values, then knowing γ, for the particular geometry of the sample, we may calculate first μ_r, and finally the magnetization M. There will be measurement errors in B and H; and γ is imprecisely known. The relative fractional error $\Delta\mu_r/\mu_r$ in the derived quantity μ_r is minimized when $\gamma \to 0$; in which case $\mu_r \to B/(\mu_0 H_2)$.

In practise, the relation between M and H is neither linear nor single-valued. The linear coefficient μ_r loses utility. In its place we write the functional relationship $B = \tilde{B}(H)$ where $\tilde{B}$ is found by measurement and B, H take their values inside the material. Now $H = H_2 - \gamma M$. Hence we may write the equivalence:

$$\tilde{B}(H) = \mu_0(H + M) \quad \text{or} \quad \tilde{B}(H_2 - \gamma M) = \mu_0[H_2 + (1 - \gamma)M] \,. \tag{1.26}$$

If γ can be made zero then the inside and outside fields are equal: $H = H_2$. Thus we may measure and record the relationship $\tilde{B}(H)$. From that result we may construct the magnetization $M(H) = \tilde{B}(H)/\mu_0 - H$. Further, by solving the second nonlinear equation 1.26 we may find the magnetization of an object with different geometry and known (non-zero) demagnetization

factor. Thus it is essential to choose a geometry for the magnetic-material sample for which the demagnetization factor γ is very small or zero in some particular direction. For that reason, needle-like objects (long and thin cylinders) or rings are employed.

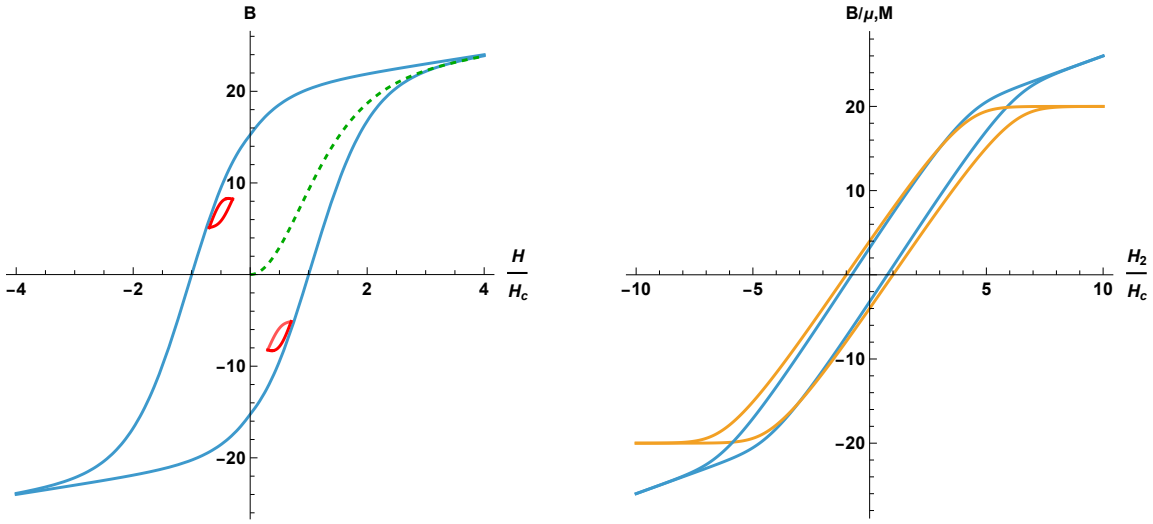

Figure 1.3: Hysteresis curves. Left: $B(H)$ main loop shown blue; virgin magnetization shown green dashed; two minor loops shown red. Right: $B(H_2)$ shown blue and $M(H_2)$ shown gold; demagnetization factor $\gamma = 0.2$. H_2 is the external applied field, and H_c the coercive field.

Eq. 1.26 is a relation between scalars. This may be generalized to a relation between vectors. The components of the demagnetizing field $\mathbf{H}_d$ is found from the magnetization $\mathbf{M}$ via a tensor $\tilde{\mathbf{N}}$. However, $\mathbf{M}$ depends on the prior history of the external magnetizing field $\mathbf{H}_2$. Let $\mathbf{H} = \mathbf{H}_2 + \mathbf{H}_d = \mathbf{H}_2 - \tilde{\mathbf{N}}\mathbf{M}$. Hence formally:

$$\mathbf{B}(\mathbf{H})/\mu_0 = (\mathbf{H} + \mathbf{M}) \quad \text{becomes} \quad \mathbf{B}(\mathbf{H}_2 - \tilde{\mathbf{N}}\mathbf{M})/\mu_0 = [(\mathbf{H}_2 - \tilde{\mathbf{N}}\mathbf{M}) + \mathbf{M}] \,. \tag{1.27}$$

1.5.2 Hysteresis curves

The relation between B and H for ferro- and ferri-magnetic materials is neither linear nor single-valued; and depends on the prior magnetisation of the sample. This effect is called hysteresis, and the trajectory $B(H)$ is an $\int\int$-shaped loop; often called a B-H curve. Example hysteresis curves are shown in Fig. 1.3. Hysteresis is a complicated phenomenon, that presupposes that the drive magnetic field is changing, albeit slowly. The essence of the hysteresis is branching: describing the existence of alternative trajectories depending on the direction of the time derivative dH/dt. We shall not treat the topic in detail here. However, the dedicated reader may pursue the review[16] by Mörée & M. Leijon of mathematical models for calculating magnetic hysteresis. One of the most popular is the model of Jiles and Atherton[17].

If there is zero prior magnetization, $B(H)$ will follow the initial (or virgin) magnetization curve – eventually to saturation. If the applied H-field is now progressively reduced, and reversed, the sample follows an $\int$-shaped curve into negative saturation. Likewise, increasing H can drive the sample back to positive saturation, but along a different/companion $\int$-curve. Thus by varying H between (symmetrical) positive and negative extremes, the sample may be cycled around its B-H loop. The loop can be considered as two branches: one for rising and another for falling H-field. All variations are assumed to be slow, or quasi-static.

But the behaviour is radically different if we stop the H-field variation part way through the cycle, and start to reverse the variation. The magnetic induction B will trace out one branch of a different hysteresis loop. If the H-variation is again stopped and then reversed, the B-field will

trace out the other branch of what is called a *minor loop*. Minor loops are sketched in Fig. 1.3. This effect is called *incremental permeability*, and the precise shape of the minor loop has to be measured for each starting point on the main B-H curve; it cannot easily be predicted. It is this type of incremental loop that is exercised when an AC or RF magnetic field is applied to a ferrite material that has been biased by a DC magnetic field into a state of prior magnetization.

The main hysteresis trajectory (B, H) is called the major loop, and is usually characterised by four values. (1) The intercept $(0, \pm H_c)$ where H_c is the coercive field (or "force"). (2) The intercept $(\pm B_r, 0)$ wher B_r is the residual magnetization. (3,4) The two saturation limits $\pm(B_s, H_s)$ where B_s is the saturation flux density, and H_s is the saturating field.

Note! Commercial hysteresis loops are usually displayed using CGS units. In the CGS system the fields B, M, H all have the same units, although for historical reasons the units of B,M are called Gauss whereas the units of H are called Oersteds. The conversion from CGS to MKS units is relatively simple: 1 Tesla= 10^4 Gauss. $10^3/(4\pi) = 79.58$ Amps/m = 1 Oersted. M in Amps/m = [4π M(in Gauss)] $\times$ 79.6. In the CGS system $B = H + 4\pi M$. The relative permeability is the same for both systems.

1.5.3 Hard versus soft magnetic materials

In hard magnetic materials, the applied field resulting in magnetic saturation is only a few times larger than the coercive field $H_{\rm c}$ which is itself considered large. Likewise, the saturation value of induction $B_{\rm sat}$ is only a few times (at most) larger than the remanent induction $B_{\rm r}$. Hard magnetic materials are initially resistant to magnetization, but once magnetized they retain their magnetization. The hysteresis loop of a hard magnetic is shown in the left side of Fig. 1.3.

In soft magnetic materials, the applied field resulting in saturation is many times larger than the corecive field which itself is considered small. Likewise, the saturation value of induction is usually many times larger than the remanent induction. Soft magnetic materials have large permeability, but a tendency to loose their magnetization over time (sometimes quickly). The hysteresis loop of a soft magnetic is shown in the right side of Fig. 1.3. Soft materials are easy to magnetize and demagnetize; indeed, very soft materials may spontaneously demagnetize due to the internal demagnetizing field. Hard magnetic materials make good permanent magnets. The ferrites employed to tune RF particle-acceleration cavities are soft magnetic materials.

The ratio of the remanent to the saturation induction $B_{\rm rem}/B_{\rm sat}$ (both taken in the same quadrant) does not follow immediately from hard versus soft material. Rather it arises from the interplay of the coercive field and the initial permeability. If the latter is large, the intercept $(B, H) = (B_r, 0)$ may lie at a significant fraction of $B_{\rm sat}$ even if the coercive field is small.

Configuration lag

Magnetization is the configuration of domains. Hysteresis is the reconfiguration lag in response to a quasi-static variation of the H-field. The magnetization always lags, and this causes a branch; and if the field is reversed again a backward branch resulting in a loop. Consider the main hysteresis loop shown in the left hand side of Fig. 1.3. It may come as a surprise, but there is negative (or reverse) magnetization in a portion of the upper right quadrant. This effect is particularly evident in hard magnetic materials. Consider first the lower right quadrant of the loop. When $H = 0$, the magnetization is large and negative $M = -B_r/\mu_0$ but not saturated. When $H = H_c$, the magnetization is weak and negative ($M = -H_c$) even though the magnetic "force" is positive. Consider now the upper right quadrant of the loop, and suppose for a moment that the hysteresis curve is locally linear about $H = H_c$. The magnetization becomes zero when $H = H_0 \approx B_r H_c/(B_r - \mu_0 H_c)$ and $H_c < H_0 < 2H_c$. The corresponding value of induction is $B_0 \approx B_r H_c \mu_0/(B_r - H_c\mu_0) > 0$; and depends on the ratio $\alpha \equiv \mu_0 H_c/B_r < 1/2$. The magnetization rises from zero as the already positive H is further increased. In the linear model, a large positive magnetization ($+B_r$) is achieved

at $H = 2H_c$. Beyond this value, the magnetization response progressively saturates. Contrastingly, in a soft magnetic material, the saturation magnetization does not arise until many times H_c has been applied.

1.5.4 Using a B-H curve

Manufacturer's hysteresis data for their magnetic materials relate the magnetic induction B and H-field inside the material. The cycle presupposes that the material has at some point been driven into (positive or negative) saturation and that we operate on the major loop of the B-H curve. Let this functional relation be $B = \tilde{B}(H)$. Suppose a magnetizable object is immersed in an external field, and the demagnetization factor γ is known for the given field orientation. To find the relation between B and the external applied field H_2, we must solve an equation of the form 1.26 for $M(H_2)$; and then substitute M to return $B(H_2)$. We shall give two examples of this procedure.

First, for simplicity, let us suppose that the hysteresis curve is locally linear about the coercive field $\pm H_c$. B_s is the saturated value of magnetic induction. To simplify expressions we define $H_s^* \equiv B_s/\mu_0$. The asterisk signifies that this value is a response rather than a drive magnetic field. Locally, the functional form is $\tilde{B}/\mu_0 = H_s^* \times (H/H_c \pm 1)$. The positive sign gives the branch at $H < 0$; and the negative sign gives the branch at $H > 0$. Now $\tilde{B}/\mu_0$ must be equal to the sum of the magnetization M and H-field inside. Further, we substitute $H = H_2 - \gamma M$.

$$(H/H_c \pm 1)H_s^* = (H + M) \quad \text{or} \quad \left[\frac{H_2 - \gamma M}{H_c} \pm 1\right] H_s^* = H_2 + (1-\gamma)M \; . \tag{1.28}$$

We solve Eq. 1.28 for the magnetization in tems of the applied field H_2.

$$M = \frac{-H_2 H_c + (H_2 \pm H_c)H_s^*}{H_c(1-\gamma) + \gamma H_s^*} \; . \tag{1.29}$$

The magnetic induction is simply $B = \mu_0[H_2 + (1-\gamma)M]$.

Now, consider a nonlinear model for the B-H curve:

$$\tilde{B}(H)/\mu_0 = M_s \tanh(H/H_c \pm 1) \; + \; H \; \equiv \; (M + H) \, . \tag{1.30}$$

Here M_s is the saturation magnetization. The $\tanh(\dots)$ term in Eq. 1.30 models saturation and the coercivity. The second term manifests that "far beyond" saturation, B is proportional to H. To find the magnetization due to an external field H_2, we substitute $H = H_2 - \gamma M$ throughout Eq. 1.30. The nonlinear equation is solved numerically for $M(H_2)$, for specific values of γ, H_c and M_s; say by Newton-Raphson iteration. The right-hand drawing in Fig. 1.3 is the example $\gamma = 0.2$, $H_c = 1$ and $M_s = 20$. The reader will notice that the magnetization saturates, while the induction B continues to rise in response to the applied field H_2.

1.5.5 Toy models for B-H branches

There are two types of toy mathematical model commonly employed to sketch B-H hysteresis branches, and each comes in three varieties. They contain analogs of coercivity and saturation, but do not necessarily contain any underlying physics. The two types are:

$$\begin{aligned} B_1/\mu_0 &= M_{\rm sat} F_j(\theta) \pm M_0 + H \\ B_2/\mu_0 &= M_{\rm sat} F_j(\theta) \times (1 \pm H/M_{\rm sat}) \; . \end{aligned}$$

The functions F_j are locally linear around $\theta = 0$, but saturate for large values of the argument: $F_j \to 1$. Here $\theta = H/H_c \pm 1$ yields the two branches. The negative/positive sign in θ gives the lower/upper branch. Because of the M_0 term, the meaning of $M_{\rm sat}$ is slightly different between B_1 and B_2. Note also that magnetization and drive-field H are distinct in B_1, but no so in B_2.

If $M_0 = 0$, B_1 has the wrong value at $H = \pm H_c$. If $M_0 = H_c$, B_1 is discontinuous between the upper and lower branches even as $H \to \pm\infty$; the jump is $2H_c$. In the case of B_2, there are four segments; one for each quadrant. Take the negative sign in $(1 \pm H)$ for $H < 0$ and the positive sign for $H > 0$. B_2 is continuous between the branches at large $|H|$. However, B_2 is discontinuous in derivative dB/dH at $H = 0$.

There are three varieties typically encountered for the functions F_j:

$$\begin{aligned} F_1(\theta) &= \tanh(a_1\theta) \\ F_2(\theta) &= (2/\pi)\arctan(a_2\theta) \\ F_3(\theta) &= [\coth(a_3\theta) - 1/(a_3\theta)] \ . \end{aligned}$$

F_3 is called the Langevin function, and has a physical basis in the statistical mechanics explanation of paramagnetism. a_1, a_2, a_3 are scale parameters. The functions may each be arbitrarily stretched or compressed. So to make a meaningful comparison, they have to be normalised. Let us insist that they have the same first derivative at $\theta = 0$. This implies $a_1 = 1$ and $a_2 = \pi/2$ and $a_3 = 3$. If the revised functions are plotted, we find that F_2 and F_3 have very similar shapes, and that F_3 may be eliminated from the menu in favour of the simpler F_2. Going forward, $F_1 = \tanh(\theta)$ and $F_2 = (2/\pi)\arctan[(\pi/2)\theta]$. F_1 approaches saturation abruptly with a knee, while F_2 saturates more gently. F_1 is better suited to model hard, and F_2 to model soft magnetic materials. Neither F_1 nor F_2 have enough free parameters to model/display the variety of saturated hysteresis curves that may be found in nature. For example, the remanent induction B_r cannot be chosen independent of $M_{\rm sat}$ or H_c. However, the flexibility can be increased by resetting the argument of tanh and arctan to be $a\,\theta + b\,\theta^3$ where a, b are adjustable constants. For example $0 < a < 1$ will reduce the remanent value B_r without changing H_c or $M_{\rm sat}$; and the rapidity of full saturation may be increased if $b > 0$. The gradient at larger values of H cannot be greater than at smaller values of $H > H_c$. Therefore, physicality demands that the third derivative $d^3F/d\theta^3$ be less than or equal zero as $\theta \to 0$.

For the B_2 type function and $F_2(a\times\theta)$, the remanent valus are $B_{\rm rem} = \pm(2/\pi)M_{\rm sat}\arctan[(\pi/2)a]$; and the discontinuity in gradient across $H = 0$ is $\Delta[\partial B/\partial H] = (4/\pi)\arctan[(\pi/2)a]$. For the B_2 type function and $F_2(a\,\theta + b\,\theta^3)$, the variable b is limited by $0 \le b \le a^3 \times (\pi^2/12) \approx a^3 \times (0.8225)$.

For the B_2 type function and $F_1(a \times \theta)$, the remanent valus are $B_{\rm rem} = \pm M_{\rm sat}\tanh(a)$; and the discontinuity in gradient across $H = 0$ is $\Delta[\partial B/\partial]H = 2\tanh(a)$. For the B_2 type function and $F_1(a\,\theta + b\,\theta^3)$, the variable b is limited by $0 \le b \le a^3/3$.

Chapter 2

Magnetic Field of Toroidal Coil

"A filament of matter, so magnetized that its strength is the same at *every section*, at whatever part of its length the section be made, is called a *magnetic solenoid*. ... the potential due to a solenoid, and consequently all its magnetic effects, depend only on its strength and the position of its ends; and not at all on its form, whether straight or curved between these points." J.C. Maxwell[1].

2.1 Introduction

In modern times, the terms "magnetic solenoid" and "helical coil" of wire are (almost) synonymous. However, in the time of Maxwell the solenoid was a uniformly magnetized iron bar or ring. The cause of magnetization was a current carrying coil, or the pole of another magnet. In the case of the ring, no combination of N-S bar magnets can induce a circuital magnetization in the ring. Only a current carrying coil wound around an azimuthal segment of the ring can produce a circuital magnetization. Such an arrangement is shown in Fig. 2.1. Often the winding has many turns and completely encloses the ring; and often no distinction is made between the solenoid (the core) and the coil. And we may have the situation that there is no iron core, and only the annular winding.

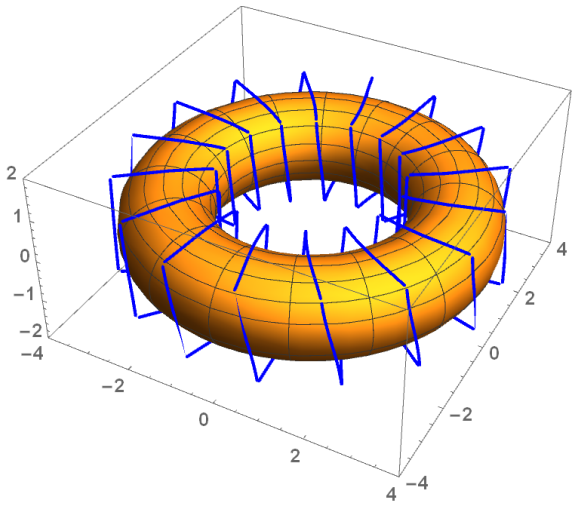

Figure 2.1: Circular iron-core solenoid with helical coil winding. The 16-turn winding, with rectangular cross-section, is show blue. The annular core is shown orange.

In many physics text books[1] on electro-magnetism it is stated that the magnetic field inside a toroidal solenoid is purely azimuthal, has no dependence on azimuth, and is given by $H_\phi = n\,I/(2\pi r)$ where n is the number of turns of the winding, I is the current in the winding, and r is the radial

[1]For example, Refs.[4, 6, 9].

(perpendicular) distance from the axis of revolution z. This statement is based on Ampère's circuital law $\oint \mathbf{H} \cdot d\mathbf{l} = I$ and a circular (azimuthal) path with centre at the rotational symmetry axis, such that the integral is $\int_0^{2\pi} H_\phi(r) r d\phi = 2\pi r H_\phi = I$. The assertions are correct for the magnetic solenoid as conceived of by Maxwell. (For Maxwell, the solenoid core and the winding are completely distinct objects.) However, what about the toroidal coil alone? Does its magnetic field have the same properties? The text books make no statement on this; and many students believe the field of the coil is essentially the same as that of the solid ring. In fact, this is not the case; the azimuthal field is not uniform. Nevertheless, Ampère's circuit law is satisfied – because the integral $\int_0^{2\pi} H_\phi(r, \phi) r d\phi$ can have precisely the same value I. This article is about the field properties of the toroidal coil.

2.2 Field Within Cylindrical Can

A toroid is a surface of revolution with a hole in the middle. The axis of revolution passes through the hole and so does not intersect the surface. The cross-section perpendicular to the azimuth may be circular or rectangular, or otherwise. Usually cylindrical polar coordinates $[r, \phi, z]$ being r radius, ϕ azimuthal angle, and z axial distance, are employed.

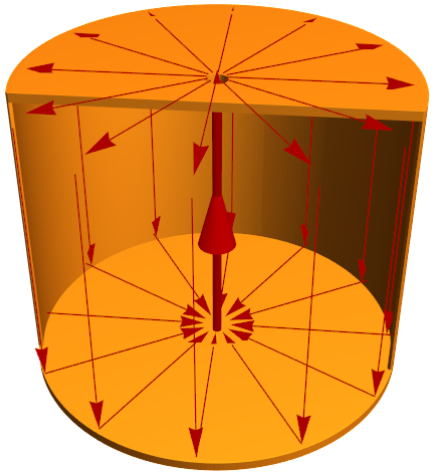

Figure 2.2: Cylindrical conducting shell (or can) with conduction currents (indicated by red arrows) flowing in the shell.

Going forward, we consider an air-core type circular solenoid with rectangular cross section. The usual derivation[2] begins by considering a cylindrical conducting[3] shell (or can) with the axis of rotational symmetry z vertical. The geometry is shown in Fig. 2.2. There is an axial upward current I_z along the centre line; this current spreads out into radial current sheets on the upper disc, flows (down) as cylindrical current sheets on the side walls, and returns as a converging radial current sheet on the lower disc. The divergence, curl and gradient operators can be written in any orthogonal coordinate system. The perfect rotational symmetry suggests they all be written in cylindrical coordinates. Let $\mathbf{u}_r$, $\mathbf{u}_\phi$ and $\mathbf{u}_z$ be radial, azimuthal and axial unit vectors. Everywhere within the can, $\nabla \cdot \mathbf{H} = 0$ and $\nabla \times \mathbf{H} = \mathbf{0}$ – except on the vertical axis z where $\nabla \times \mathbf{H} = \mathbf{J} = J_z(r)\mathbf{u}_z$. The curl is also non-zero at the radial-directed current sheets on the top and bottom discs, and the axial-directed current sheet on the cylindrical side walls. Application of symmetry and Ampere's circuital law tells us that there is no magnetic field outside the can. Therefore, the field is discontinuous on the walls of the can. Let the radius of the can be R and the height be $2L$.

[2]For example, Zangwill[13] Chap. 10.3.

[3]The material is unimportant. The shell is a structure to enable/support the current sheets.

The curl equations imply:

$$-\frac{\partial H_\phi}{\partial z} = J_r(r,z)\,, \qquad \frac{\partial H_r}{\partial z} - \frac{\partial H_z}{\partial r} = 0\,, \qquad \frac{1}{r}\frac{\partial}{\partial r}(rH_\phi) = J_z(r,z)\,. \tag{2.1}$$

Let $\delta(x)$ be the Dirac delta function. The localized current distributions are

$$\mp J_r(r)\delta(z \pm L) \quad \text{and} \quad J_z(r,z) = I_z\delta(r) \;-\; I_z/(2\pi R)\delta(r-R)\,. \tag{2.2}$$

Let $H_\phi \equiv I/(2\pi r)$ The solution of these equations has two parts: (1) $\mathbf{H} = \mathbf{u}_\phi H_\phi$ inside; and (2) $\mathbf{H} = \mathbf{0}$ outside the can. Given that H_ϕ appears to be independent of z and rH_ϕ indepednent of r, it is not obvious that $\mathbf{H}$ satisfies the components of the curl Eq. 2.1. Note, the field is discontinuous at $r = R$ and $z = \pm L$. The Heaviside or unit step function is $\Theta(x)$ such that $\Theta(x > 0) = 1$ and $\Theta(x < 1) = 0$. The derivative of Θ is the Dirac delta function $\delta(x)$ such that $\delta(0) \to \infty$ and $\delta(|x| > 0) = 0$ and $\int \delta(x)dx = 1$. So we write the field more carefully as $H_\phi(r,z) = I/(2\pi r)\Theta[R-r]\Theta[L-z]\Theta[L+z]$. Forming the derivative at the locations where H_ϕ is discontinuous results in the form Eq. 2.1.

Another way to understand that $\mathbf{u}_\phi H_\phi$ really is the solution, is to think of integrating the field across the discontinuity. The change in H_ϕ must be equal to a surface current. This also happens to be the boundary condition normal to the surface:

$$\mathbf{H}_{\text{out}} - \mathbf{H}_{\text{in}} = \mathbf{J} \times \hat{\mathbf{n}} \quad \text{where } \hat{\mathbf{n}} \text{ is the ouward normal.} \tag{2.3}$$

The current density on the upper and lower discs is $\mathbf{J}_\pm = \pm\mathbf{u}_r H_\phi$, and that on the cylindrical wall is $\mathbf{J}_c = -\mathbf{u}_z I/(2\pi R)$. The matching conditions on the end discs and side wall are the identities:

$$\mathbf{0} - H_\phi\mathbf{u}_\phi = \mathbf{J}_\pm \times (\pm\mathbf{u}_z) \quad \text{and} \quad \mathbf{0} - H_\phi\mathbf{u}_\phi = \mathbf{J}_c \times \mathbf{u}_r\,, \quad \text{respectively.} \tag{2.4}$$

The field $\mathbf{H}_\phi$ is the gradient (in cylindrical coordinates) of the scalar potential $H_\phi\phi$. For a cylinder field that is uniform in the axial direction between planes at $z = \pm L$, there must be an axial variation at those planes. But the scalar potential functions do not contain an explicit z-dependence – unless we choose to write them with unit step functions $\Theta[L-z]\Theta[L+z]$. Nevertheless, implictly, the unit steps are always there.

2.2.1 Confined radial currents

The next step is to propose replacing the can by a series of rectangular current loops. Each loop consists of two axial segments (of length $2L$) placed at $r = \rho$ and $r = R$, and two radial segments (of length $R - \rho$) placed at $z = \pm L$. Here $0 < \rho < R$. The n loops are arranged uniformly in azimuth, with an angle $\Delta\phi = 2\pi/n$ between them. It is then suggested (in a typical text book) that the arrangement of current loops continues to have cylindrical symmetry, and that the magnetic field is purely azimuthal with value $H_\phi = nI_z/(2\pi r)$. Some text books concede that this occurs in the limit of a large number of current loops.

However, the geometry of the current loops has only radial symmetry. The rotational invariance is broken, as may be seen from the expressions for the current densities:

$$\mp J_r(r)\delta(z\pm L)\delta[\phi - 2\pi(m/n)]\,, \qquad J_z(r,z) = \delta[\phi - 2\pi(m/n)]\times[I_z\delta(r-\rho) - I_z/(2\pi R)\delta(r-R)]\,. \tag{2.5}$$

Here the integer m runs form 0 to $n-1$. The solution for the magnetic field must respect the n-fold symmetry of the field sources (the currents).

2.3 Field With n-Fold Symmetry

We continue with the circular solenoid and suppose the solenoid winding is composed of n discrete rectangular current loops. Suppose the axial height is very much greater than the radial width of the loops. To simplify matters, we consider field sources to be line charges and line currents: charge Q on long straight insulating filament, and current I in a straight conductive wire of infinite length. In such a case, the radial currents are moved to infinity and have no effect; and electro-magnetism becomes two-dimensional (2D); with spatial variation confined to the plane perpendicular to the lines sources. (The three-dimensional case will be returned to later.) In 2D, the electric (E) and magnetic (H) force laws become $E \propto Q/r$ and $H \propto I/r$ respectively.

We adopt cylindrical coordinates r, θ, z. The magnetic scalar potential is multi-valued: $V = -H_0\theta$ where $H_0 = I/(2\pi)$. V satisfies Laplace's equation. The magnetic field vector is $\mathbf{H} = -\text{Grad}\, V = [H_r, H_\theta, H_z] = [0, H_0/r, 0]$. The same field in Cartesian coordinates x, y, z is $[H_x, H_y, H_z] = [-H_0 y/r^2, H_0 x/r^2, 0]$ where $x^2 + y^2 = r^2$. The axial component H_z will always be zero. Going forward we shall omit H_z, and write $\mathbf{H}$ as a 2D vector. Suppose we move the origin to $(x = a\cos\phi, y = -a\sin\phi)$. The components in the cylindrical system become:

$$[H_r, H_\theta] \;=\; \left[-\frac{aH_0\sin(\theta-\phi)}{a^2+r^2-2ar\cos(\theta-\phi)},\; \frac{H_0[r-a\cos(\theta-\phi)}{a^2+r^2-2ar\cos(\theta-\phi)}\right] . \tag{2.6}$$

If the Cartesian radius vector is oriented locally parallel to the cylindrical radius vector, then $\phi = \theta$ and $[H_r, H_\theta] = [0, H_0/(r-a)]$.

We now consider the case that there are n line currents all set at radius a with respect to the cylindrical origin, and equally spaced in azimuth at angles $\phi_m = m \times (2\pi/n)$ with integer $m = 0, 1, 2, \ldots, n-1$. The sum of the contributions is given by

$$\mathbf{H}(r,\theta,\rho) \;= [H_r, H_\theta] \;=\; \left[\frac{-n\sin n\theta}{r[\rho^{-n}+\rho^n-2\cos n\theta]},\; \frac{n(\rho^n-\cos n\theta)}{r[\rho^{-n}+\rho^n-2\cos n\theta]}\right] H_0 \quad \text{with} \;\; \rho = \frac{r}{a} . \tag{2.7}$$

In the case $r > a$ and $\rho^n \gg 1$, the limiting form is:

$$[H_r, H_\theta] \;=\; \left[-\frac{n\sin n\theta}{r\rho^n},\; \frac{n}{r} \;-\frac{n\cos n\theta}{r\rho^n}\right] \;\to\; \left[0,\; \frac{n}{r}\right] . \tag{2.8}$$

In the case $r < a$ and $\rho^n \ll 1$, the limiting form is:

$$[H_r, H_\theta] \;=\; -\frac{n\rho^n}{r}[\sin n\theta,\, \cos n\theta] \;\to\; [0,\, 0] . \tag{2.9}$$

To complete the picture we must include the effect of distant field sources; and for the annular solenoid they are essential to the description. There are n return line currents at radius $r = b > a$ also equally spaced in azimuthal angle. The return currents are oppositely directed to those at radius $r = a$. These currents contribute a field of the form Eq. 2.7, but with $\rho = r/b$ and a negative sign applied. The total field is $\mathbf{H}(r,\theta,r/a) - \mathbf{H}(r,\theta,b/r)$, the sum of the contributions from the opposite (and equal) line currents arranged at $r = a$ and $r = b$. In the region $r > b$ the contributions almost cancel. In the region $0 < r < a$, both contributions are individually very small, and they add together. In the annular region $a < r < b$, the field is dominated by the contribution from the lines sources at $r = a$; but, nevertheless, there is a portion due to the sources arranged at $r = b$.

Figure 2.3 shows magnetic field in the (x, y)-plane. The coloured contours correspond to the field strength modulus, and the field lines (shown red or blue) indicate the direction of the field. Where the arrow heads are reversed, the field strength is actually negative. The left figure represents the field from eight line currents alone (all set at radius $a = 1$). The right figure shows the superposition of fields from 8 positive and 8 negative line currents set at radius $r = a = 1$ and $r = b = 3$ respectively. The field cancellations at $r > b$ and $r < a$ are quite obvious. As the number

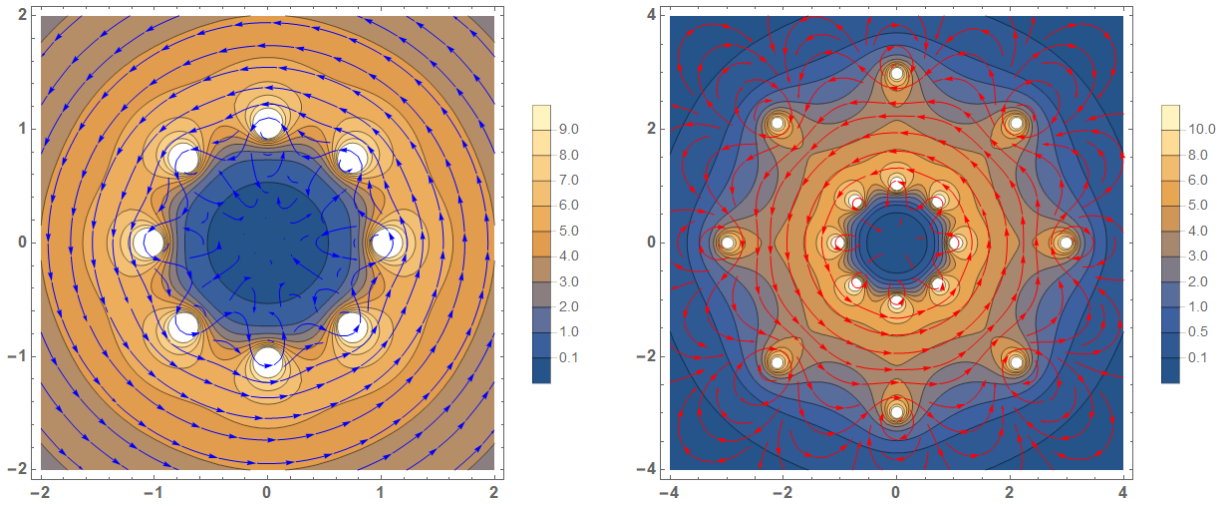

Figure 2.3: Magnetic field. Left: field due to 8 line currents at $r = 1$. Right: field of circular air-core solenoid due to 8 positive line currents at $r = 1$ and 8 negative currents at $r = 3$.

of line currents is increased, the cancellations become more complete; and in the limit of $n \to \infty$ there is no field beyond $r = b$ and no field within $r = a$.

In a practical situation, the magnetic field is more uniform than this analysis suggests. First, it is typically the case that instead of separate current loops, there is the helical winding of a single conducting filament; this yields a slight improvement in uniformity. Second, and far more effective, a ferro-magnetic annular core is placed inside the current winding. The material becomes magnetized and concentrates the field lines parallel to its own azimuthal axis. And, of course, the winding has a large number of turns n. The geometry of an iron-core solenoid with helical winding solenoid is sketched in Fig. 2.1. We note that Mirin[15] *et al* have found an analytic expression for the interior magnetic field due to a helical winding on an air-core torus.

2.4 Ampère's Circuit Law

Let the vector element of length be $d\mathbf{l}$. Ampère's circuital law concerns the vector path integral: $\oint \mathbf{H} \cdot d\mathbf{l} = I$. Applied to the circular path (centred at $r = 0$) in the region $a < r < b$, the integral is expected to yield $\oint H_\theta r d\theta = nI$. How is this to be reconciled with the field appearing in Eq. (2.7) ? The path integral looks formidable, particularly so because H_θ has contributions from both $\mathbf{H}(r, \theta, \rho = r/a)$ and $\mathbf{H}(r, \theta, \rho = r/b)$. But, consider the sources at $r = a$ and $r = b$ one at a time. If we think of x and y as being directions in the complex plane, then the field due to sources at $r = a$ is the sum $H_0 \sum_m^{n-1} 1/[r - a \exp i(\theta - \phi_m)]$. Thus we may use the methods of complex analysis[37]. Cauchy's residue theorem tells us that if the integration path $r > a$ encircles all the singularities, then the integral is the sum of residues equal to $2\pi n$; and if the path is taken at $r < a$ the integral is exactly zero. Likewise, the contribution from current sources at $r = b$ to a path integral at $r < b$ is identically zero. Now $H_0 = I/(2\pi)$, and so the contour integral performed at $a < r < b$ is precisely $n \times I$. If the circular path is taken at $r > b$, the residues from the positive and negative line currents cancel exactly; and the integral is zero.

In fact, complex analysis tells us something even more surprising and wonderful. The integration path does not have to be circular, it can be any path we choose in the (x, y)-plane – and the result will be the same. The value of the integral depends only on whether it includes singularities (called *poles*) of the form $1/(r - r_0)$.

2.4.1 Fields from short straight wires

Now we return to the case of a three dimensional geometry: the rectangular current loops each have height $2L$ and width $b-a$. The magnetic field due to a finite length wire is smaller than that from an infinite straight wire. As before, we take a cylindrical coordinate system with the z axis coincident with the wire. We consider a source element Idz located at z in the wire; and an observation point (r,θ,ζ). The vector from source to point is $\mathbf{r}=[r,0,z-\zeta]$ and the parallel unit vector is $\hat{\mathbf{r}}=\mathbf{r}/(\mathbf{r}\cdot\mathbf{r})$. The Biot-Savarat law gives the field contribution from the source to the observation point:

$$d\mathbf{H}=\frac{I}{4\pi}\frac{dz\,\mathbf{u}_z\times\hat{\mathbf{r}}}{\mathbf{r}\cdot\mathbf{r}}=\frac{I}{4\pi}\left[0,\ \frac{dz\,r}{[r^2+(z-\zeta)^2]^{3/2}}\,,\ 0\right]\ . \tag{2.10}$$

This element is integrated over z from $-L$ to $+L$. The result is

$$H_\theta(r,z{=}\zeta)\ =\ \frac{I}{4\pi r}\left[\frac{L+\zeta}{\sqrt{r^2+(L+\zeta)^2}}\ +\ \frac{L-\zeta}{\sqrt{r^2+(L-\zeta)^2}}\right]\ . \tag{2.11}$$

The field at middle and ends of the wire is:

$$H_\theta(r,z{=}0)\ =\frac{I}{2\pi r}\frac{L}{\sqrt{L^2+r^2}}\,,\qquad H_\theta(r,z{=}\pm L)\ =\frac{I}{2\pi r}\frac{L}{\sqrt{4L^2+r^2}}\ . \tag{2.12}$$

In the case $L\gg r$, these become $H_\theta(z=0)=I/(2\pi r)$ and $H_\theta(z=\pm L)=I/(4\pi r)$. How are these fields to be reconciled with Ampere's circuit law? Once again, we must apply to the fields from distant sources. Each current loop has radial-directed segments at heights $z=\pm L$ above the mid-plane; and both these (additively) contribute field to the observation point. When these fields are included, the circular path integral at radius r is exactly equal I independent of axial position ζ.

The rectangular loop is an example of a more general understanding of the relation between the Biot-Savarat law and the Ampère law. Consider a current loop of any shape, and the contour integral formed on a plane perpendicular to the wire's local direction. Provided the contour encircles the wire, the integral of $\mathbf{H}$ is always the current I. The contour can be taken *anywhere* (around the current filament) because the field is contributed from current elements *everywhere* (along the current filament). The filament must, of course, close on itself to form a loop. The infinite straight current-carrying wire is a special case. The field integral around the wire at *any* axial location is I because we have summed contributions to the field from *everywhere* along its (infinite) length.

2.5 Cylindrical Harmonics

Text books often contain artificial examples. The annular shell with a harmonic (sine or cosine) current density in its surface is artificial, but serves the purpose of demonstrating that (in general) two types of scalar potential function are needed: (1) the multi-valued[4] type around a line current, and (2) the usual, single-valued (conservative) potential functions. Consider the annulus with rectangular cross section, and height $2L$ as before. There are cylindrical inner and outer side walls at radius $r=a$ and $r=b$ respectively; where $a<b$. These walls carry current densities $J_a=+I[1+\cos n\theta]/(2\pi a)\delta(r-a)$ and $J_b=-I[1+\cos n\theta]/(2\pi b)\delta(r-b)$ with integer $n=1,2,3,\ldots$. These axial currents are uniform within $z=\pm L$ and zero outside. There are annular discs at top and bottom which carry radially directed current density also with the azimuthal dependence $[1+\cos n\theta]$ and radial dependence $1/r$.

To account for that part of the axial currents which do not vary with azimuth, we need the multi-valued potential θ. To account for the azimuthal variation of fields and sources, we use

[4]Maxwell Article 606 is vehement that the magnetic scalar potential for a line current is multi-valued, accruing a fixed increment (2π) for each turn about the current.

cylindrical harmonics: solutions of the Laplace equation in cylinder coordinates. Within the can, fields are axially uniform; so we set the partial derivative $(\partial^2 V/\partial z^2) \to 0$. Thus the harmonics are $V(r,\theta) = F_n(r)[c_3 \cos n\theta + c_4 \sin n\theta]$ where $F_n(r) = c_1 r^n + c_2 r^{-n}$, and the constants c_1, c_2, c_3, c_4 are chosen to fit geometry-dependent boundary conditions. In regions where $r \to 0$, $c_2 = 0$; and where $r \to \infty$, constant $c_1 = 0$. Both potentials, θ and $V(r,\theta)$ satisfy Laplace's equation, and generate vector fields with zero curl and divergence.

To match the two concentric current densities, we take the following combination of functions:

$$\begin{aligned} V_a &= r^n\,[A_a + A_b]\sin n\theta & 0 \le r < a & \quad (2.13)\\ V_\rho &= [r^{-n}C_a + r^n A_b]\sin n\theta - B_a\theta & a \le r < b & \quad (2.14)\\ V_b &= r^{-n}C_b \sin n\theta + B_b\theta - B_a\theta & r \ge b & \quad (2.15) \end{aligned}$$

where the constants $A_{a,b}, B_{a,b}, C_{a,b}$ will be determined. We form the gradient to find the corresponding fields $\mathbf{H}_a, \mathbf{H}_\rho, \mathbf{H}_b$. The next step is to consider boundary conditions at the inner and outer cylinders. The radial component is continuous, so

$$\mathbf{u}_r \cdot [\mathbf{H}_\rho(r{=}a) - \mathbf{H}_a(r{=}a)] = 0 \quad \text{and} \quad \mathbf{u}_r \cdot [\mathbf{H}_b(r{=}b) - \mathbf{H}_\rho(r{=}b)] = 0\,. \tag{2.16}$$

The azimuthal component is discontinuous, with a jump equal to the current density on the cylindrical wall; thus:

$$\mathbf{u}_\theta \cdot [\mathbf{H}_\rho(r{=}a) - \mathbf{H}_a(r{=}a)] = J_a \quad \text{and} \quad \mathbf{u}_\theta \cdot [\mathbf{H}_b(r{=}b) - \mathbf{H}_\rho(r{=}b)] = J_b\,. \tag{2.17}$$

Because there are constant terms and sinusoidal terms present in Eqs. 2.16 and 2.17, these constitute six linear equations for the unknowns. The solutions are: $B_a = B_b = I/(2\pi)$, as may have been guessed, and

$$A_a = a^{-n}I/D\,, \quad A_b = -b^{-n}I/D\,, \quad C_a = -a^n I/D\,, \quad C_b = (b^n - a^n)I/D\,, \quad D \equiv 4n\pi\,. \tag{2.18}$$

These values are substituted in $V_{a,\rho,b}$ and $\mathbf{H}_{a,\rho,b}$. For example,

$$V_a = \chi\frac{(b^n - a^n)}{b^n}(r/a)^n\,, \;\; -V_\rho = \frac{I\theta}{2\pi} + \chi[(a/r)^n + (r/b)^n]\,, \;\; V_b = \chi\frac{(b^n - a^n)}{r^n}\,, \;\; \chi \equiv \frac{I\sin n\theta}{4n\pi}\,. \tag{2.19}$$

The field is dominant in the region $a < r < b$; but a small residual (or fringe) extends into the regions $r < a$ and $r > b$. The moduli of the fringe fields are:

$$|\mathbf{H}_a(r)| = [1 - (a/b)^n](r/a)^n\frac{I}{4\pi r} \quad \text{and} \quad |\mathbf{H}_b(r)| = \frac{(b^n - a^n)}{r^n}\frac{I}{4\pi r}\,. \tag{2.20}$$

Due to the power law dependence $(r/a)^n$ for $r < a$ and $(b/r)^n$ for $r > b$, the fringe fields diminish extremely quickly as the harmonic number n is increased. Figs. 2.4,2.5 show an example for $n = 6$ and $a = 1$, $b = 3$.

The fringe fields also extend above and below the planes $z = \pm L$. In these regions, there are no axial currents; and so the magnetic potential is a purely conservative function. However, finding this function and matching the coefficients across the boundaries $z = \pm L$ is extremely difficult. In the case of infinite line currents, Sec. 2.3, this difficulty was avoided by moving the boundary to infinity.

2.6 Vector Potential

The magnetic field in Sec. 2.3 was derived from a scalar potential V that satisfies Laplace's equation. The same field $H_\phi = I/(2\pi r)$ appeared in Sec. 2.2, where we found the treatment of surface currents is not straight forward. Some readers may be aware of the magnetic vector potential, and wonder if

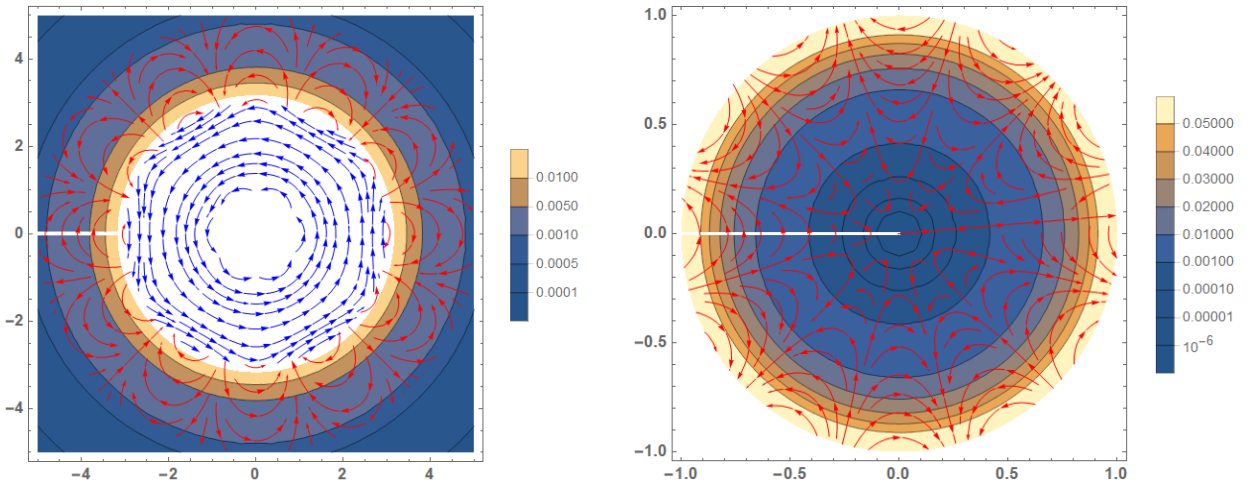

Figure 2.4: Magnetic field lines and modulus. Left: region $r > a$; and in region $r < b$ field lines only. Right: region $r < a$.

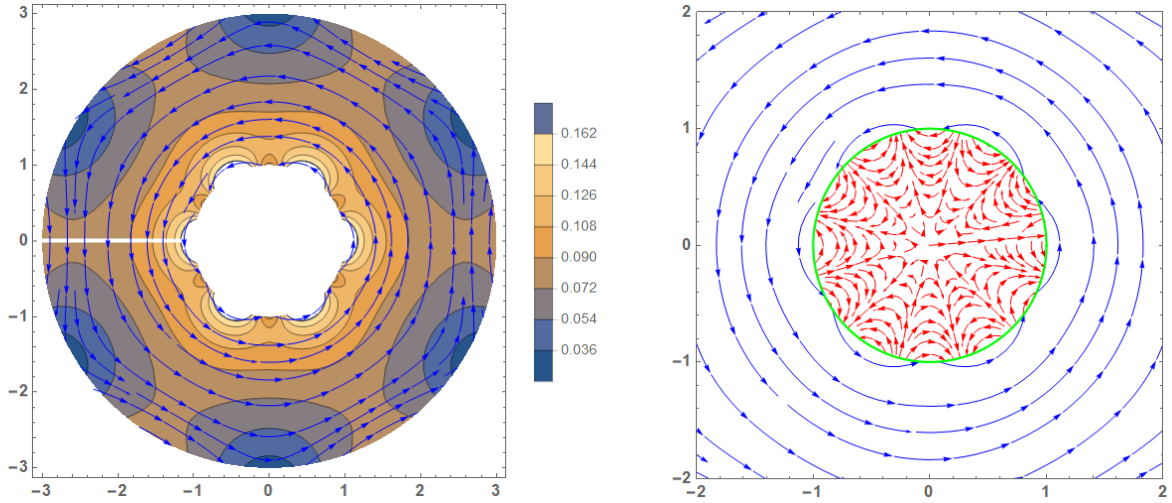

Figure 2.5: Magnetic field line and modulus for six-sector current can. Left: region $a < r < b$. Right: region $0 \le r < (2/3)b$ field lines only.

it simplifies the effect of surface current; it does not. The vector potential is used in regions where there are *volume* currents, that is a finite volume sufficiently large that the observation point may lie inside the volume. These currents may be due to flow of charge or displacement currents resulting from time-varying electric fields. We compare the scalar and vector potential for the cylindrical magnetic field. We define the vector potential $\mathbf{A}$ by

$$\nabla \cdot \mathbf{H} = 0\,, \quad \nabla \times \mathbf{H} = \mathbf{J}\,, \quad \mathbf{H} = \nabla \times \mathbf{A}\,, \quad \nabla \cdot \mathbf{A} = 0\,. \tag{2.21}$$

The last condition is called the Coulomb (or transverse) gauge; this constraint is not essential. We begin with some simple single-component potentials.

$$\mathbf{A} = \mathbf{u}_r A_r(z)/r \;\text{ leads to }\; \mathbf{H} = \mathbf{u}_\theta(\partial A_r/\partial z)/r \;\text{ and }\; \mathrm{Curl}\,\mathbf{H} = -\mathbf{u}_r(\partial^2 A_r/\partial z^2)/r\,.$$

$$\mathbf{A} = \mathbf{u}_z, A_z(r,\theta) \;\text{ leads to }\; \mathbf{H} = [(\partial A_z/\partial\theta)/r, -(\partial A_z/\partial r), 0]$$

and $\mathrm{Curl}\mathbf{H} = -\mathbf{u}_z[\partial^2 A_z/\partial\theta^2/r^2 + (\partial A_z/\partial r)/r + \partial^2 A_z/\partial r^2]$. The two examples suggest that if we want radial and axial current densities, we should consider a two component potential $\mathbf{A} =$

$\mathbf{u}_r A_r + \mathbf{u}_z A_z$. If we insist that axial field $H_z = 0$, azimuthal current $J_\theta = 0$, and H_θ is single-valued and independent of z, then the choice of potential is narrowed to $\mathbf{u}_r A_r(r) + \mathbf{u}_z A_z(r)$. Thus $\nabla \cdot \mathbf{A} = A_r(r)/r + (\partial A_r/\partial r) = 0$ and $\mathbf{H} = \mathrm{Curl}\,\mathbf{A} = \mathbf{u}_\theta(\partial A_z/\partial r)$. There are two scenarios. First, if field varies with radius $H_\theta = G/r$ the components are $A_r = c_1/r$ and $A_z = c_2 - G\ln(r)$; yielding $\mathbf{H} = \mathbf{u}_\theta G/r$ and $\mathrm{Curl}\,\mathbf{H} = \mathbf{0}$. This is the same field, as was given by the scalar potential; and the arbitrary constants of integration c_1, c_2 may be set to zero. Secondly, if H_θ is independent of radius, then $A_r = c_1/r$ and $A_z = -H_\theta r + c_2$; yielding $\mathbf{H} = \mathbf{u}_\theta H_\theta$ and $\mathrm{Curl}\,\mathbf{H} = \mathbf{u}_z H_\theta/r$. This solution maybe used inside a hollow cylinder of volume current density.

2.7 Complex Analysis

Complex analysis is perfectly suited to the description of electro-magnetic fields in two dimensions. Following Morse & Feshbach[37] Chap. 4.1, let us state the main results. Let $i \equiv \sqrt{-1}$. Let x, y be Cartesian coordinates, and define the complex variable $z = x + iy$ and its conjugate $z^* = x - iy$. Rotation by an angle θ in the $x - y$ plane is performed by the operator $\exp(i\theta)$. Let there be a complex function with components along the real and imaginary directions: $f = u + iv$ and $g = s + it$. The sums and product of functions f^*g obey the usual axioms for real numbers. In vector language, there is the analogue $\mathbf{f} = [u, v]$ and $\mathbf{g} = [s, t]$. Comparing products we find:

$$f^*g \;=\; (us + vt) + i(ut - vs) \;=\; \mathbf{f}\cdot\mathbf{g} \;+ i\,\mathbf{f}\times\mathbf{g}\,. \tag{2.22}$$

Thus f^*g contains both the scalar and vector product of $\mathbf{f}$ and $\mathbf{g}$. We introduce the complex gradient ∇, whose operation immediately gives both the divergence and curl of a complex function (or its equivalent vector form):

$$\nabla \;\equiv\; \frac{\partial}{\partial x} + \,i\,\frac{\partial}{\partial y} \;\equiv 2\frac{\partial}{\partial z}\,, \quad \text{and} \quad \nabla^* g = \mathrm{Div}\,\mathbf{g} \;+\; i\;\mathrm{Curl}\,\mathbf{g}\,, \tag{2.23}$$

where Div and Curl are 2D versions of the vector calculus operators.

Consideration of $\nabla(u + iv)$ yields the Cauchy-Riemann conditions:

$$\partial u/\partial x = +\partial v/\partial y \quad \text{and} \quad \partial u/\partial y = -(\partial v/\partial x)\,. \tag{2.24}$$

Any function which satisfies Eqs. 2.24 is called an *analytic function* of the complex variable $z = x + iy$.

Suppose that some field E is derivable from a potential $V(x, y)$, both being complex, such that $E = \nabla V$. Then we can write $E = 2\partial V/\partial z^*$, and since $\partial E/\partial z = 0$, we have Laplace's equation:

$$4\frac{\partial^2 V}{\partial z \partial z^*} \;=\; \frac{\partial^2 V}{\partial x^2} \;+\; \frac{\partial^2 V}{\partial y^2} \;=\; 0\,. \tag{2.25}$$

Given that the potential may be written $V = \Psi(x, y) + i\Phi(x, y)$, it is clear that Ψ and Φ are each, individually, solutions of the 2D Laplace equation.

The fundamental field due to a unit line source is

$$F \;=\; -2\ln(z) \;= -\ln(x^2 + y^2) \;- 2i\arctan(y/x) \;= -2\ln(r) \;- 2i\theta \;= -2\ln[r \times e^{i\theta}]\,. \tag{2.26}$$

If this field is due to a unit/length electric line charge, then $\Psi = -\ln(x^2 + y^2) = -\ln(zz^*)$ and $-\partial F^*/\partial z = 2/z^*$ is the electric intensity vector, pointed along the radius vector z and inversely proportional to $|z|$. If the magnetic field is due to a unit/length charge current, then $\Phi = -2\arctan(y/x) \equiv -2\theta$ is the magnetic potential, $\Psi =$ constant gives its lines of force, and $i\partial F^*/\partial z = -i(2/z^*)$ is the magnetic intensity, pointed perpendicular to the radius vector in the clockwise direction for a positive current.

We may integrate a complex function along a path in the complex plane (x, iy). The geometry of the path has to be specified. If the path closes on itself, the result is called a contour integral and denoted by $\oint f(z)dz$. We shall use, but not prove, Cauchy's theorems for contour integrals of complex functions. Suppose that $f(z)$ is analytic everywhere inside and on a closed contour C, then $\oint f(z)dz = 0$. Suppose that (complex) a is a point within C, then $f(z)/(z-a)$ is singular at $z = a$. Cauchy's integral formula states:

$$\oint \frac{f(z)}{(z-a)}dz \;=\; 2\pi\, i\, f(a) \times \begin{cases} 1\,; & \text{if } a \text{ within } C \\ \frac{1}{2}\,; & \text{if } a \text{ on } C \text{ (principal value)} \\ 0\,; & \text{if } a \text{ outside } C. \end{cases} \tag{2.27}$$

Cauchy's integral theorem is a statement, in the notation of analytic functions, of Gauss' theorem for electrostatics or Ampère's theorem for magnetostatics.

2.7.1 Two-dimensional electric fields

In the absence of charges, Maxwell's equations for electric field $\mathbf{E}$ state that $\mathrm{Div}\,\mathbf{E} = 0$ and $\mathrm{Curl}\,\mathbf{E} = \mathbf{0}$. These statements are equivalent to $(\partial E/\partial z) = 0$; which implies $E = E(z^*) = u - iv$. Contrarily, $E^* = E^*(z) = u + iv$.

Concerning the path integrals. If the region is devoid of charge, then $\oint E^* dz = 0$. If the region inside the contour includes a line charge, Q per unit length, perpendicular to the (x, y)-plane, then $\oint E^* dz = 4\pi Q$. In general, there is a field $E_0^*(z)$ due to sources outside the contour, and a field $E_1^* = 2Q/(z - z_1)$ due to the line-charge inside the contour. The total field is $E_0^* + E_1^*$.

2.8 Conclusion

The superficially simple case of the toroidal coil serves very well to exemplify the magneto-static physics of current carrying wires. In particular, the implications of vector fields that have everywhere zero curl and divergence *except* at field sources where locally the field posses rotation. To be clear, there is rotation about the current-density vector and yet (nevertheless) the field has zero curl at all points in space except those within the current. The current loops also cause us to recognize that distant currents are important and crucial to the sanctity of Amperè's magnetic circuit law. Moreover, the physics of current loops and magnetic field demonstrate to us that the Ampère law and the Biot-Savarat law are inextricably linked.

Chapter 3

Ferro- and Ferri-Magnetism

3.1 Introduction

Ferro-magnets have a subatomic crystal lattice with a single type of (nett) electron spin site. Ferri-magnets have two or more types of spin site. With the obvious exception that ferro-magnets are conductors, while ferri-magnets are insulators, the ferro- and ferri- magnetic materials have many properties in common and which share a common explanation. The (simpler) theory of ferro-magnetism, was developed (in the 1930's) before that of ferri-magnetism. There are many modern text books[54, 55] on magnetic properties and detailed calculation thereof. But for an introductory account of the underlying principles, it suffices to adapt material from a historic collection of papers[38, 39, 40, 41] that marks the moment that "ferrites arrived" in communication electronics. The story of magnetism is essentially that of four kinds of energy: (I) the Zeeman, (II) the magnetic dipole, (III) the exchange, and (IV) the anisotropy energy. By far the most important of these is the exchange energy, which is the underlying cause of magnetism; and so we begin with that.

3.2 Exchange Interaction

The exchange interaction[1] (EI) is one of the most singular and surprising predictions of quantum mechanics (QM). The EI is a purely quantum property with no classical analogue. The EI is subtle and fundamental. The manifestations of EI are confirmation that the physical world is "quantum".

The EI and exchange energy is a consequence and manifestation of four of the postulates of quantum mechanics: (i) that there is a wave function; (ii) that it obeys the mathematical operation of linear superposition; (iii) that what we call "observables" are expectation values; and (iv) the phase of the wave function is not a physical observable (i.e. only the modulus leads to an expectation value). The EI is an embodiment of QM and testament that the tenets of QM are not merely "just postulates" but an underlying component of physical reality. Superposition is an axiom of quantum mechanics, and it applies to the joint state of two quantum objects.

The wave function of indistinguishable particles[44] is subject to exchange symmetry. Let $\psi(1,2)$ be the wave function of two indistinguishable particles, indexed 1 and 2. Because the particles are identical, an equally valid wave function is $\psi(2,1)$. We introduce the exchange operator P which acting on a state interchanges all coordinates (space and spin) of particles 1 and 2. (The operation is also called permutation, which is why we use the symbol P.) Hence $P\,\psi(1,2) = \psi(2,1)$ and $P^2\,\psi(1,2) = \psi(1,2)$. Thus the operator has eigenvalues ± 1. The corresponding eigenstates are the superpositions $\psi^+\sqrt{2} = \psi(1,2) + \psi(2,1)$ and $\psi^-\sqrt{2} = \psi(1,2) - \psi(2,1)$. Now $P\,\psi^+ = \psi+$ is symmetric and $P\,\psi^- = -\psi^-$ is anti-symmetric with respect to the interchange operator. The operator P commutes with the Hamiltonian, and so the permutation symmetry P is a constant of motion. Note, this symmetry is an intrinsic property of the particles, not of the system preparation.

[1] Postulated (i.e. discovered mathematically) independently by Heisenberg and Dirac in 1926.

To summarise, the joint wave function either (i) changes sign or (ii) remains unchanged when two identical particles are exchanged. We call property-(i) objects fermions; and we call property-(ii) objects bosons.

In a simple one-dimensional system with two identical particles in two states ψ_a and ψ_b, the joint wave functions are

$$\sqrt{2}\,\psi^{\pm} = \psi_a(x_1)\psi_b(x_2) \pm \psi_a(x_2)\psi_b(x_1)\ . \tag{3.1}$$

$\psi^{\pm}(1,2)$ is the joint probability amplitude for finding a particle at location x_1 and another at position x_2. The probability density is $\psi \times \psi^*$ where * denotes complex conjugate. Exchange symmetry alters the expectation value of the distance between two indistinguishable particles when their wave functions overlap:

$$\langle (x_1 - x_2)^2 \rangle_{\pm} \ = \ \langle x^2 \rangle_a + \langle x^2 \rangle_b - 2\langle x \rangle_a \langle x \rangle_b \ \mp |\langle x \rangle_{ab}|^2\ .$$

For fermions the expectation value of the distance increases, and for bosons it decreases (compared to distinguishable particles). Two indistinguishable fermions cannot be in the same state, because the only mathematical quantity that is unchanged by sign/polarity reversal is zero - which is the absence of a quantum object. Bosons and fermions both have an additional quantum property: spin. That bosons have integer spins, and fermions have half integer spins $(2n+1)/2$, does not have a simple explanation.

The symmetric ψ^+ and antisymmetric ψ^- combinations in Eq. 3.1 did not include the spin variables (α = spin-up; β = spin-down); there are also antisymmetric and symmetric combinations of the spin variables: $\sqrt{2}\,\phi^{\pm} = \alpha(1)\beta(2) \pm \alpha(2)\beta(1)$. To obtain the overall wave function, these spin combinations have to be coupled with Eq. 3.1. The resulting overall wave functions, for fermions, are anti-symmetric under interchange of particle index. Hence: When the orbital wave function is symmetrical, the spin function must be anti-symmetrical; and vice versa. For the same reason that electrons in the same position within an atom cannot have the same spin, the electrons of neighbouring atoms in a solid ferromagnetic object must have the same spin. The electron spin carries a magnetic moment. The exchange interaction stabilises the aligned elementary magnets, i.e. the atomic spins, in magnetic materials. This is the only reason why the parallel alignment of the elementary magnets in ferromagnets is so stable.

There are two combinations of the wave functions of two indistinguishable particles: symmetric and anti-symmetric. Nature did not have to furnish examples of both types, but it does: bosons and fermions. And the implication of the EI is that these fundamental objects are truly indistinguishable. Quantum field theory supplies an explanation for this: that they are excitations of an underlying quantum field. Quantum fields are matter. As concerns "identity", one excitation is the same as another. In a quantum field theory, what we perceive as particles are excitations of the quantum field itself. The quantum field is a complicated object. In part this is because it contains all of physics: the field can describe vast numbers of particles, interacting in a myriad of different ways.

3.3 Theory of Ferro-magnetism

The story of ferro- (and ferri-) -magnetism is essentially that of four kinds of energy.
(I) The Zeeman is the magnetic energy of elementary magnets in an applied field $\mathbf{H}$: $-2\beta \sum_i \mathbf{H} \cdot \mathbf{S}_i$ where β is the Bohr magneton and $\mathbf{S}_i$ is the spin angular momentum vector of atom i measured in units of Planck's constant/$2\pi \equiv \hbar$.
(II) The classical magnetic dipolar energy, of mutual interaction between elementary magnets:

$$\sum_{j>i} \frac{g_e^2 \beta^2}{r_{ij}^3} \left[\mathbf{S}_i \cdot \mathbf{S_j} \ - 3 \frac{(\mathbf{r}_{ij} \cdot \mathbf{S}_i)(\mathbf{r}_{ij} \cdot \mathbf{S}_j)}{r_{ij}^2} \right]$$

Here the electron g-factor $g_e \approx 2$. Despite being long range, the coupling is too small by a factor 10^4 to align the spins in a ferromagnetic material. The dipolar energy involves the angles between the spin vectors $\mathbf{S}_i, \mathbf{S}_j$ and a given direction $\mathbf{r}_{ij}$, and so is not spatially invariant.
(III) P.A.M. Dirac wrote the exchange energy in the form $-2\sum_{j>i} J_{ij}(\mathbf{S}_i \cdot \mathbf{S}_j)$ where the factor J_{ij} is the quantum mechanical exchange integral connecting atoms i and j. The Dirac potential simplifies calculation, but hides how uncanny and bizarre is the exchange interaction (EI). This interaction is very short range, a few atoms at most. The exchange energy is responsible for two key conditions: (i) the electron spins in filled atomic orbitals are anti-parallel pairs (resulting in no net spin); and (ii) if there is an incomplete outer shell (such as d or f orbitals) then neighbour atoms have parallel spins, leading to large net spin angular momentum. A purely quantum effect, the EI is responsible for the alignment of spins in a ferromagnetic material. Because the scalar product $\mathbf{S}_i \cdot \mathbf{S}_j$ of two vectors is invariant under a rotation, the EI is isotropic; it cannot explain why most ferromagnetic materials are more easily magnetized along certain directions than others.
(IV) The anisotropic exchange energy is the modification to (III) that arises from spin-orbit coupling. This coupling makes the spin feel the anisotropy of the charge distribution which is not spherically symmetric in high orbital levels or excited states. The anisotropy energy explains preferential magnetization along certain directions in a crystal.

3.3.1 Free Energy of Magnetic Material

The whole problem of magnetism is simply to determine which spin configuration gives the lowest free energy, in the thermodynamic sense, when one includes simultaneously the four energies I, II, III, and IV (or IV'). These energies have roughly the following orders of magnitude: I $\simeq 10^{-4}$, II $\simeq 0.1$, III $\simeq 10^3$, IV $\simeq 10$. The estimate (IV) applies only to non-cubic crystals. With cubic symmetry, the relevant estimate is IV' ranges 0.1 to 1.

The first simplification is to study the energetic and alignment behaviour which results when exchange coupling alone is present, and the action of the other atoms on a given atom i is approximated by an effective field $\mathbf{H}_{\text{eff}}$. (III) is replaced by $\sum -g_e\beta \sum_i \mathbf{S}_i \cdot \mathbf{H}_{\text{eff}}$. Weiss assumed that the effective field was linear in the magnetization M. Quantum mechanics furnishes a real foundation for this assumption of linearity, since (III) implies that the mean exchange potential coupling a spin i to its surroundings is proportional to the expectation value of the spin angular momentum of neighbouring atoms. This model may be used to find the temperature dependence of spontaneous magnetization and the saturation value at T=0 kelvin. The next step is to include anisotropy. The anisotropic exchange mechanisms give the proper directional dependence of the energy of anisotropy dictated by the crystal structure.

3.3.2 Weiss domains

The interactions (III & IV) which we have included so far are able to explain the existence of magnetization and preferential directions, but they are completely inadequate to describe the hysteresis and other phenomena associated with aligning the magnetization parallel to the applied field. Irreversible processes are found even in very weak fields. The difficulty is that with the mechanisms III and IV alone present, (along with the energy I due to the applied field) there is no reason why the average positions of all the elementary magnets should not be parallel throughout the entire crystal. A mechanism is needed which will provide small domains of magnetization, called Weiss[2] domains (discovered in 1906). The requisite mechanism is provided by (II) the classical magnetic interaction between dipoles. This is a long range coupling; and as a result it is energetically unfavourable for dipoles to be aligned perpendicular to the bounding surfaces of the specimen. In consequence, a lower energy is achieved when the direction of magnetization is different in different small regions, called domains. This subject was first properly investigated by Landau and Lifshitz[45] in 1935.

[2]Pierre Ernest Weiss (1865-1940) was a French physicist who developed the domain theory of magnetism.

The domain structure seems to account[46] quite well for the various phenomena of hysteresis, remanence, etc. When an applied field shifts the direction of magnetization, this readjustment can be achieved in either of the two ways: rotation of the magnetization in a domain of given size, or by expansion of the domains. The second of these processes is usually the more important, and of course involves migration of the domain boundaries. The transition region between two domains is named a Bloch wall or domain wall. The wall is not a barrier, rather it is an interface (about 100 atoms wide) shared by two domains. Roughly speaking, domain walls can move at (upto) the speed of sound in the material. It is the growth and/or rotation of domains in response to an external applied magnetic field that is responsible for hysteresis and the $\int\int$-shape of the magnetization curve in the B-H plane. The behaviour is cartooned in Fig. 3.1.

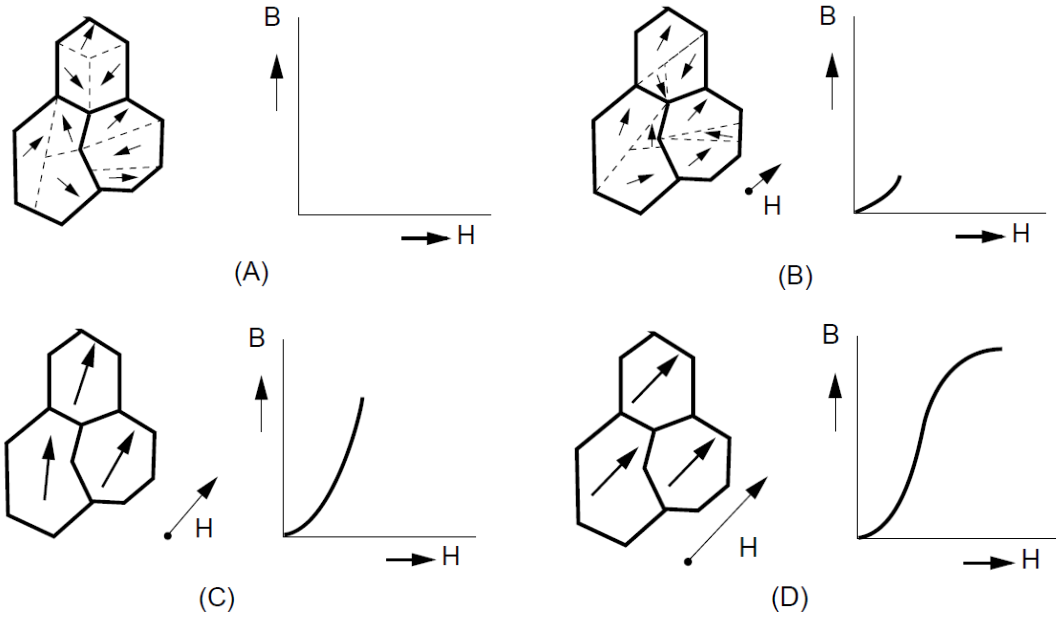

Figure 3.1: Progress of magnetization. Cartoon adapted from Philips Ferroxcube Handbook. Domain walls movement is dominant at lower bias, with domain rotation becoming dominant at higher bias. (A) Unmagnetized state with 9 domains. (B) Some domains grow at the expense of others. (C) Three partially aligned domains. (D) Magnetic domains aligned in saturation.

3.4 Theory of Ferri-magnetism

A positive exchange integral is a necessary condition for ferro-magnetism (in order to minimize free energy). This stipulation, however, is only essential as long as all atoms have the same spin. If two (near-neighbour) atoms of unlike spin are antiparallel, there can be a net resultant magnetic moment. Thus an exchange coupling which favours an antiparallel short-range order can lead to an overall/residual magnetic moment. Neel[47] first proposed this type of mechanism, wherein magnetism can occur even when the exchange integral has the (normal) negative sign. He also suggested the name ferri-magnetism, a felicity as the ferrites are the prototype case. The various general energetic considerations presented for ferro-magnets apply perfectly well to ferrites.

In the case of ferri-magnetism the two (or more) magnetic subsystems are coupled strongly by their mutual exchange interaction. They are not separated in space as in the domain problems but are interspersed as inter-penetrating lattices throughout the ferrite crystal. In a two-component system, the two types of spin site are referred to as A-sites and B-sites. Since the exchange coupling between the two subsystems is so strong, it may be expected that in many respects it will behave as one single (ferro-magnetic) system. This expectation is borne out by experiment and for many

applications the discussion in terms of a single net magnetization is adequate. However, there are effects where the two-component character of A and B sites is manifest; and these are called specifically ferri-magnetic. One such example is discussed in Sec. 3.5.6.

3.5 Magnetic Resonance in Ferrites

Thus far, we have considered the DC or low frequency properties of magnets. But what happens if the material is subject to an electro-magnetic (EM) wave? One particular effect, among many that a ferrite can display, is the ferro magnetic resonance (FMR). Thin, plate-like samples of ferromagnetic material were probed with radio-frequency (RF) waves in the early 1900's. The samples display resonant absorption phenomena, now called FMR. The metallic samples must be thin, otherwise the EM wave does not penetrate into their interior. Contrastingly, ferrites are insulators and EM waves pass freely into and through them. Ferrites also display resonant absorption, and have become the exemplar of FMR.

Magnetization arises from the alignment of individual electron spins with respect to one another (spontaneous magnetization) and with respect to an externally applied DC field. Landau[45] realized that the spins will precess (rotate or gyrate) about the applied field, and wrote a semi-classical equation of motion for the spin magnetic moments. Landau also realized that in the presence of an applied RF field, there will be resonance effects if the field oscillation frequency is equal to the spin gyration frequency. Before we can write Landau's equation, we must introduce the gyromagnetic ratio.

3.5.1 Gyromagnetic ratio

Suppose that we have a uniformly rotating sphere of uniform charge density and uniform mass density. This sphere will have a magnetic moment $\mathbf{M}$, having units of current $\times$ area, and an angular momentum $\mathbf{L}$ having units of mass $\times$ area divided by time. The ratio $\gamma \equiv |\mathbf{M}|/|\mathbf{L}|$ is called the gyromagnetic ratio, and has the units of electrical charge divided by mass. For a classical sphere, $\gamma = q/(2m)$ where q, m are the total charge and mass of the object, respectively.

Consider now the electron which has intrinsic spin. The electron is a diffuse quantum object, not a classical sphere. Nevertheless, the electron does have a gyromagnetic ratio $\gamma_e = g_e[-q_e/(2m_e)]$ where the subscript e denotes "electron-value". Here g_e, called the electron g-factor, accounts for the quantum nature of the electron. g_e is computed by Quantum Electro-Dynamics (QED) to have the value $2.002319\ldots$ The deviation from 2 is due to loop corrections. The gyromagnetic ratio is sometimes written $\gamma_e = -g_e[(\beta/2)/(\hbar/2)]$ where $\hbar/2$ is the spin angular momentum of the electron and $\beta/2$ is the electron magnetic moment in terms of the Bohr magneton (β). The "natural unit" of atomic-level magnetic moment (β) has the value $9.27401\cdots \times 10^{-24}$ in SI units.

3.5.2 Motion of spin magnetic moment

The response of an electron spin angular momentum $\mathbf{s}$ to a torque $\mathbf{T}$ is $d\mathbf{s}/dt = \mathbf{T}$. Now the magnetic moment $\mathbf{m}$ of an electron is related to the spin $\mathbf{s}$ by $\mathbf{m} = \gamma_e \mathbf{s}$. The torque exerted on a magnetic moment by a magnetic field $\mathbf{B} = \mu_0 \mathbf{H}$ is $\mathbf{T} = \mathbf{m} \times \mathbf{B}$. Combining the relations, the equation of motion for the magnetic moment of an electron spin is

$$d\mathbf{m}/dt = \mu_0 \gamma_e \, \mathbf{m} \times \mathbf{H} \,. \tag{3.2}$$

Now, if the electron spin is in a constant state of precession ω_0 about $\mathbf{H}$, it follows that $\mathbf{T} = \omega_0 \, \mathbf{s}$ and $\omega_0 = \mu_0 \gamma_e \, |\mathbf{H}|$ is the Larmor angular frequency.
Note that in the frequently employed CGS sytem, B, M, H all have the same units; and therefore the μ_0 pre-multiplier is absent from the equation of motion. Note also, there is some inconsistency between authors whether the gyromagnetic ratio is a signed quantity or a modulus. And

this introduces minor discrepancies (sign changes) between different presentations of the Landau-Lifshitz (LL) equation (3.2). For example Bloembergen[40] and Gilbert[57, 58] take $\gamma < 0$, whereas Shapiro[61] and Tsutaoka[104] take $\gamma > 0$.

Eq. 3.2 is summed over all atoms in a crystal to find the net spin and magnetization: $\mathbf{M} = (1/\Delta V)\sum_i^N \mathbf{m}$ where ΔV is the volume of the atomic spin site. In this summation, it becomes clear that $\mathbf{H}$ is the sum of any externally applied field *and* all the internal magnetic fields due to each of the atomic spins; in other words the effective field. Typically we first look for a steady-state solution $d\mathbf{M}/dt = 0$ that is consistent with minimizing the magnetic free energy; and then consider the evolution of deviations of the magnetization. Eq. 3.2 summed over all atoms is the core of the Landau-Lifshitz theory[45] of ferromagnetic resonance. If all the spin sites are aligned, the sum yields the uniform mode. Alternatively, if the alignment (of spin sites) varies periodically in space and time, the sum permits spin-wave modes (called magnons).

If in addition to the applied DC magnetic field, there is a radio-frequency magnetic field $\mathbf{h}e^{i\omega t}$ then this field may drive the spin gyrations to large amplitude if ω is equal to the Larmor frequency. The resonance can be found/graphed either as a function of applied field (at fixed RF) or a function of radio frequency at fixed magnetic bias. The DC bias creates a preferred direction about which the spins precess; and thus the response to an alternating magnetic field depends on whether the RF magnetic component is parallel or perpendicular to the bias. The effect is described by the Polder[49] complex permeability tensor[3]. Lax & Button[54], Appendix 4-1, outline the derivation of effective susceptibility components including loss and demagnetizing factor.

3.5.3 Conditions for FMR

When a homogeneous bias magnetic field sufficient for uniform magnetization to saturation is applied, the ferrite becomes a single domain, uniform precession of its magnetic moment is possible, and the conditions for FMR are ideal. If the bias field is insufficient and significantly inhomogeneous, and if a ferrite sample is comparatively large, then there could be many domains in the ferrite sample. Magnetic moments in different parts (domains) of the sample will have different orientations with respect to the crystallographic axes and the bias field (if the latter is applied), and therefore, the magnetic resonance conditions will be different in different parts of the sample. This leads to a weaker and broader resonance with less specificity concerning the relative orientation of bias and RF wave. There is a theory[89, 90, 91] of FMR in partially saturated ferrites, but it is more complicated.

Natural FMR

The crystallographic anisotropy field is the cause of an internal bias field (or fields) with specific directionality. This field sets conditions for a natural FMR. However, the gyration (resonance) frequency is typically very high; in the tens of GHz range.

3.5.4 Demagnetizing factor

Shortly after the experimental verification of the Landau theory of FMR by Griffiths[48], the researcher Kittel[51] pointed out that the effective field may be very different from the externally applied DC magnetic field because of the demagnetizing field as discussed in Sec. 1.4. Subsequently, Kittel[52] introduced the RF demagnetizing field, and asserted the DC and RF demagnetizing factors are equal. This might be true, but it is not self-evident. Clearly, the field equations are different between statics (DC) and dynamics (RF). The field solutions are different. It is possible that the fractions of the solutions outside versus inside the sample are the same for DC and RF,

[3]The tensor depends only on direction and not on position and so reduces to a matrix relation (double index rather than triple index).

but needs to be demonstrated. Because $\nabla \times \mathbf{H} \neq \mathbf{0}$ and $\nabla \times \mathbf{E} \neq \mathbf{0}$ when fields are time varying, it follows that field shapes change. Whereas the scalar potential is suited to static irrotational fields, the vector potential is suited to time-varying fields with non-zero curl. Nevertheless, the fields share some of the geometric symmetries of the material object. So equal DC and RF demagnetization factors cannot immediately be ruled out.

3.5.5 Importance of damping

Damping is essential to align the spins with the external field, and is discussed in Chap. 4. Damping is introduced in a phenomenological way through several possible models, such as those of Landau, Gilbert and Bloch[4]. The Landau and Gilbert models conserve the magnitude $|\mathbf{M}|$; the Bloch model[53] does not. The damping factor is difficult to estimate, and so is obtained from experiment. In the 1950's efforts to clarify the basic damping mechanism led to experiments at high microwave power level in order to study the dissipation of absorbed magnetic energy. Two effects were discovered: frequency doubling, and saturation of the magnetization due to nonlinearity. Contrastingly, a decline of permeability may occur at surprisingly low RF power levels: spin-wave modes having the same frequency of precession as the uniform mode can grow at the expense of the uniform mode.

3.5.6 Ferri-magnetic resonance

In ferro-magnets there is one type of spin site repeated throughout the crystal lattice. In ferrimagnets, there are two (or more) types of spin site. Thus it is proper to introduce two magnetizations (with different g-factors, anisotropy fields, etc.) into the summation over A and B spin sites. There is one low frequency mode in which the ferrite behaves apparently as a simple ferromagnetic system. In that mode, the two sets of spins precess in the same rotational sense and are in phase. There is one high frequency mode (usually in the infrared) in which the material displays ferrimagnetic character: the two sets of spins (one for each sub-lattice) precess in the same sense but out of phase. The resonance frequency is high because it takes place in the internal molecular field, which is considerably larger than the external magnetic fields normally available in the laboratory. The matter is discussed by Lax & Button[54] Chaps. 6.1. & 6.2.

3.6 Simple Ferrite Structures

3.6.1 Spinel structure

Consider now the spinel structure. The name spinel comes from the Latin word spinella, a diminutive form of spine, in reference to its pointed crystals. The spinel is a ferrous oxide (Fe_3O_4) lattice with some of the Fe^{2+} substituted by other divalent atoms such as Ni, Mn, Co, Zn, etc. A spinel unit-cell is made up of eight face-centred cubic (FCC) cells made by oxygen ions in the configuration $2 \times 2 \times 2$, so it is a big structure consisting of 32 oxygen atoms, 8 A atoms and 16 B atoms. In general, the A and B atoms may differ. The structure is two interpenetrating lattices of tetrahedral sites and octahedral sites, which we label T and O respectively. In the *normal* spinel structure, all A^{2+} cations occupy the tetrahedral sites, and all B^{3+} ions occupy the octahedral sites. In the *inverse* spinel structure, half of the B^{3+} cations occupy the tetrahedral sites and the remaining half B^{3+} and all A^{2+} cations occupy the octahedral sites. Only this inverse structure has ferri-magnetic properties. We can think of this more simply as an arrangement as eight molecules each with chemical formula $B^{3+}(A^{2+}B^{3+})O_4$. There are two sites per molecule which we name O and T. The

[4]Felix Bloch (1905-1983) was a Swiss-American physicist. He shared the 1952 Nobel prize with Edward Mills Purcel for the development of Nuclear Magnetic Resonance.

T site has a single cation, and the O site has two cations per molecule. In the case that the spinel is a ferrite, the B atoms are iron Fe; and the A atoms may be Fe, Ni, Mn, Co, Zn, etc.

Consider, the particular case of the loadstone molecule Fe_3O_4. Neel, proposed the structure, wherein the T site has a ferric ion (Fe^{3+}), and the O site contains a ferric (Fe^{3+}) and a ferrous (Fe^{2+}) ion. Neel assumed that the O-T exchange interactions are stronger than those of the O-O or T-T category. The geometry of the lattice is such that the spins of the atoms on the O sites cannot be antiparallel to those of the neighboring atoms on the T sites unless the O-site atoms are all mutually parallel, pointing say North, and those of the T-site atoms all pointing in the opposite direction, e.g. South.

$$\begin{array}{cccc} \overleftarrow{B^{+++}} & \overrightarrow{A^{++}}\,\overrightarrow{B^{+++}} & \overleftarrow{B^{+++}} & \overrightarrow{A^{++}}\,\overrightarrow{B^{+++}} \\ \text{T} & \text{O} & \text{T} & \text{O} \\ \overleftarrow{Fe^{+++}} & \overrightarrow{Fe^{++}}\,\overrightarrow{Fe^{+++}} & \overleftarrow{Fe^{+++}} & \overrightarrow{Fe^{++}}\,\overrightarrow{Fe^{+++}} \\ \text{T} & \text{O} & \text{T} & \text{O} \end{array}$$

The spins of the Fe^{2+} and Fe^{3+} ions are respectively 2 and 5/2. According to the Neel model sketched above, the saturation magnetization per molecule of Fe_3O_4 at T=0 should be

$$g_e\left[-\frac{5}{2}+\left(2+\frac{5}{2}\right)\right] \simeq \text{ 4 Bohr magnetons, because } g_e \approx 2.$$

The observed value is 4.2. All told, the saturation moments of the various ferrites, and the analogous compounds with varying amounts of magnetically inert substituents conform very well to the predictions of theory.

3.6.2 Garnet structure

Garnets are represented by the general formula $R_3Fe_5O_{12}$, containing two magnetic ions one being iron (Fe) and the other a rare earth (R) such as yttrium (Y) or a lanthanide. The unit cell is cubic and contains 8 formula units i.e. 160 atoms, quite complex. The cations are located in three sublattices: dodecahedral (D), octahedral (O) and tetrahedral (T). Such structure can be described by the general formula of $\{R_3\}[Fe_2](Fe_3)O_{12}$, where { }, [ ] and ( ) brackets indicate the positions in the D, O and T sub-lattice sites, respectively. As a rule, R^{3+} occupies the D sites and Fe^{3+} ions occupy the O and T sites in the ratio of 2:3. The spin configurations (of Fe atoms) at O and T sites are anti-parallel, while the spins (of R atoms) at the D sites are parallel to those at O sites. In garnet ferrites, the orbital contribution of iron is quenched leaving only the spin contribution. The rare earth ions contribute both orbital and spin magnetic moment. Each Fe^{3+} ion contributes spin 5/2, and each rare earth ion contributes spin $S_R = (2n+1)/2$ with $n = 0, 1, 2, 3$. Although the lattice sites are three-dimensional, the magnetic moments are either parallel or anti-parallel; so we can sketch a linear diagram to sum the nett contribution.

$$\begin{array}{ccc} \overleftarrow{3R^{3+}} & \overrightarrow{3Fe^{+++}} & \overleftarrow{2Fe^{+++}} \\ \text{D} & \text{T} & \text{O} \end{array}$$

The saturation magnetization per molecule should be:

$$g_e\left[-3\times S_R\ +3\times\frac{5}{2}\ -2\times\frac{5}{2}\right] \simeq 5\ -3(2n+1)\ \text{ Bohr magnetons, because } g_e \approx 2.$$

Of course, this is a gross simplification. Modern studies[56] show that YIG may display multiple ferro-and ferri-magnetic phases. Here phase means state of matter. $Y_3Fe_5O_{12}$ or YIG is the most typical of the garnet-ferrites. In the fields of microwave electronics, materials based on YIG are widely used owing to their low magnetic damping, controllable saturation magnetization, high electrical resistivity, and large magneto-optical Faraday rotation.

Chapter 4

Landau-Lifshitz-Gilbert Equation

4.1 History

This chapter presents nonlinear solutions of the Landau-Lifshitz-Gilbert Equations 4.1 and 4.2. Although the Landau and Gilbert versions of the spin equation of motion happen to be algebraically equivalent, they have somewhat different roots and physics perspective. The significance and historical context of the Landau version is discussed by Bar'yakhtar[59]. Landau introduced the effective magnetic field to be the sum of several physical contributions which result in the field energies (I,II,III,IV) introduced in Chap. 3. The triple-product relaxation term in the Landau equation is specifically identified (by Landau) as a (small) relativistic correction term, though details are not given. The rich range of physics that can be included in the effective field, and the consequent beautiful and complex varieties of nonlinear motion, is described by Lakshmanan[60].

Contrastingly, Gilbert set out to recast the spin equation of motion in a Lagrangian form and to introduce viscous damping effects while retaining the spin-modulus conservation property. Thus the physics underlying the parameter α appearing in the vector triple-product of Landau, and the dissipation parameter α pre-multiplying $\mathbf{M} \times \dot{\mathbf{M}}$ in the Gilbert equation have completely different motivation. If, however, we view α as a purely phenomenological parameter, whose value is found from measurement, these distinctions may become lost. We shall consider only the most elementary (and simplest) form of the effective magnetic field.

4.2 Effective magnetic field

A modern account of the five[1] terms in the effective field is given by Wei[20] Chap. 2.3.1. The minimalist effective field contains three terms: an applied field, the dipole-dipole field, and the exchange field. The corresponding field energies are the Zeeman (I), the classical dipolar energy (II), and the exchange energy (III). In addition to aligning domains the dipole-dipole field (II) is responsible for the demagnetizing field.

The ferro-magnetic resonance (FMR) occurs when the magnetic material has DC and RF applied magnetic fields. Authors vary in the precision with which they define the applied fields. Some treatments[63, 64, 12] of the FMR assume that the magnetic material is an infinite medium; in which case, there is no distinction between inside and outside the material. When the magnetic medium is infinite in extent, any surface density of magnetic dipoles (such as occurs at the poles of a magnet) are moved to infinity, and are therefore inconsequential. In such a case, there is no demagnetizing field. However, a more practical and realistic arrangement has a magnetic material of finite size immersed in an external applied field. In this set up, there is definitely a distinction between the fields inside (the material) and outside (in vacuum); and there will be a demagnetizing field present

[1] The fifth term is due to the magneto-elastic effect: the energy associated with the change in a material's magnetic properties due to mechanical stress or strain.

(inside) related to the magnetization of the material. The importance of this demagnetizing field was first recognized by Kittel[51, 52], and is taken up in the text books by Lax & Button[54] and Koledintseva & Tsutaoka[104].

4.3 Spin-Magnetization Equation of Motion

The Landau-Lifshitz and Gilbert versions of the spin relaxation equation of motion are identical, in the same way that the left and right sides of the vector triple product identity $\mathbf{p} \times (\mathbf{q} \times \mathbf{r}) \equiv (\mathbf{p} \cdot \mathbf{r})\mathbf{q} - (\mathbf{p} \cdot \mathbf{q})\mathbf{r}$ are equal. The Landau and Gilbert equations have precisely the same solutions.

Although the Gilbert variety was conceived in the context of permalloy[2], which has a comparatively large value of α, both mathematical versions have the same range of validity for the relaxation parameter α.

In writing the spin relaxation equation, we follow the conventions employed in Refs.[40, 43, 58, 61]. $\mathbf{H}$ will be the effective field. For brevity, we write the time derivative $d\mathbf{M}/dt \equiv \dot{\mathbf{M}}$ and the modulus $M \equiv |\mathbf{M}|$ or $M^2 = \mathbf{M} \cdot \mathbf{M}$. The Landau-Lifshitz equation:

$$\dot{\mathbf{M}} = g\mathbf{H} \times \mathbf{M} + g\frac{\alpha}{M}\,\mathbf{M} \times (\mathbf{H} \times \mathbf{M}) \tag{4.1}$$

The Gilbert version:

$$\dot{\mathbf{M}} = g(1+\alpha^2)\mathbf{H} \times \mathbf{M} + \frac{\alpha}{M}\,\mathbf{M} \times \dot{\mathbf{M}} \tag{4.2}$$

Here $g \equiv \mu_0\gamma_e$. All quantities appearing in these equations are those *inside* the material. We shall demonstrate the equivalence of these two forms. Following Baartman[65], we understand that it is slightly easier to go from the Gilbert version to the Landau form. We form the vector cross product of Eq. 4.2 with $\mathbf{M}$. The left side becomes $\mathbf{M} \times \dot{\mathbf{M}}$. We use the triple product identity $\mathbf{M} \times (\mathbf{M} \times \dot{\mathbf{M}}) \equiv (\mathbf{M} \cdot \dot{\mathbf{M}})\mathbf{M} - (\mathbf{M} \cdot \mathbf{M})\dot{\mathbf{M}}$ to expand that part of the right side which contains $\dot{\mathbf{M}}$. Now it is a fundamental property of the Landau-Lifshitz equation that the modulus of the magnetic moment is conserved, because forces are always perpendicular to motion; and so $\mathbf{M} \cdot \dot{\mathbf{M}} = 0$. Hence:

$$\mathbf{M} \times \dot{\mathbf{M}} = g(1+\alpha^2)\mathbf{M} \times (\mathbf{H} \times \mathbf{M}) - \alpha M\dot{\mathbf{M}} \tag{4.3}$$

We now substitute expression (4.3) into the right side of Eq. 4.2. We move the term in $\dot{\mathbf{M}}$ to the left, divide throughout by $(1+\alpha^2)$ and recover the Landau form Eq. 4.1. It is a matter of choice whether to use the Landau or Gilbert forms of the spin-magnetization equation; we shall employ the former. The LLG equation admits steady-state solutions, but does not generate them. For the steady-state, we must apply the equations of magneto-statics. We assume the bias field is sufficiently strong to align all the magnetic domains into a single domain; so the material is near/at saturation. Because of the demagnetizing field, both the DC and RF fields inside the material differ from the outside applied values. The following discussion and formulae concern the fields inside. We denote static values by upper case letters, and dynamic values by lower case.

The demagnetizing field is $\mathbf{H}_d = \bar{\mathbf{N}}\mathbf{M}$ with magnetization $\mathbf{M}$ and tensor $\bar{\mathbf{N}}$. However, $\mathbf{M}$ depends on the prior history of the external applied $\mathbf{H}_2$ which penetrates into the interior. The DC internal field is $\mathbf{H} = \mathbf{H}_2 + \mathbf{H}_d = \mathbf{H}_2 - \mathbf{N}\mathbf{M}$. Hence formally

$$\mathbf{B}(\mathbf{H})/\mu_0 = (\mathbf{H} + \mathbf{M}) \quad \text{becomes} \quad \mathbf{B}(\mathbf{H}_2 - \mathbf{N}\mathbf{M})/\mu_0 = [(\mathbf{H}_2 - \mathbf{N}\mathbf{M}) + \mathbf{M}]\,. \tag{4.4}$$

The steady-state $\mathbf{M}$ and $\mathbf{H}_2$ are self-consistent solutions of Eq. 4.4. The steady-state quantities are substituted in the LLG equation, yielding the condition $(\mathbf{H}_2 - \bar{\mathbf{N}}\mathbf{M}) \times \mathbf{M} = \mathbf{0}$.

[2]Permalloy is a nickel-iron magnetic alloy, with about 80 % nickel and 20 % iron content. Invented in 1914 by physicist Gustav Elmen at Bell Telephone Laboratories, it is notable for its very high magnetic permeability, which makes it useful as a magnetic core material in electrical and electronic equipment, and also in magnetic shielding to block magnetic fields. Commercial permalloy alloys typically have relative permeability of around 10^5, compared to several thousand for ordinary steel.

In order to find the dynamics, we add an AC/RF term $\mathbf{h}_2$ to the external H-field. This will apply an alternating torque to the spins, causing them to precess. Summing over all the spins leads to a gyrating magnetic moment $\mathbf{m}$. In general, this gyrating internal moment will lead to an alternating bound surface current, or equivalent surface dipole density; and this is the source of an alternating demagnetizing field $\mathbf{h}_d = -\bar{\mathbf{n}}\mathbf{m}$. Here $\bar{\mathbf{n}}$ is the AC/RF demagnetization tensor, which may differ from the DC tensor. The AC internal field is $\mathbf{h} = \mathbf{h}_2 - \bar{\mathbf{n}}\mathbf{m}$. Hence, with respect to the LLG equation, we make the substitutions:

$$\mathbf{M} \to \mathbf{M} + \mathbf{m} \quad \text{and} \quad \mathbf{H} \to (\mathbf{H}_2 - \bar{\mathbf{N}}\mathbf{M}) + (\mathbf{h}_2 - \bar{\mathbf{n}}\mathbf{m}) \,. \tag{4.5}$$

The steady-state condition is used to set some of the product terms to zero, yielding the nett dynamical equation:

$$\begin{aligned} \dot{\mathbf{m}} &= g[\mathbf{h} \times (\mathbf{M} + \mathbf{m}) - (\bar{\mathbf{n}}\mathbf{m}) \times \mathbf{M} + \tilde{\mathbf{H}} \times \mathbf{m}] \qquad (4.6) \\ &+ (g\alpha/M)[\mathbf{m} \times (\mathbf{h} \times \mathbf{m}) + \mathbf{m} \times [\mathbf{h} \times \mathbf{M} - (\bar{\mathbf{n}}\mathbf{m}) \times \mathbf{M} + \tilde{\mathbf{H}} \times \mathbf{m}] \\ &+ (g\alpha/M)[\mathbf{M} \times (\mathbf{h} \times \mathbf{m}) + \mathbf{M} \times [\mathbf{h} \times \mathbf{M} - (\bar{\mathbf{n}}\mathbf{m}) \times \mathbf{M} + \tilde{\mathbf{H}} \times \mathbf{m}] \\ \tilde{\mathbf{H}} &= \mathbf{H}_2 \; - \bar{\mathbf{N}}\mathbf{M} \; - \bar{\mathbf{n}}\mathbf{m} \,. \qquad (4.7) \end{aligned}$$

In explicit component form, this equation contains a large number of terms; and, moreover, non-linearity up to cubic terms. This complexity is dealt with by taking single-component forms for $\mathbf{H}_2$ and $\mathbf{h}_2$; and assuming that the coordinate axes are taken parallel with the symmetry axes of the magnetized object or sample, in which case, the matrices $\bar{\mathbf{N}}$ and $\bar{\mathbf{n}}$ take diagonal form. The diagonal elements are (N_1, N_2, N_3) and (n_1, n_2, n_3) respectively.

We adopt a locally orthogonal coordinate system, which could be Cartesian (x, y, z) or cylindrical (r, ϕ, z) or spherical (r, θ, ϕ), depending on the shape of the material and shape of the applied fields. The form of the spin equation of motion is invariant when the coordinate system is changed because the spin motion does not contain translation. For example, the equation of spin motion in cylinder coordinates is identical in form to that of the Cartesian components; $\mathbf{m} = [m_x, m_y, m_z]$ is simply substituted by $\mathbf{m} = [m_r, m_\phi, m_z]$. Thus, without loss of generality, we may take a Cartesian system and the DC bias aligned with the z-axis such that $\mathbf{H}_2 = [0, 0, H_z]$. We assume the bias field is strong, so the magnetic material is near saturation with domains aligned. The static magnetization is $\mathbf{M} = [0, 0, M_z]$.

4.4 RF Parallel to Bias

We consider the case that an external RF magnetic field is applied parallel to an external DC magnetic bias field. The angular frequency of the RF field is ω. $\mathbf{h} = [0, 0, h_z \cos(\omega t)]$ and $\mathbf{m} = [m_x(t), m_y(t), m_z(t)]$. The combination $g \times H$ has the dimensions of angular frequency.

4.4.1 Linearized solution

Suppose that product terms of the form $m_i m_j$ and $h_z m_j$ are set to zero, with i, j coordinate indices. In this case, the drive term $\cos(\omega t)$ disappears; and the LLG equation is much simplified. For brevity, we define $H_p \equiv H_z + M_z(n_1 - N_3)$ and $H_q \equiv H_z + M_z(n_2 - N_3)$; and $M_z \equiv \rho M$. The LLG equation becomes:

$$\begin{aligned} \dot{m}_x &= -g(H_q m_y + H_p m_x \alpha\rho) \qquad (4.8) \\ \dot{m}_y &= +g(H_p m_x - H_q m_y \alpha\rho) \qquad (4.9) \\ \dot{m}_z &= 0 \qquad (4.10) \end{aligned}$$

The solution of these equations is a damped precession of the moments m_x, m_y at frequency ω_0, and m_z a constant.

$$\begin{aligned} m_x(t) &= \exp(-\beta t/2)[c_1 \cos\omega_0 t \ - (g/\omega_0)(c_1(H_p - H_q)\alpha\rho/2 \ + c_2 H_q)\sin\omega_0 t] && (4.11)\\ m_y(t) &= \exp(-\beta t/2)[c_2 \cos\omega_0 t \ + (g/\omega_0)(c_2(H_p - H_q)\alpha\rho/2 \ + c_1 H_p)\sin\omega_0 t] && (4.12)\\ \omega_0 &= g\sqrt{H_p H_q + (H_p - H_q)^2(\alpha\rho/2)^2}\ , \qquad \beta \equiv g(H_p + H_q)\alpha\rho\ . && (4.13) \end{aligned}$$

The constants of integration c_1, c_2 are chosen to match initial conditions. Note that typically $0 \le \alpha \ll 1$ and $0 < \rho < 1$, and so the damping rate β is usually small. The full nonlinear equation also has a damped precession of m_x, m_y, but the axial component m_z relaxes to a final value greater than the initial.

4.4.2 Near-linear solution

Suppose that product terms only of the form $m_i m_j$ are set to zero. Further, suppose the magnetized object is in the form of a cylinder (or bar of square cross section) with symmetry axis along z, such that $n_1 = n_2$. (Because the fields are both applied along z, it is not essential to set $N_1 = N_2$.) The DC internal field becomes $\tilde{H}_z = H_z + (n_1 - N_3)M_z$. The LLG equation is simplified:

$$\begin{aligned} \dot{m}_x &= -g(\tilde{H}_z + h_z\cos\omega t)[M m_y + \alpha m_x M_z)]/M && (4.14)\\ \dot{m}_y &= +g(\tilde{H}_z + h_z\cos\omega t)[M m_x - \alpha m_y M_z]/M && (4.15)\\ \dot{m}_z &= 0 && (4.16) \end{aligned}$$

For the purpose of brevity and compactness, we define R and r by the relations $(\omega/g)R \equiv \tilde{H}_z$ and $(\omega/g)r \equiv h_z$. Further, set $\rho = M_z/M$; and $s = \omega t$ and $m' \equiv dm/ds$; and $\chi(s) = R\,s + r\sin s$. The approximate equations have an exact solution:

$$\begin{aligned} m_x(s) &= \exp(-\alpha\rho\chi)[c_1\cos\chi - c_2\sin\chi]\\ m_x(s) &= \exp(-\alpha\rho\chi)[c_1\cos\chi - c_2\sin\chi]\\ m_z(s) &= m_z(t{=}0) \end{aligned}$$

The constants of integration c_1, c_2 are chosen to match initial conditions.

4.4.3 Nonlinear solution

We now address the case that all product terms are retained. However, a simplification is needed to make the system of equations tractable. We take the case of a sphere or cube with equal demagnetizing factors $N_1 = N_2 = N_3$ and $n_1 = n_2 = n_3$. However, we admit the possibility that AC and DC factors are not identical; and that $n_1 \neq N_3$. $\mathbf{H}$ and $\mathbf{M}$ are substituted in the Landau Eqn. 4.1, leading to equations of motion for the three components of magnetization:

$$\begin{aligned} \dot{m}_x &= -g(\tilde{H}_z + h_z\cos\omega t)[M m_y + \alpha m_x(M_z + m_z)]/M && (4.17)\\ \dot{m}_y &= +g(\tilde{H}_z + h_z\cos\omega t)[M m_x - \alpha m_y(M_z + m_z)]/M && (4.18)\\ \dot{m}_z &= +g\alpha(\tilde{H}_z + h_z\cos\omega t)(m_x^2 + m_y^2)/M && (4.19) \end{aligned}$$

It is noteworthy that almost the same set of equations arise if $n_1 = n_2 = n_3 = 0$ and $N_1 = N_2 = N_3 = 0$. Thus the symmetry of the sphere makes its response almost like an infinite medium. If $n_1 = N_3$ then $\tilde{H}_z = H_z$ is the externally applied field, and the sphere behaves exactly like an infinite medium.

As before, we make the definitions $(\omega/g)R \equiv \tilde{H}_z$ and $(\omega/g)r \equiv h_z$; and $s = \omega t$ and $m' \equiv dm/ds$. When $R = 1$, the drive frequency becomes $\omega = gH_z$ which can be considered the resonance

frequency, or more correctly the gyration frequency. The ratio $r/R = h_z/\tilde{H}_z$. This is the most economical notation; but if we wish to keep the fields H_z, h_z fixed while the drive frequency is varied, then R and r must be updated. In terms of these reduced variables, the equations assume a briefer form:

$$m'_x = -g(R + r\cos s)[Mm_y + \alpha m_x(M_z + m_z)]/M \quad (4.20)$$
$$m'_y = +g(R + h_z\cos s)[Mm_x - \alpha m_y(M_z + m_z)]/M \quad (4.21)$$
$$m'_z = +g\alpha(R + r\cos s)(m_y^2 + m_x^2)/M \quad (4.22)$$

The magnitude of the magnetization is preserved by the LLG equations, and so we may replace $(m_y^2 + m_x^2)$ by $M^2 - m_z^2$ in the equation for m'_z. When the bias and static magnetization are both zero ($H_z = 0, M_z = 0$), Eq. 4.25 has solution $m_z(s) = M\tanh(Mc_1 + \alpha r\sin s)$. This guides us toward the general solution Eq. 4.25. The solution m_z is then substituted in Eqs. 4.20, 4.21, and these solved for the time-varying magnetizations:

$$m_x(s) = \mathrm{sech}[Mc_1 + \alpha\chi][c_2\cos\chi - c_3\sin\chi] \quad (4.23)$$
$$m_y(s) = \mathrm{sech}[Mc_1 + \alpha\chi)][c_3\cos\chi + c_2\sin\chi] \quad (4.24)$$
$$m_z(s) = M\tanh[Mc_1 + \alpha\chi] - M_z \quad (4.25)$$

As before, $\chi(s) = R\,s + r\sin s$. The constant of integration c_1 is chosen to yield the initial value of m_z. Thus $\tanh(Mc_1) = m_z(0)/M$. At large times $m_z \to (M - M_z)$ and $m_x, m_y \to 0$. The reader may recognize that $\cos(r\sin s)$ and $\sin(r\sin s)$ are representations of the Bessel functions, and may be Fourier analysed into a spectrum with frequency components at multiples of ω (the drive frequency). The form of m_x, m_y indicates a precession of the spin, with fundamental frequency proportional to H_z/g and modulations whose amplitudes are related to h_z. The case of an infinite magnetized medium has the same equations and solution, with the exception that $\tilde{H}_z = H_z$.

4.4.4 Magnetization equations for cylinder

In the case of a cylinder (or square rod), the demagnetization factors $N_1 = N_2 \neq N_3$ and $n_1 = n_2 \neq n_3$. When all product terms are retained, the components of the magnetization become Eqs. 4.17-to-4.19 with $(\tilde{H}_z + h_z\cos\omega t)$ replaced by $[\tilde{H}_z + h_z\cos\omega t + (n_1 - n_3)m_z(t)]$ throughout. We remind the reader that the equations in cylindrical-polar form (m_r, m_ϕ, m_z) take the same form. Unfortunately, there is no closed-form solution.

4.5 RF Perpendicular to Bias

We consider the case that an external RF magnetic field is applied perpendicular to an external DC magnetic bias field. The DC bias aligned with the z-axis such that $\mathbf{H}_2 = [0, 0, H_z]$. The angular frequency of the RF field is ω. $\mathbf{h} = [0, h_y\cos(\omega t), 0]$ and $\mathbf{m} = [m_x(t), m_y(t), m_z(t)]$.

4.5.1 Linearized solution

The linearization conditions are $m_i \times m_j = 0$ and $h_y \times m_j = 0$ where i, j are the coordinate indices. The solution of the linearized LLG equation is well known as the Polder[49, 50] tensor[3]. But in fact, Polder himself references Kittel[51, 52] as the originator; and, moreover, neither author considered a damping term in the form of a triple-vector product.

Usually $h_y(t)$ is written in complex form $h_y\exp(i\omega t)$ and the solution for $[m_x, m_y, m_z]$ given as complex amplitudes. However, we shall write the drive as $h_y(t) = h_y\cos(\omega t)$, and the solution in

[3]This is a tensor of rank 2, usually called a matrix.

pure real form. As above, we define $H_p \equiv H_z + (n_1 - N_3)M_z$ and $H_q \equiv H_z + (n_2 - N_3)M_z$; and $M_z \equiv \rho M$. The linearized LLG equation is:

$$\begin{aligned} \dot{m}_x &= g(h_y M_z \cos\omega t \; - H_p m_x \alpha\rho \; - H_q m_y) && (4.26)\\ \dot{m}_y &= g H_p m_x + g\alpha\rho(h_y M_z \cos\omega t \; - H_q m_y) && (4.27)\\ \dot{m}_z &= 0 && (4.28) \end{aligned}$$

The solution is the sum of a complementary function, which decays, and a particular integral that is the steady state. For brevity we set $s \equiv \omega t$ and $\delta \equiv \alpha\rho$; typically $\delta \ll 1$. We substitute the trial solution

$$[m_x, m_y, m_z] = [A_x \cos s + B_x \sin s, A_y \cos s + B_y \sin s, c_3] \; . \tag{4.29}$$

The coefficients of $\cos s$ and $\sin s$ must all be zero. This leads to a system of algebraic equations, two for each of the magnetization components. The particular integral is:

$$\begin{aligned} m_x &= g h_y M_z \omega [g(H_p + H_q)\omega\delta \cos s \; + (\omega^2 - g^2 H_p H_q(1+\delta^2)) \sin s]/D && (4.30)\\ m_y &= g h_y M_z \left\{ g[g^2 H_p^2 H_q(1+\delta^2) + \omega^2(H_q\delta^2 - H_p)] \cos s \; + \omega\delta[\omega^2 + g^2 H_p^2(1+\delta^2)] \sin s \right\} / D \\ D &= \omega^4 + (g^2 H_p H_q)^2(1+\delta^2)^2 + \omega^2 g^2[-2H_p H_q + (H_p^2 + H_q^2)\delta^2] && (4.31) \end{aligned}$$

D is a resonant denominator, and the gyromagnetic resonance condition is $\omega^2 = g^2 H_p H_q(1+\delta^2)$. When driven at that specific frequency, the response is:

$$\begin{aligned} m_x(t) &= \frac{h_y M \cos\omega t}{(H_p + H_q)\alpha} && (4.32)\\ m_y(t) &= \frac{h_y M_z \cos\omega t}{(H_p + H_q)} \; + \frac{h_y M \sin\omega t}{(H_p + H_q)\alpha} \sqrt{(H_p/H_q)(1+\delta^2)} && (4.33) \end{aligned}$$

Evidently, the in-phase component of m_x and the quadrature component of m_y are boosted by $1/\alpha$. $m_z = c_3$ is constant. Note as follows: both m_x and m_y are perpendicular to the bias; h_y drives precession in the x, y plane; an applied RF component h_x would also drive precession in the x, y plane. If the split $|n_1 - n_2| \ll 1$ is small, the amplitude of the spin precession at resonance is $\sqrt{m_x^2 + m_y^2} \approx h_y M_z/[(H_p + H_q)\delta]$.

The susceptibility is $m_y(t)/h_y(t)$. The in-phase (quadrature) component of m_y/h_y is the real (imaginary) part of complex susceptibility χ_{yy}. Thus at resonance, the material becomes very lossy; and the incremental permeability $\mu_\Delta = 1 + M_z/(H_p + H_q)$. Likewise the components of m_x/h_y are related to the complex cross-susceptibility χ_{xy}.

4.5.2 Magnetized cylinder

In the case of a magnetized cylinder aligned with z, the factors $n_1 = n_2$ and $H_p = H_q$; and so the expressions simplify. As above, we define $(\omega/g)R \equiv \tilde{H}_z$ and $s = \omega t$ and $M_z \equiv \rho M$. The general solution is the sum of a complementary function $\exp(-Rs\alpha\rho)[c_1 \cos(Rs) + c_2 \sin(Rs)]$, which decays, and particular integral that gives the steady state. For brevity we set $\delta \equiv \alpha\rho$. Further, we introduce the scaled drive frequency S by $\omega = g\tilde{H}_z \, S\sqrt{1+\delta^2}$. The resonant denominator becomes

$$D = (g\tilde{H}_z)^4(1+\delta^2) \times E \quad \text{with} \quad E = [(1-S^2)^2 \; + \; (1+S^2)^2\delta^2] \; . \tag{4.34}$$

$m_z = c_3 = 0$. The other magnetic moments are:

$$\begin{aligned} m_x &= \frac{h_y M_z}{\tilde{H}_z E} \left[2S^2\delta \cos\omega t \; - \; S(1-S^2)\sqrt{1+\delta^2} \sin\omega t \right] && (4.35)\\ m_y &= \frac{h_y M_z}{\tilde{H}_z E} \left[[(1-S^2) + \delta^2(1+S^2)] \cos\omega t \; + \; S(1+S^2)\delta\sqrt{1+\delta^2} \sin\omega t \right] \; . && (4.36) \end{aligned}$$

When the drive frequency equals the gyration frequency, $S \to 1$, the moments are boosted:

$$m_x(t) = \frac{h_y M_z}{2\tilde{H}_z\,\delta}\cos\omega t \quad \text{and} \quad m_y(t) \approx \frac{h_y M_z}{2\tilde{H}_z\,\delta}\sin\omega t\,. \tag{4.37}$$

Typically $\delta \ll 1$; and so the in-phase component of m_x and the quadrature (lossy) component of m_y rise to large amplitude. In the limit of low frequency $S \to 0$, the components become $m_x = 0$ and $m_y = (h_y M_z/\tilde{H}_z)$.

4.5.3 Polder tensor

We now discuss the elements of the susceptibility tensor. Evidently, we may write Eqs. 4.35 and 4.36 in the form:

$$m_x(t)/h_y = \Re[\chi_{xy}e^{i\omega t}] \quad \text{where} \quad \chi_{xy} = (M_z/\tilde{H}_z)[\chi'_{xy} + i\chi''_{xy}] \tag{4.38}$$

$$m_y(t)/h_y = \Re[\chi_{yy}e^{i\omega t}] \quad \text{where} \quad \chi_{yy} = (M_z/\tilde{H}_z)[\chi'_{yy} + i\chi''_{yy}] \tag{4.39}$$

$$m_z(t)/h_y = \Re[\chi_{zy}e^{i\omega t}] = 0\,. \tag{4.40}$$

$\chi_{xy}, \chi_{yy}, \chi_{zy}$ are the complex elements of the Polder susceptibility tensor. There are corresponding elements for an excitation $h_x e^{i\omega t}$. Fig. 4.1 shows the in-phase (real) and quadrature (imaginary) components of the complex susceptibility m_y/h_y and cross-susceptibility m_x/h_y versus (normalised) frequency at fixed bias field. $S = w/\omega_0$ is the ratio of applied frequency to the gyromagnetic resonance frequency $\omega_0 = g\tilde{H}_z\sqrt{1+\delta^2}$.

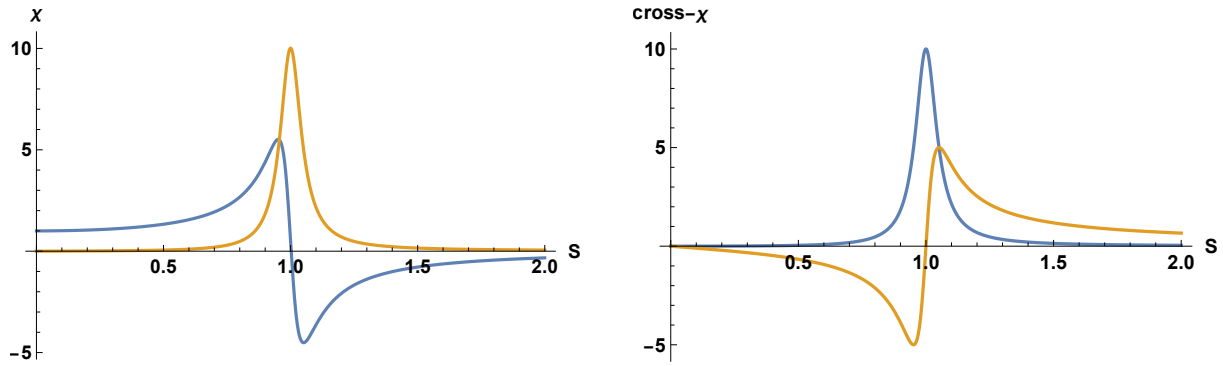

Figure 4.1: Complex susceptibility components of m_y (left graph) and m_x (right graph). $\delta = 0.05$ The in-phase (real) component χ' shown blue; the quadrature (imaginary, lossy) component χ'' shown gold. The bias field is fixed, as is the scale parameter between angular frequency ω and S.

Remarkably, the incremental permeability $\mu_\Delta = 1 + \chi$ due to m_y/h_y may become negative for $S = \omega/\omega_0 > 1$. This means that the spins lag the RF wave in such a way that m_y opposes h_y. This surprising behaviour is confirmed experimentally be several authors[106].

χ_{yy} is of the form: scale factor $(M_z/\tilde{H}_z)$ multiplied by pure functions $\chi'_{yy}(S)$ and $\chi''_{yy}(S)$. It is instructive to consider particular values of S in the limit $\delta \ll 1$.

S	1	1/2	0
χ'_{yy}	1/2	$4(3+5\delta^2)/(9+25\delta^2) \approx 4/3$	1
χ''_{yy}	$\sqrt{1+\delta^2}/(2\delta) \approx 1/(2\delta)$	$10\delta\sqrt{1+\delta^2}/(9+25\delta^2) \approx 10\delta/9$	0

Evidently for $S \leq 1/2$, the real part of χ_{yy} is essentially independent of $\delta = \alpha \times (M_z/M)$. The maximum of χ'' occurs at precisely $S = 1$. The zero of χ' occurs at $S = \sqrt{1+\delta^2}/\sqrt{1-\delta^2} \approx$

$1+\delta^2$. The minimum and maximum of χ' occur at $S=\sqrt{1-\delta}/\sqrt{1+\delta}$ and $S=\sqrt{1+\delta}/\sqrt{1-\delta}$, respectively. The corresponding value of χ' are $(1+\delta)^2/(4\delta)$ and $-(1-\delta)^2/(4\delta)$.

Bias varied at fixed RF

When the bias is varied at fixed RF, the expression for magnetic moments becomes:

$$\frac{m_x}{h_y} = \frac{gM_z}{\omega\, E}\left[2R\delta\cos\omega t \;+\; [1-R^2(1+\delta^2)]\sin\omega t\right] \tag{4.41}$$

$$\frac{m_y}{h_y} = \frac{gM_z}{\omega\, E}\left[R[-1+\delta^2+R^2(1+\delta^2)]\cos\omega t \;+\; \delta[1+R^2(1+\delta^2)]\sin\omega t\right] \tag{4.42}$$

$$E = 1-2R^2(1-\delta^2)+R^4(1+\delta^2)^2\ . \tag{4.43}$$

We may examine the in-phase and quadrature components to find the complex susceptibility. We may plot these components (χ',χ'') as a function of bias field at fixed frequency. In this case, the abscissa is $R=g\tilde{H}_z/\omega$. Because $R=1/S$, the inversion of "above versus below" flips the plots (Fig. 4.1) about the line $S=R=1$, and distorts the curves. Note, the incremental permeability $(1+m_y/h_y)$ is negative for $R=\omega_0/\omega<1$. Thus bias values must be selected above the gyromagnetic resonance value $H_{\rm res}=\omega/g$. This places the RF drive frequency below the gyromagnetic resonance.

4.6 Sphere with RF perpendicular to bias

The linearized equations of motion 4.26-to-4.28, and their solution, do not conserve the magnitude of the magnetization. The full nonlinear LLG equation is so complicated that single-component forms for $\mathbf{H}_2=[0,0,H_z]$, $\mathbf{M}=[0,0,M_z]$ and $\mathbf{h}=[0,h_y(t),0]$, and diagonal forms for $\bar{\mathbf{N}}$ and $\bar{\mathbf{n}}$, are insufficient to make the problem tractable. Additional symmetries are needed.

4.6.1 Nonlinear solution for sphere

In the case of the sphere or cube $n_1=n_2=n_3$, and assuming the DC and AC factors are equal $n_1=N_3$. $\mathbf{H}$ and $\mathbf{M}$ and $\mathbf{m}=[m_x(t),m_y(t),m_z(t)]$ are substituted in the Landau Eqn. 4.1, leading to equations of motion for the three components of magnetization:

$$0 = \dot{m}_x \;-(g/M)\left[-(Mm_y\;+\alpha m_xU_z)H_z\;-(\alpha m_xm_y-MU_z)\,h_y\cos\omega t\right] \tag{4.44}$$

$$0 = \dot{m}_y \;-(g/M)\left[+(Mm_x\;-\alpha m_yU_z)H_z\;+\alpha\,(m_x^2+U_z^2)\,h_y\cos\omega t\right] \tag{4.45}$$

$$0 = \dot{m}_z \;-(g/M)\left[+\alpha(m_x^2+m_y^2)H_z\;-(Mm_x+\alpha m_yU_z)\,h_y\cos\omega t\right] \tag{4.46}$$

Here $U_z(t)\equiv M_z+m_z(t)$. These equations do not have an exact analytic solution. However, the method of *harmonic balance* may find an approximate Fourier series steady-state solution. Unfortunately, except by numerical solution of the LLG Eqns., we cannot address the nature of the transient that may precede the steady-state conditions. We take the trial solution:

$$\mathbf{m}(t)=[A_x\cos(s+p_x),\;A_y\sin(s+p_y),\;m_0+A_z\sin(2s+p_z)]\quad\text{with}\quad s\equiv\omega t\ . \tag{4.47}$$

Here A_j are adjustable amplitudes and p_j are adjustable phases, both to be determined; and the index $j=x,y,z$. Note that we have included a DC term, m_0, and a frequency doubling in the third component $m_z(t)$. We must foresee that products of terms in $\cos\omega t$ and $\sin\omega t$ will generate sub-harmonics and super-harmonics.

The exact solution conserves the magnitude M^2. However, the trial solution may introduce periodic modulations – which must be minimized. Hence in addition to the three equations for $\dot{m}_j$, there is a constraint equation for the modulus of the magnetization: $0=[\mathbf{M}+\mathbf{m}(t)]^2-M^2$. We call this the *zeroth* equation.

The trial form is substituted into the zeroth Eqn. and the three LLG Eqns.; we label this set $0, 1, 2, 3$ respectively. Given that all expressions are equal to zero, it follows that all the harmonic components must equal zero. The four equations are Fourier analyzed. Let $[\cos s, \sin s]$ be fundamental components; and $[\cos ns, \sin ns]$ be n^{th} harmonics. We label the n^{th} harmonic cosine and sine components of Eq. number j as C_{jn} and S_{jn} respectively. When performing the analysis, we must replace powers of cosine and sine by their Fourier components. For example:

$$[\cos s + \sin s]^2 \equiv (\cos s)^2 + 2\cos s \sin s + (\sin s)^2 \equiv (1 + \cos 2s)/2 \ + (\sin 2s) \ + (1 - \cos 2s)/2 \ .$$

The trial form has seven (7) adjustable parameters. In principle, Eq. 0 contains harmonics upto $n = 4$, and Eq. 1 harmonics upto $n = 3$, and Eq. 2 harmonics upto $n = 5$, and Eq. 3 harmonics upto $n = 4$. Hence there are more equations than unknowns. The strategy is to minimize (in fact make equal to zero) the lowest harmonics, and push the error into more rapidly oscillating higher harmonics[4]. Hence, we shall solve the system of equations

$$C_{00} = 0, \ \ C_{11} = 0, \ \ S_{11} = 0, \ \ C_{21} = 0, \ \ S_{21} = 0, \ \ C_{32} = 0, \ \ S_{32} = 0, \tag{4.48}$$

for the vector of unknowns $\mathbf{x} \equiv [m_0, A_x, p_x, A_y, p_y, A_z, p_z]$. The remainder harmonic components C_{jn} and S_{jn} are considered to be errors, which we hope are small. The only way to reduce the errors is to add additional Fourier harmonics to the trial solution. For example, at the next order of precision we must add to Eq. 4.49 the increment $[B_x \cos(3s + q_x), \ B_y \sin(3s + q_y), \ B_z \sin(4s + q_z)]$ with six more adjustable parameters.

The expressions for C_{jn} and S_{jn} are long and complicated; their details are presented in Sec 4.6.2. The set Eq. 4.48 are a system of coupled, nonlinear algebraic equations. They are solved numerically, by Newton-Raphson iteration, for given values of the parameters M, M_z, H_z, h_y, α. It is convenient to use reduced quantities. $g \times H_z$ and $g \times h_y$ have the dimensions of Hz, and so we write them as frequencies. The most economical notation is that they be written in terms of the drive frequency ω. Thus $gH_z \equiv \omega R$ and $gh_y \equiv \omega r$. Evidently $r/R = h_y/H_z$; and this ratio is a measure of the degree of nonlinearity. When $R < 1$, the resonance frequency is below the drive frequency; $R = 1$ corresponds to resonance; when $R > 1$, the resonance frequency lies above the drive frequency.

The behaviour of the system is investigated by setting R fixed, and then systematically varying r over the range $[0, 1]$. The process is repeated for $R > 1$, $R = 1$ and $R < 1$. Typically, A_x, A_y initially rise linear with r, but then plateau[5] at surprisingly small values of r/R. Contrastingly, A_z initially rises quadratic with r, but then rises linear. m_0 initially varies quadratic, then changes sign (opposes M_z), then varies steeply with r, and then plateaus. In the plateau[6] region of r, all amplitudes vary slowly and linearly.

These predictions have been confirmed by direct numerical solution of the LLG equations for the same parameter values. In all cases, the Gilbert damping $\alpha = 0.05$. The numerical integrations were continued until the transient response is completed and the steady-state periodic response emerges. Data from the periodic regime was then Fourier analyzed. Fig. 4.2 for the case $R = 1.2$ compares the analytic values of A_x, A_y, A_z, m_0 against those extracted from numerical simulation. Fig. 4.3 makes a similar comparison for the case $R = 1.0$; note that amplitudes A_x and A_y are indistinguishable and therefore become overlayed. In both these cases, $R = 1.2$ and $R = 1$, the analytic solutions provide good predictions of the response across the entire range $r = [0, 1]$. Fig. 4.4 compares analytic and numerical predictions for the magnetization amplitudes when $(R = 0.8)$ the drive frequency is above the resonance frequency; the agreement is good upto $r = 0.8$, but diverge thereafter.

[4] With the hope that error amplitudes diminish increasingly with harmonic number.

[5] "Plateau" is here used as a verb.

[6] "Plateau" is here used as an adjective.

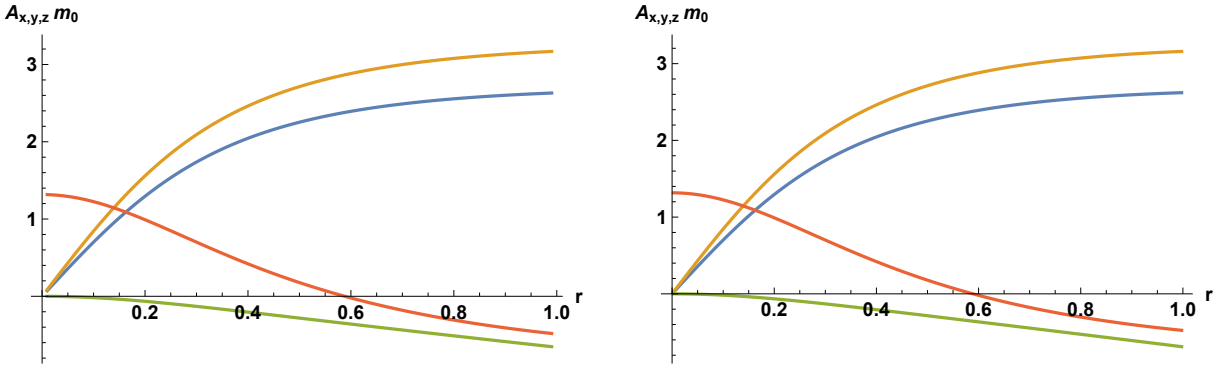

Figure 4.2: Magnetization components (A_x, A_y, A_z, m_0) versus drive amplitude r. Blue $= A_x$, gold $= A_y$, green $= A_z$, coral $= m_0$. Resonance frequency $(R = 1.2)$ above drive frequency. Left: values found by harmonic balance. Right values from numerical simulation.

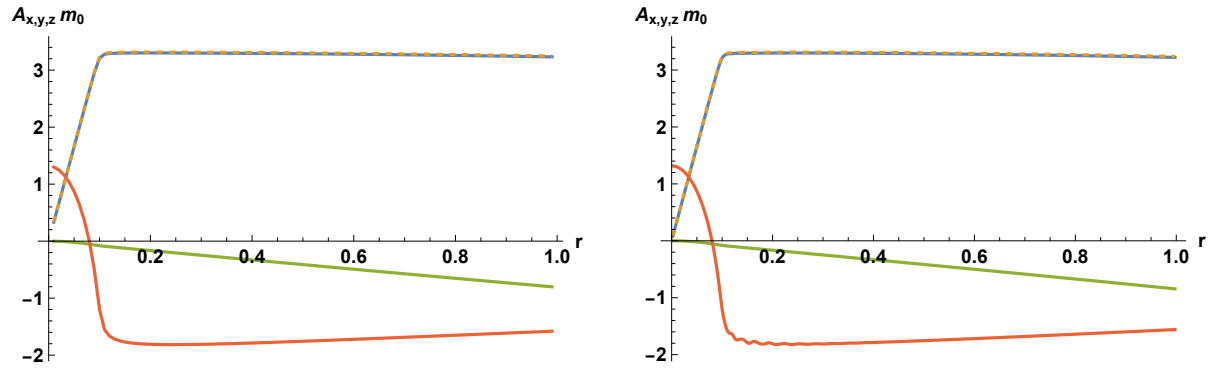

Figure 4.3: Magnetization components (A_x, A_y, A_z, m_0) versus drive amplitude r. Blue $= A_x$, dashed gold $= A_y$, green $= A_z$, coral $= m_0$. Resonance frequency $(R = 1.0)$ equal to drive frequency. Left: values found by harmonic balance. Right values from numerical simulation.

The reader will recall that solution of the linearized LLG Eqn. showed the components m_x, m_y to be proportional to h_y, and to be boosted at resonance. In the nonlinear theory m_x, m_y saturate at surprisingly low values of h_y/H_z; and m_z (which is zero in the linear theory) slowly increases parallel to the magnetic bias field. This has a simple explanation: there is a finite quantity of spin-sites available to be gyrated by the RF drive; when they are all used up, there can be no further increase in the magnetization **m**.

Note that at resonance, Fig. 4.3, saturation sets in at $r \approx 0.1$; whereas when the drive frequency is below (Fig. 4.2), or above (Fig. 4.4) resonance, saturation does not emerge until $r \approx 0.6$ or greater. This is straight forward to explain. For given excitation r, the response is greater at resonance; and so saturation will set in at lower values of r. Contrastingly, the zero response ($A_x \to 0$ and $A_y \to 0$) displayed in the numerical simulation for $R = 0.8$ (Fig. 4.4 Right) is mystifying.

Magnetized cylinder

The cylinder has lower symmetry than the sphere, and so the equation of motion for the magnetic moments is more complicated because there is less opportunity for cancellation between the demagnetiztion terms. It is appropriate to take $n_1 = n_2$. If in addition we insist that the AC and DC demagnetization factors $n_3 = N_3$, the system of equations for the cylinder is 4.44-to- 4.46 with H_z replaced by $H_z + (n_1 - n_3)U_z$ throughout. The method of harmonic balance could be used

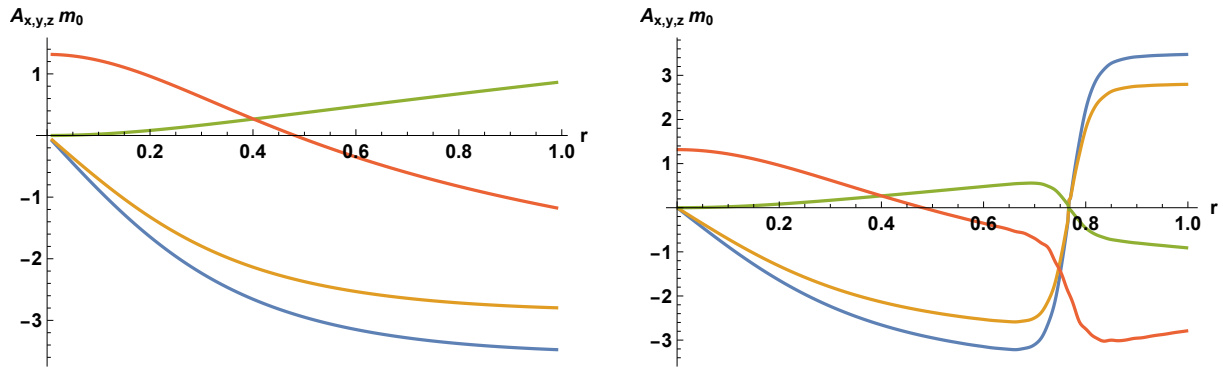

Figure 4.4: Magnetization components (A_x, A_y, A_z, m_0) versus drive amplitude r. Blue $= A_x$, gold $= A_y$, green $= A_z$, coral $= m_0$. Resonance frequency $(R = 0.8)$ below drive frequency. Left: values found by harmonic balance. Right values from numerical simulation.

to find the steady state precession, but we have not done so. But it is evident that there will be an additional periodical modulation, and that the system will display saturation with respect to increase of the RF drive amplitude h_y.

Literature

The results of this chapter, Sec. 4.4.2 and Sec. 4.4.4, and also Sec. 4.6, were derived by the author (Koscielniak) February to April 2025, and not reported elsewhere. Subsequently, it comes to the authors attention that a team[62] from Lanzhou University, China, has also attempted to find an analytical solution of the nonlinear LLG equation for the magnetized sphere with microwave field perpendicular to bias. Their solution contains the fundamental and second harmonic Fourier components; but does not include the DC term m_0 which arises as a subharmonic of the product of 1st and 2nd harmonics. This DC term is an essential feature of the saturation phenomemon that occurs close to and at resonance. In particular, note that that m_0 displays significant variation, and even sign reversal prior to saturation.

Conclusion

The electron spins cannot be more than 100% aligned. Hence there is saturation: we may increase the H-field, but there is no corresponding increase in the magnetization.

4.6.2 Equations for Fourier harmonics

The starting point is Chap. 4.6.1. The LLG Eq. has trial solution:

$$\mathbf{m}(t) = [A_x \cos(s + p_x),\ A_y \sin(s + p_y),\ m_0 + A_z \sin(2s + p_z)] \quad \text{with} \quad s \equiv \omega t\ . \tag{4.49}$$

Equation zero

Eq. zero is the constraint of constant magnitude of magnetization: $0 = [\mathbf{M} + \mathbf{m}(t)]^2 - M^2$. Here $\mathbf{M} = [0, 0, M_z]$. We substitute the trial leading to:

$$0\ = [A_x \cos(s + p_x)]^2 + [A_y \sin(s + p_y)]^2 + [M_z + m_0 + A_z \sin(2s + p_z)]^2\ - M^2 \tag{4.50}$$

We Fourier analyze. The DC component is

$$C_{00} \equiv (A_x^2 + A_y^2 + A_z^2)/2\ + (M_z + m_0)^2\ - M^2\ . \tag{4.51}$$

The 1st harmonic (or fundamental) and 3rd harmonic content is identically zero. The 2nd harmonic components are

$$C_{02} = [A_x^2 \cos 2p_x - A_y^2 \cos 2p_y + 4A_z(M_z + m_0)\sin p_z]/2 \quad (4.52)$$

$$S_{02} = 2A_z(M_z + m_0)\cos p_z + [-A_x^2 \sin 2p_x + A_y^2 \sin 2p_y]/2\ . \quad (4.53)$$

The 4th harmonic components are

$$C_{04} = -(A_z^2/2)\cos 2p_z \quad \text{and} \quad (A_z^2/2)\sin 2p_z\ . \quad (4.54)$$

Equation 1

Eq. one is Eq. 4.44 containing $\dot{m}_x$. We substitute the trial solution and Fourier analyze. The DC, and 2nd and 4th and 5th harmonic terms are automatically zero. The cosine and sine 1st harmonics, respectively, are

$$\begin{aligned} C_{11} &= \omega[-4M(M_z + m_0)r + 4A_x(M_z + m_0)R\alpha\cos p_x - 4A_xM\sin p_x - 2A_xA_yr\alpha\sin(p_x - p_y) \\ &+ 4A_yMR\sin p_y + A_xA_yr\alpha\sin(p_x + p_y) - 2A_xA_zR\alpha\sin(p_x - p_z) - 2A_zMr\sin p_z]/(4M) \quad (4.55) \\ S_{11} &= \omega[-4A_xM\cos p_x + 4A_yMR\cos p_y + A_xA_yr\alpha\cos(p_x + p_y) + 2A_xA_zR\alpha\cos(p_x - p_z) \\ &- 2A_zMr\cos p_z - 4A_x(M_z + m_0)R\alpha\sin p_x]/(4M) \quad (4.56) \end{aligned}$$

The cosine and sine 3rd harmonics, respectively, are

$$\begin{aligned} C_{13} &= [\omega(A_xA_yr\alpha\sin(p_x + p_y) - 2A_zMr\sin p_z + 2A_xA_zR\alpha\sin(p_x + p_z))]/(4M) \quad (4.57) \\ S_{13} &= [\omega(A_xA_yr\alpha\cos(p_x + p_y) - 2A_zMr\cos p_z + 2A_xA_zR\alpha\cos(p_x + p_z))]/(4M) \quad (4.58) \end{aligned}$$

Equation 2

Eq. two is Eq. 4.45 containing $\dot{m}_y$. We substitute the trial solution and Fourier analyze. The DC, and 2nd and 4th harmonic terms are automatically zero. The cosine and sine 1st harmonics, respectively, are

$$\begin{aligned} C_{21} &= \omega[-2(A_x^2 + A_z^2 + 2(M_z + m_0)^2)r\alpha - 4A_xMR\cos p_x + 4A_yM\cos p_y \\ &+ \alpha(-A_x^2 r\cos 2p_x + 2A_yA_zR\cos(p_y - p_z) + 4(M_z + m_0)(A_yR\sin p_y - A_zr\sin p_z))]/(4M) \quad (4.59) \\ S_{21} &= \omega[4A_y(M_z + m_0)R\alpha\cos p_y - 4A_z(M_z + m_0)r\alpha\cos p_z + 4A_xMR\sin p_x \\ &+ A_x^2 r\alpha\sin 2p_x - 4A_yM\sin p_y + 2A_yA_zR\alpha\sin(p_y - p_z)]/(4M) \quad (4.60) \end{aligned}$$

The cosine and sine 3rd harmonics, respectively, are

$$\begin{aligned} C_{23} &= -[\omega\alpha(A_x^2 r\cos 2p_x + A_z(-A_zr\cos 2p_z + 2A_yR\cos(p_y + p_z) + 4(M_z + m_0)r\sin p_z))]/(4M) \quad (4.61) \\ S_{23} &= [\omega\alpha(A_x^2 r\sin 2p_x - 2A_zr\cos p_z(2(M_z + m_0) + A_z\sin p_z) + 2A_yA_zR\sin(p_y + p_z))]/(4M) \quad (4.62) \end{aligned}$$

The 5th harmonic components are:

$$C_{25} = +[A_z^2 r\omega\alpha/(4M)]\cos 2p_z \quad \text{and} \quad S_{25} = -[A_z^2 r\omega\alpha/(4M)]\sin 2p_z\ . \quad (4.63)$$

Equation 3

Eq. three is Eq. 4.46 containing $\dot{m}_z$. We substitute the trial solution and Fourier analyze. The 1st, 3rd and 5th harmonic terms are automatically zero. The DC component is

$$C_{30} = [\omega(2A_xMr\cos p_x + \alpha(-2(A_x^2 + A_y^2)R + A_yA_zr\cos(p_y - p_z) + 2A_y(M_z + m_0)r\sin p_y))]/(4M) \quad (4.64)$$

The cosine and sine 2nd harmonics, respectively, are

$$\begin{aligned} C_{32} &= \omega[A_xMr\cos p_x - A_x^2 R\alpha\cos 2p_x + 4A_zM\cos p_z \\ &+ A_y\alpha(A_yR\cos 2p_y + r\sin p_y(M_z + m_0 + A_z\sin p_z))]/(2M) \quad (4.65) \\ S_{32} &= \omega[-A_xMr\sin p_x + A_x^2 R\alpha\sin 2p_x + A_yA_zr\alpha\cos p_z\sin p_y \\ &+ A_y\alpha\cos p_y((M_z + m_0)r - 2A_yR\sin p_y) - 4A_zM\sin p_z]/(2M) \quad (4.66) \end{aligned}$$

The 4th harmonic components are:

$$C_{34} = -[A_y A_z r\omega\alpha/(4M)]\cos(p_y + p_z) \quad \text{and} \quad S_{34} = +[A_y A_z r\omega\alpha/(4M)]\sin(p_y + p_z)\ . \tag{4.67}$$

Expressions $C_{00}, C_{11}, S_{11}, C_{21}, S_{21}, C_{32}, S_{32}$are used to determine $\mathbf{x} = [m_0, A_x, p_x, A_y, p_y, A_z, p_z]$. Expressions $C_{02}, C_{04}, C_{13}, S_{13}, C_{23}, S_{23}, C_{25}, S_{25}, C_{30}, C_{34}, S_{34}$ are all treated as errors.

Chapter 5

RF Permeability of Ferrites

In this article we discuss the permeability and hysteresis and saturation properties of ferrites for applications in the frequency range 100 kHz to 100 MHz. The article on near-DC permeability and hysteresis in Chap. 1.5 was simplistic and naive; several important aspects were not even mentioned.

- The major hysteresis loop (performed near DC) may be taken in a single B-H quadrant (either upper right or lower left), or taken concentric with the origin $(B, H) = (0, 0)$; and the magnetization changes considerably between them. Likewise, minor loops will differ depending on the parent major loop. Thus the choice of a unipolar or bipolar current source for the bias can have an appreciable impact on μ_Δ. For instance, μ_Δ at the remanent field B_r has a rather different value if the bias is unipolar instead of bipolar. Hysteresis loop models are reviewed by Mörée and Leijon[16].
- It is simply not possible for a hysteresis cycle performed in a quasi-static manner to display resonance behaviour. Therefore relying on the near-DC behaviour can be misleading. In fact, phenomena such as domain-wall vibration and ferro-magnetic-resonance (FMR) occur when the magnetic fields oscillate.
- Although the energy to drive a magnetic material through a hysteresis cycle is proportional to the area enclosed by the B-H curve, the dissipative effect is not immediately apparent for near-DC variation of H. Contrastingly at kHz and beyond, there is obvious heating and phase-lag when the material is driven hard by a sinusoidal oscillation. The description of this effect requires the concept of permeability to be broadened to a complex quantity; this was encountered in Chap. 4.5.3.
- Symmetric oscillatory magnetic fields alone, or superposition of DC and oscillatory fields were not considered. With drive fields of this type, there arises frequency dependence and the influence of magnetic bias; and also consideration of the relative orientation of DC and RF field components.
- The major hysteresis loops depend on temperature. Thermal agitation tries to randomise the orientation of the microscopic magnetic domains. At any temperature above absolute zero, it is not possible to align all the domains. The fraction (which is a statistical quantity) which cannot be aligned increases with temperature, until at the Curie[1] temperature the cooperative effect of interacting magnetic moments is overcome and magnetization is lost. Thus at higher temperature, the saturation values of M and B are lower.
- Permeability depends also on mechanical stress and the RF amplitude.

We now elaborate these more sophisticated aspects of permeability.

[1]Named after French physicist and radiochemist Pierre Curie (1859-1906), the co-discoverer of polonium and radium. His collaborator was polish-born Madame Marie Curie, née Marya Sklodowska. In addition, with older brother Paul-Jacques, he was co-discoverer of piezo-electricity.

5.1 Incremental permeability

The usual B-H hysteresis curve is measured quasi-DC: the cycle around the loop is taken at kHz frequencies in automated procedures; and much more slowly if completed manually. But this measure of permeability $B/(\mu_0 H)$ is irrelevant to RF variation of the H-field.

The aspect of permeability that is relevant to the speed of an electromagnetic wave (travelling in a medium) is the change of the magnetic induction (B) arising from a change in magnetization (M) in response to a change in magnetic field (H). Because of hysteresis, the relation between B and H is non-linear. And, therefore, the (DC) absolute permeability ratio $B/(\mu_0 H)$ is irrelevant to calculating the speed of an EM wave in the ferrite. Moreover, the differential permeability dB/dH taken tangential to the DC hysteresis curve is not precisely the measure of permeability for calculating the wave speed. *Hysteresis is inescapable.* There is an energy barrier to changes in magnetization; and there will be a configuration lag between $\Delta\mathbf{H}$ and $\Delta\mathbf{M}$ that always leads to a B-H minor loop when H is made to dither up and down. Thus, a small forward and back variation $\pm\Delta H$ leads off the major loop[2] of the hysteresis curve onto a minor loop. The minor loop has the (relative) incremental permeability given by $\mu_\Delta = \Delta B/(\mu_0 \Delta H)$. This incremental value is the quantity relevant to computing the wave speed; and it varies with the frequency, amplitude and polarization ($\parallel$ or $\perp$) of the oscillation. The name *reversible permeability* is sometimes given to the incremental permeability in the limit of vanishingly small AC or RF amplitude. The minor loop is composed of two branches: a lower for $dH/dt > 0$ and an upper for $dH/dt < 0$. In detail, the value of μ_Δ is slightly different for each branch. By convention, the incremental permeability is taken to mean the average of the two branches. At low frequency, for parallel bias, this average value is approximated by the local value of $\partial B/\partial H$ on the parent (DC) major loop.

If evidence be needed for the disconnect between differential and incremental permeability, it is the FMR which yields permeability in the saturated regime vastly different from the differential of the B-H curve, and that depends on field orientation.

5.1.1 Naming and notation

The incremental μ_Δ and RF permeability μ_r are different names/notations for essentially the same dynamical permeability: it depends on temperature, DC bias, frequency, RF amplitude, respective orientation of bias and RF components, and can be represented by a complex quantity which accounts for the dissipative property. The different symbols seem to have arisen from history and an individual authors wish to stress one dependence over the others. Thus μ_Δ tends to be used for the real part of the parallel-to-parallel component of μ_r at low frequency < 10 MHz. And often μ_r is taken to mean the signal-level value, as if there was no dependence on amplitude ΔH.

5.2 Magnetic-bias dependence

We remind the reader that in the unmagnetized state, the material is a vast number of microscopic magnetic domains (of various sizes) randomly oriented. Magnetization proceeds by growth in size of some domains (at the expense of others) and by their rotation into alignment, which necessitates the movement and destruction of domain walls. Both mechanisms are always present, but which of them is more dominant varies with the degree of magnetization. Rotation following growth is the norm.

Away from saturation, and in the absence of resonance, the same processes (growth and rotation) occur in an AC minor loop as occur in the next increment along a major loop; and so μ_Δ is well approximated by the tangent $\partial B/\partial H$ to the major loop. In this regime, there is little difference between parallel and perpendicular biasing. Typically, the range of DC to a few MHz is resonance

[2]The main loop carries the material from one saturated state to the opposite (in polarity) state.

free. At higher magnetization, differences between biasing will be come evident. For parallel bias at low frequency, incremental μ_Δ continues to be approximated by the differential $\partial B/\partial H$. For perpendicular bias at low frequency, μ_Δ is approximated by $1 + M_z/H_z$ where M_z is the saturation magnetization. It is for this reason that some authors (e.g. Smythe[97]) suggest the parallel and perpendicular components of incremental permeability are $\mu_\parallel = \partial B/\partial H$ and $\mu_\perp = B/H$, respectively. However, it must be understood that the frequency must be low; and further that the AC/RF amplitudes must be sufficiently small that $B(H)$ can be treated as locally linear.

5.3 Major-loop dependence

The value of $\mu_\Delta = \Delta B/(\mu_0 \Delta H)$ depends on the parent major loop, and therefore on the history of the quasi-DC magnetization. The shape of the major loop differs greatly depending on whether the current source (producing the magnetizing field) is unipolar or bipolar. The bipolar source is capable to exercise the hysteresis curve through all four quadrants, yielding full forward ($H > 0$) and full reversed saturation ($H < 0$). The B-H curve, and the corresponding differential permeability $\partial B/\partial H$ is sketched in Fig. 5.1.

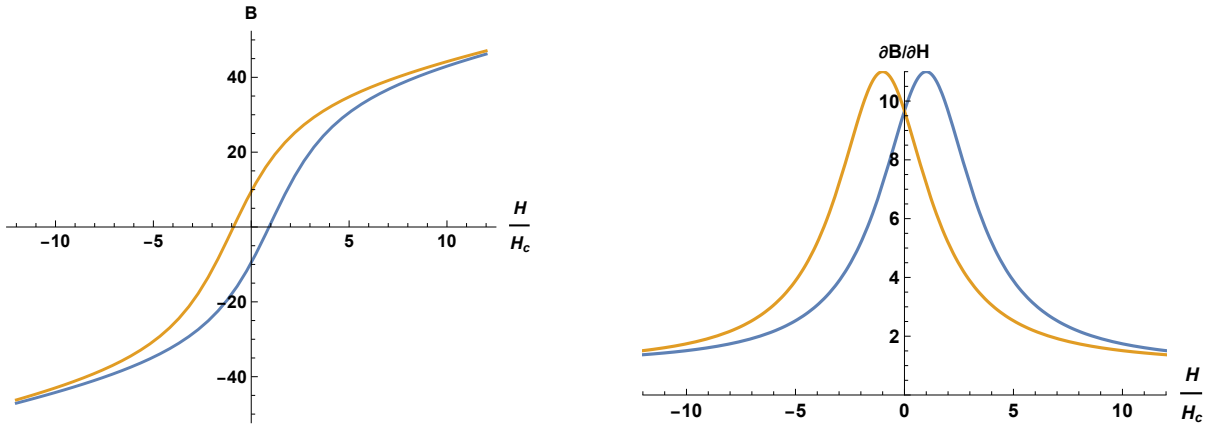

Figure 5.1: Hysteresis and differential permeability for magnetic material with bipolar bias-current supply. Left: $B(H)$. Right: $\partial B/\partial H$. The forward path $dH/dt > 0$ is shown blue. The reverse path $dH/dt < 0$ is shown gold.

The unipolar current source cycles the magnetization in a single quadrant only; suppose it is the region $H \geq 0, B > 0$. The upper branch of the major loop emanates from full saturation, when the time derivative $dH/dt < 0$, and moves toward the remanent value $(B, H) = (B_r, 0)$. The lower branch emanates from the remanent value, when the time derivative $dH/dt > 0$, and follows a different path with slightly smaller magnetization than the upper branch; until finally saturation is achieved again. In the vicinity of $(B, H) = (B_r, 0)$, the path from upper to lower branch is reminiscent of a particle colliding with an object and then recoiling. Thus the B-H trajectory when the drive speed dH/dt changes sign without the magnetic field passing through saturation is called a recoil path. Consider now the variation of the differential permeability along the upper and lower branches. The derivative is continuous (same-valued) at the extreme of saturation. But the derivative $\partial B/\partial H$ is discontinuous at the recoil point, larger on the descending branch and smaller on the ascending branch (for this particular quadrant). The recoil point is that at which the time variation dH/dt changes sign - when the material is not in saturation. The effect is sketched in Fig. 5.2.

This example of the unipolar major loop reveals that the essence of the hysteresis is branching. The effect is general, not just reserved for the remanent point. Whenever the sign of dH/dt is reversed, there is a recoil path; so a path that never enters saturation but cycles through all four

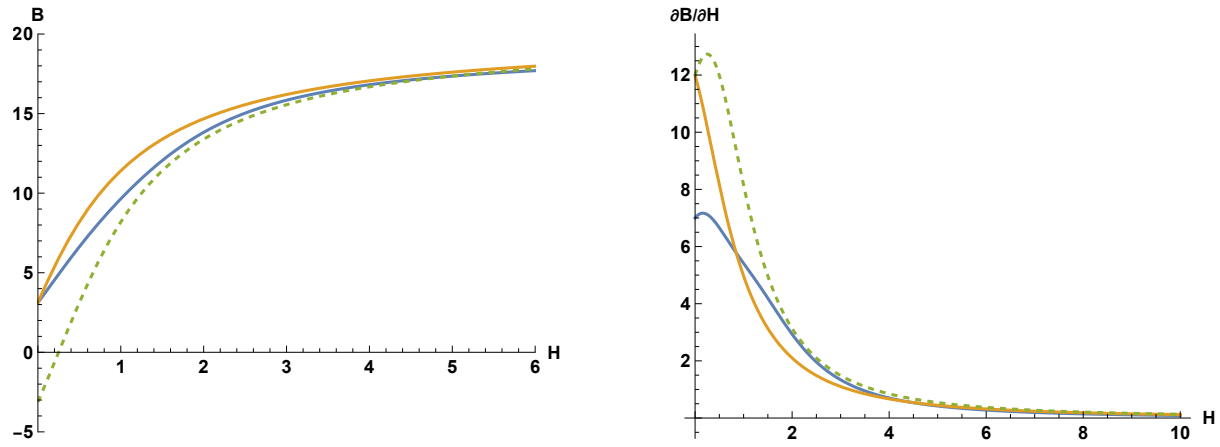

Figure 5.2: Hysteresis and differential permeability for magnetic material with unipolar bias-current supply. Left: $B(H)$. Right: $\partial B/\partial H$. The reverse path $dH/dt < 0$ is shown gold. The forward (or recoil) path $dH/dt > 0$ is shown blue. For comparison, the forward path starting from negative saturation (and passing through negative $|B_{\rm rem}|$) is shown green-dashed.

quadrants has two recoil points, at opposite ends of the loop.

5.4 Frequency dependence

Frequency dependence emerges when the magnetization cannot respond sufficiently quickly to a change in drive field H. The exchange interaction (EI) and crystal anisotropy determine the magnetization within a single domain. The EI is essentially instantaneous, and so does not participate in dynamical/relaxation effects. The crystal anisotropy gives rise to an intrinsic resonance: certain directions within a crystal having large effective field can provide an axis for spin precession. However, this occurs at very high frequency, in the tens of GHz.

Magnetization proceeds by rotation of domains and/or the movement of domain walls so that some grow at the expense of others. These mechanisms are not instantaneous, and therefore we should expect some frequency dependence when an AC or RF magnetic field is present alone (without bias). Furthermore, rapid cycling around a minor loop provides the opportunity for domain wall vibration and resonance. Depending on the ferrite composition, there is a low frequency regime (a few tens MHz) where the incremental permeability is almost (or roughly) constant, followed by an intermediate regime (roughly 10-100 MHz) where the permeability begins to drops rapidly and the material becomes lossy (mostly) due to the domain wall resonance. Thus the permeability must be described by a complex quantity $\mu_r = \mu' + i\mu''$ whose imaginary part μ'' accounts for losses. For the spinel ferrites, the losses start to rise above 0.1 MHz, peak around 10 MHz and then fall again; becoming negligible above 100 MHz. For the garnet ferrites, the onset of losses is delayed to about 1 MHz. In the absence of bias field, the spinel (Mn-Zn and Ni-Zn) and YIG ferrites show similar properties - except that both components of μ_r are about one hundred times smaller for the garnets. Examples are shown in Figs. 5.3 and 5.4. The behaviour does not change much at small values of the bias. Of course, if the material is biased toward saturation, the FMR will become evident and strong differences between the frequency dependence of $\mu_{\|}$ and $\mu_{\perp}$ will emerge. The spinel and garnet ferrites both display an FMR, but it is more pronounced for the latter as shown in Fig. 5.5.

The log-log scale and the vast range of frequency in these plots may give the illusion[3] that it is the frequency dependence of μ_r' that limits their use to below (roughly) 10 MHz. However,

[3]Logarithms compress values greater than unity, but they stretch fractions less than one.

the variation when plotted on a linear scale is quite modest: ferrites with a near-DC permeability μ_r less than a few hundred display a relative change $\mu_r(f)/\mu_r(0)$ of less than 10 percent over the first 10 MHz. Actually, it is the rise of μ_r'' toward a maximum around 10 MHz, and the resulting reduction of the magnetic quality factor $Q_m = \mu'/\mu''$, that limits the ferrites use to approximately 10 MHz or less.

Although the losses diminish rapidly towards 100 MHz, two factors curtail ferrite use in that frequency region: (i) the permeability is significantly smaller; and (ii) cavity size above 100 MHz is already reasonable. So 10 MHz and below would be the end of the road for ferrite-loaded cavities, if it were not for perpendicular biasing - which offers high magnetic Q above 30 MHz (but at the cost of more complicated bias-field geometry).

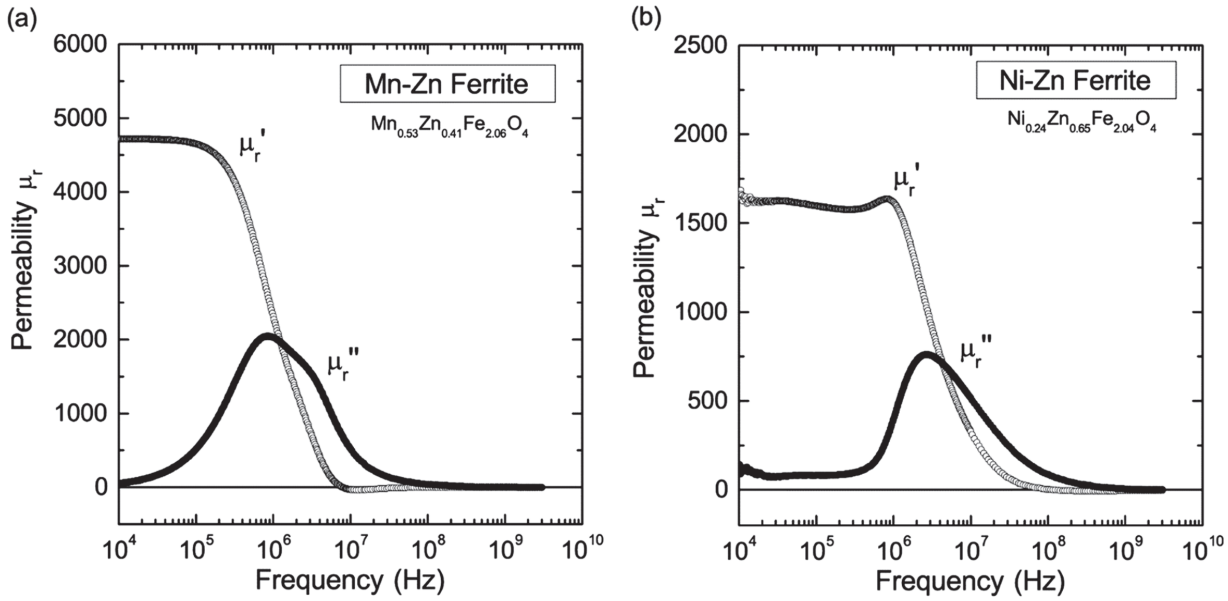

Figure 5.3: Permeability spectra of spinel ferrites (a) Ni–Zn ferrite and (b) Mn–Zn ferrite under zero external field; adapted from Ref. [105].

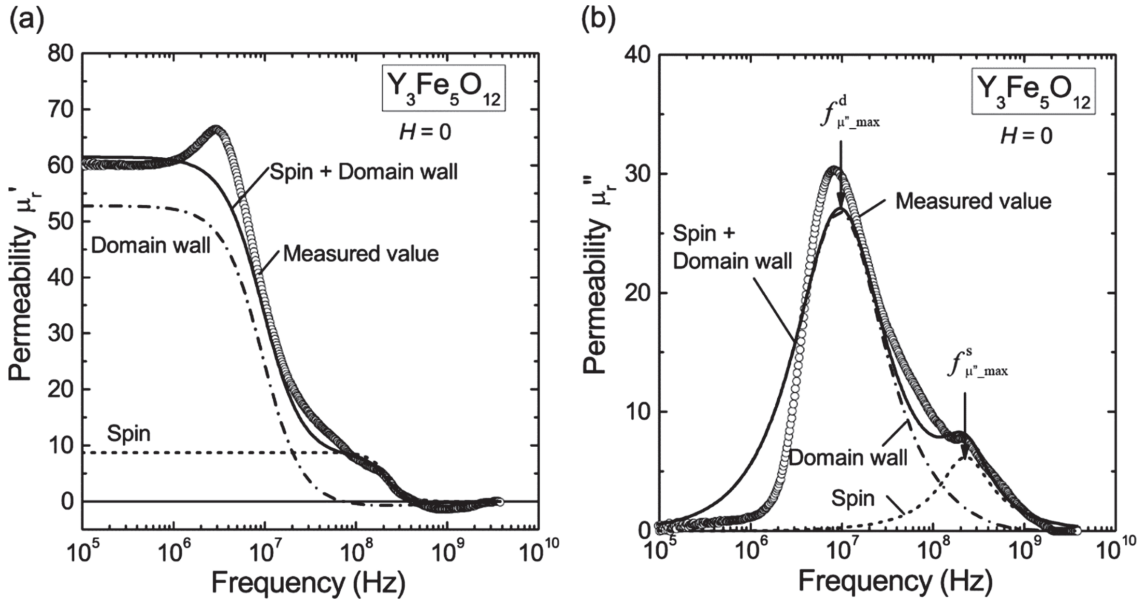

Figure 5.4: Permeability spectra of YIG under zero external field; adapted from Ref. [106].

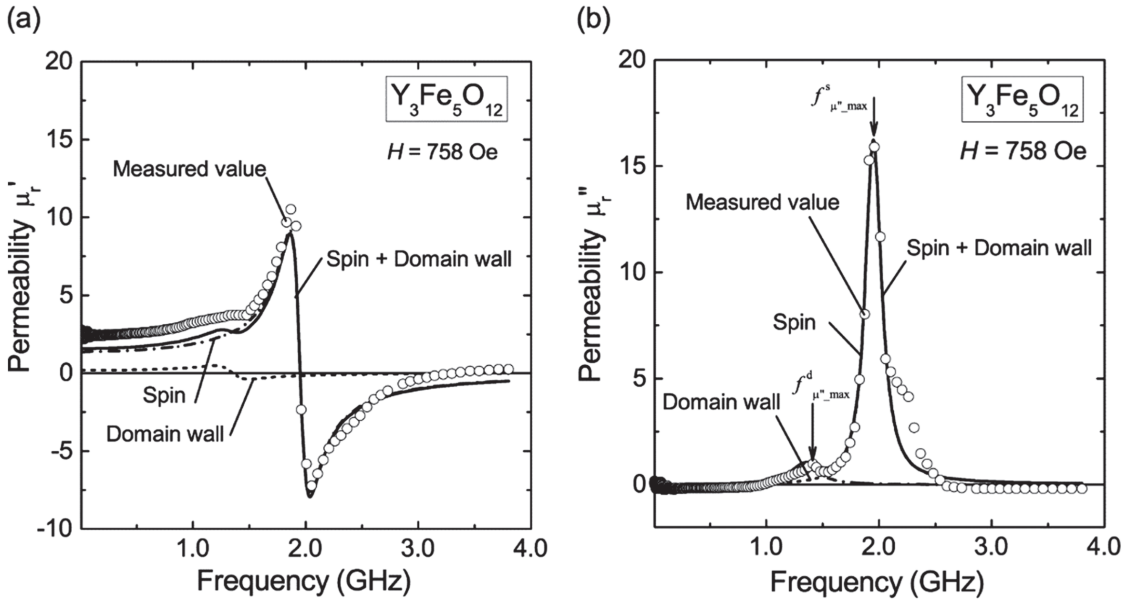

Figure 5.5: Permeability spectra of YIG under 758 Oe external field; adapted from Ref. [106].

5.4.1 Snoek's law

The shape of the permeability curves versus frequency, in the absence of magntic bias, is similar across a range of ferrite material compositions and grades. However, the frequency at which the material's dynamic magnetic properties start to diminish is in inverse proportion to the static permeability. This observation is known as Snoek's law[67]. The law does not describe the material property, rather it sets an upper bound on the properties a material may posses. Snoek's law is the envelope of possible material properties. The law is $\mu_r' = C/f$ where C is a constant and f is RF. If RF is in MHz, then C is roughly 10^4. In a log-log plot, Snoek's law is a straight line with slope equal -1, as in Fig. 5.6. The figure also sketches the individual properties of some hypothetical materials. These are phenomenological curves of the form $\mu_r'(f) = A_i \exp[-B_i \times (f\,A)_i^n]$ where A_i, B_i, n_i are individual material constants. Obviously $A = \mu_r'(f=0)$ for a particular material. For the Fig. 5.6, the B_i are similar but not identical; and the power law index $n = 1.5$. (If the index is varied over the range $n = [1, 2]$, there is little change to the plot except the slope as $\mu_r \to 1$.)

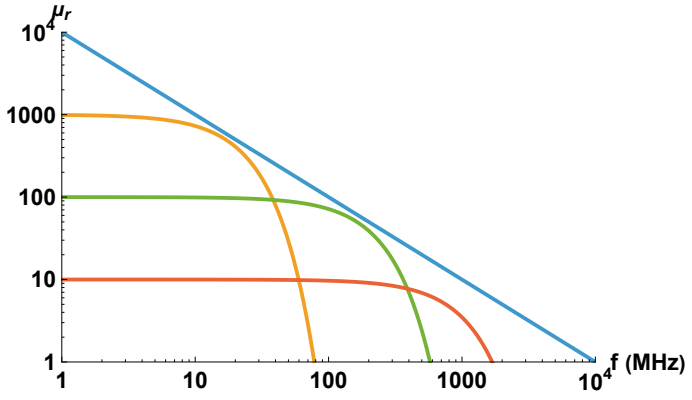

Figure 5.6: Snoek's law, the upper bound, is shown blue. Individual material properties are shown gold, green and coral.

In fact, if B and n are held fixed, and A is varied this will generate a family of curves such that their gradient at the knee frequency is equal to that of the Snoek's curve C/f. The locus of

the μ'_r values at the respective knee frequencies is parallel to the Snoek curve. Let us demonstrate this property. Let $Y = \ln(C/f) = \ln(C) - \ln(f)$ and $X = \ln(f)$. The log-log gradient of the Snoek curve is $dY/dX = -1$ and the intercept $Y(f=1) = \ln(C)$. Let $Z = \ln[A\exp[-B \times (A\,f)^n]]$ be the logarithm of permeability. Then the log-log gradient of permeability is $dZ/dX = -B(A\,f)^n$. The knee frequency f_k is the solution of $dY/dX = dZ/dX$, namely $A \times f_k = 1/(B \times n)^{(1/n)}$. This value is substituted into Z yielding $Z(f_k) = \ln(A) - 1/n$. The envelope of the points $[X(f_k), Z(f_k)]$ lies on a line $y(f) = \ln(c) - \ln(f)$ where $0 < c < C$ is to be determined. Evidently $y(f_k) = Z(f_k)$; and this may be solved for $c = \exp(-1/n)(B \times n)^{(-1/n)}$. Thus the envelope of curves $\mu'_r(f)$ with differing initial permeability A share precisely the same intercept $\ln(c)$ at $f = 1$, and the value of c depends only on the family parameters B and n. Although there is no materials science underlying the form $\mu'_r(f) = A\exp[-B \times (f\,A)^n]$ where $A = \mu'_r(f=0)$, we speculate that curve fitting of the five grades of Ferroxcube 4A-4E shown in Brockman[77] Fig. 13 would have similar values of B and n.

5.5 Orientation dependence

The relative orientation of the DC and RF magnetic components plays a role in the incremental permeability. The B-H curve assumes that all fields (H,M,B) are always parallel. The fields are vectors, and so the quantities $\mathbf{H} + \Delta\mathbf{H}$, $\mathbf{M} + \Delta\mathbf{M}$ and $\mathbf{B} + \Delta\mathbf{B}$ must each be added vectorially. If the fields are parallel, the addition is straight forward. If the fields are perpendicular, $\Delta\mathbf{M}$ is in a different direction to $\mathbf{M}$. If the ferrite is far from saturation, the crystals/domains have a large variety of orientations and enough them will always follow $\Delta\mathbf{H}$ to give a semblance of the incremental μ of the B-H curve. However, near saturation the number of sites available to be aligned is different for a $\Delta\mathbf{H}_\perp$ versus a $\Delta\mathbf{H}_\parallel$. Fortunately, the saturated regime is also that for which we have a simple theory, the Landau-Lifshitz-Gilbert theory of FMR, which predicts how the incremental susceptibility and permeability differ depending as the RF magnetic field is parallel or perpendicular to the bias. In principle, the reversible permeability can be different for parallel verus perpendicular orientation of the AC or RF magnetic field component.

5.5.1 Approximate dual dependence $\mu_r(H, \nu)$

Although incremental permeability is a function of applied DC field and the EM wave frequency, it is customary to present is properties as one or the other is varied but not both. However, due to the behaviour of ferrites (encapsulated by Snoek's law) it follows that over a limited frequency range, the dominant variation in $\mu_\Delta(\nu, H)$ is that due to the bias field. Thus, for parallel bias, from DC to audio frequencies, permeability is approximated by $\mu_0\mu_\Delta = \mu'_r(\nu=0)\partial B/\partial H$ where $B(H)$ is some class of major hysteresis loop. Further, for materials with moderate (i.e. not excessive) DC relative permeability (say up to several hundred), the roll-off (reduction) in permeability is not severe; and so the dual dependence upto a few MHz can be approximated by the product

$$\mu_0\mu_\Delta = \mu'_r(\nu)|_{H=0} \times \partial B/\partial H|_{\nu=0}\ . \tag{5.1}$$

For given DC permeability, Snoek's law provides an indication of the knee frequency, $\nu_k = C/\mu'_t(0)$, up to which Eq. 5.1 is useful. Better still, given experimentally measured data, the knee frequency is that at which $d\ln[\mu_r(\nu)]/d\ln(\nu) = -1$. Above the knee frequency, incremental permeability μ_Δ is not necessarily estimated by the product of the individual dependencies.

5.6 Measurement of RF permeability

The method of measurement depends on the frequency range. Above 1 GHz, material samples may be placed inside a terminated waveguide of practical size, and excited by an RF wave of known polarization. An external large dipole magnet is rotated about the waveguide to produce parallel or perpendicular bias. The material properties are inferred from reflection and transmission coefficients. The calculation depends only on the dimensions of the rectangular waveguide and the spherical specimen, and so the inference is direct. Details of this measurement type are given in Refs. [54, 65, 104].

Below 1 MHz, waveguide size is prohibitive but a lumped-element approach is possible for high permeability materials. A ferrite core is wound with excitation and sensing windings[4]; and the core may be biased either parallel by an additional winding or perpendicular by placing the core between the pole pieces of a dipole electro-magnet.

The frequency range of roughly 10–100 MHz, is problematic. Material properties are inferred from the properties (resonance frequency and quality factor) of full size cavity prototypes with and without the ferrite; and with the appropriate magnetic biasing. Toward the lower end of the frequency range, the cavity resonance may be mathematically modeled by an LCR circuit. The inference of material parameters then becomes model dependent.

5.6.1 Network permeability

Klingbeil[81] develops a simple mathematical model[5] for the resonance property of a ferrite-loaded quarter wave cavity. He begins with Maxwell's equations and ends with a lumped-element LCR resonator whose element values are related to the components of the complex permeability. In brief: the capacitance C is dominated by that of the accelerating gap. So large is the permeability, that the inductance is dominated by the ferrite cores even if they do not fill the entire volume. So large are the core losses that they dominate over the ohmic loss in the cavity metallic walls. There are N cores of thickness T and inner/outer radius ratio ρ. The cores are characterised by $\Gamma \equiv [N \times T/(2\pi)] \ln \rho$. Klingbeil takes a circuit with two parallel arms, one containing the capacitance, and the other the inductance L_s and resistance R_s in series. The impedance of the inductive arm is

$$Z_s = j\omega L_s + R_s \quad \text{where} \quad L_s = \Gamma\mu' \quad \text{and} \quad R_s = \omega\Gamma\mu'' \,. \tag{5.2}$$

Evidently, R_s and L_s are related according to $R_s = \omega L_s/Q$ where the quality factor of the cores is $Q = \mu'/\mu'' \equiv 1/\tan(\delta)$. The total admittance of the two arms is $Y = (1/Z_s) + j\omega C$.

It is important to note that when the complex permeability is formed from network measurements, it is the reflection and transmission coefficients that are measured. The permeability becomes a *calculated* quantity and ceases to be a *bona fide* property of the material. The permeability becomes a property of the electrical network; and changes if the network model changes. Thus, if the series-LCR model is substituted by a parallel-LCR model, the values of the complex permeability components will change. Klingbeil is aware of this issue, and provides an alternative formulation for the parallel-LCR impedance. The relations between parallel and series components, subscripted p and s respectively, are as follows:

$$R_p/R_s = (\omega L_p)(\omega L_s) = R_s^2 + (\omega L_s)^2 \tag{5.3}$$

$$Q \equiv \frac{\omega L_s}{R_s} = \frac{\mu_s'}{\mu_s''} = \frac{R_p}{\omega L_p} = \frac{\mu_p''}{\mu_p'} \tag{5.4}$$

And thus $\mu_p' = \mu_s'[1 + 1/Q^2]$ and $\mu_p'' = \mu_s''[1 + Q^2]$. Evidently, formulated this way, the permeability components and the network model become inseparable; another network would result in different values.

[4] Below $\simeq 1$ MHz, it is legitimate to excite the ferrite with a cable winding, but not at much higher RF.

[5] The same model as Brockman.

5.6.2 Ferrite data tables

Manufacturer's data tables (for example Philips[71, 72]) of ferrite properties may contain the following measured magnetic properties/values:

- the initial (DC) permeability (i.e. in the virgin or demagnetized state)
- the B-H curve measured quasi-DC and at a few kHz
- the incremental permeability (as function of H) measured quasi-DC and at a few kHz
- the frequency dependence of μ' and μ'' measured either in the virgin state or in the remanent state. The frequency range is typically DC to 10 MHz (or less).
- At the customer's request, the manufacturer may measure the incremental permeability (at signal level) as a function of bias for a prescribed fixed RF.

The commercial catalog tables usually contain temperature dependence, the Curie temperature and other physical properties such as resistivity and dielectric constant. The types of data required for accelerator applications is so specialist that it is essential to make measurements $\mu_r(H, \nu)$ for the specific ferrite variety and intended bias and frequency range; and not to rely on the limited manufacturer's data.

Chapter 6

Magnetically Biased Ferrites for RF Cavity Tuning

"The practical achievement of modern magnetic ferrites was announced just 10 years ago. They are ceramic-like materials, with permeabilities ranging up to several thousand combined with specific electrical resistivities over a million times those of metals... It is intriguing to consider this modern ferrite as a rebuilt version of lodestone, the first magnetic material discovered by man...
The advantages of the combined high permeability and high resistivity announced[66] by the Philips Company in 1946 were apparent immediately to engineers." C. Dale Owens[41], October 1956.

6.1 Prologue

The behaviour of magnetic materials, and their explanation, is the domain of condensed matter theory. The detailed properties of ferrites is the speciality of ferrite technology. Neither is the usual province of accelerator physics, so we have introduced the physical principles that underlie ferrite properties in the preceding chapters: classical magnetism, demagnetization factors, permeability and hysteresis in Chap. 1; the magnetic field of toroidal windings mounted on an annular solenoid in Chap. 2; the quantum explanation of magnetism, including the contributions to the effective field, and the spinel and garnet lattice structure of ferri-magnets in Chap. 3; the Landau-Lifshitz-Gilbert equations for the precession of spin magnetic moments in Chap. 4; and the incremental permeability behaviours of Ni-Zn and YIG ferrites at frequencies up to 100 MHz in Chap. 5. Throughout the text, there are sprinkled historical references.

6.2 Article structure

We begin with a statement of the problem: the need for tuning and the need to shrink RF cavity size. In certain circumstances, ferrites answer this problem. We introduce the relationship between cavity resonance frequency and incremental permeability. Followed by the individual theory of resonance tuning by parallel and by perpendicular magnetic bias. We describe implementations of biasing using current carrying coils and windings. After a brief discussion of the conditions under which Ni-Zn or YIG, and parallel or perpendicular bias, is employed there follow literature reviews exploring the development of these tuning methods: (i) the use of parallel-biased spinel ferrites employed at relatively low radio frequency; and (ii) the use of perpendicular-biased garnet ferrites employed at higher RF frequency. Finally, there is a discussion and explanation of the nonlinear behaviour observed at high RF field in the presence of perpendicular bias.

6.3 Introduction

Metallic cavities, resonant at radio-frequency, are used to accelerate charged particles such as electrons and protons. This article contrasts two types of resonance tuning: (1) parallel bias of spinel ferrites; and (2) perpendicular bias of garnet ferrites. Bias refers to the imposition of a DC magnetic field that establishes a preferential direction for alignment of the magnetic spins. Parallel versus perpendicular refers to the orientation of an RF magnetic field with respect to the bias field. "Tuning" means to bring the resonance frequency into coincidence with the drive frequency. Although ferrites are employed in both types of tuning, the physics of each is very different. This article is not about RF cavity design and engineering, rather it serves to contrast the two types of tuning.

All orientations are equal until the bias field is applied. Therefore, we should say the RF field is parallel or perpendicular to the bias. However, the technological application usually has a specific orientation for the RF component; in which case the bias direction becomes the secondary consideration. Thus the vernacular phrasing has become "the bias is parallel or perpendicular to the RF field".

6.3.1 Motivation

Particle acceleration results in higher kinetic energy and speed. Provided that the orbit in the synchrotron does not change, both the orbital speed and frequency increase monotonically. The cavity drive frequency must be perfectly matched to an integer multiple of the particle revolution frequency. If the particles accelerate, there will be a programme of values drive-frequency versus time called a *frequency law*; and the cavity resonance must be tuned to follow this law. Ferrite offers an electro-magnetic means to tune an RF cavity that is faster and wider ranging than can be achieved by electro-mechanical tuning (cavity deformation or variable capacitors).

6.3.2 Narrow versus wide band resonator

Narrow-band copper cavity resonators have quality factor in the range $\simeq 10^3$ to $\simeq 10^4$, and can achieve high fields with moderate power requirements. Wideband resonators have quality factor in the range $\simeq 1$ to $\simeq 100$, and are very lossy. Tuning of the resonance frequency is a requirement for narrow band resonators. Contrastingly, a wideband cavity may have resonance sufficiently broad to encompass the entire frequency law without tuning. Following their successful introduction[68] at the Japan Proton Accelerator Research Complex (J-PARC), wideband magnetic-alloy (MA) filled cavities are considered a useful alternative to ferrite-loaded resonators. For example, MA cavities were employed[69] at the CERN Low Energy Ion Ring (LEIR) to cover the frequency range $0.35 - 5$ MHz without tuning. The very thin magnetic alloy tapes wound into cores offer permeability ten times higher than ferrites, and lead to very compact cavity designs. However, the topic of MA materials and cavities is outside the scope of this article.

6.3.3 Transit time factor

If the RF cavity frequency is too high, the electric field may reverse during the transit time of the particle across the accelerating gap, resulting in no nett acceleration. This effect is quantified by the transit time factor $T \equiv \sin(\tau)/\tau \approx 1 - \tau^2/6$ and $\tau = \omega L/(2v)$ where ω is angular frequency, L is gap width, and v is the particle speed. If the speed is too low, as occurs for non-relativistic particles such as low energy protons or heavy ions, the frequency must be lowered. The non-relativistic regime is also that in which increasing kinetic energy is associated with rising speed. So low frequency and the need for frequency tuning go hand in hand. Contrastingly, for relativistic particles (whose speed approaches that of light), transit times are quick and there is almost no change in speed. In this case, high frequency cavities with little or no tuning may be used.

6.3.4 Ferrites in a nutshell

Ferrites are special materials that have both high magnetic permeability and high electrical resistivity. The magnetic properties of both ferro- and ferri-magnetic materials are due to spin magnetic moments (SMM). The ferro-materials have one SMM per crystallographic unit cell. The ferri-materials have two (or more) interpenetrating lattices that result in two SMMs in their (complicated) unit cell; the two magnetic moments are oppositely oriented but unequal, resulting in an nett SMM for the cell. Ferrites are micro-crystalline ceramics, made by sintering iron oxide with metals such as Mn, Ni, Zn or the rare earths (Y, La, etc), possessing significant magnetic properties due to the over-expressed spin magnetic moments of electrons on the external shell of the atoms of these metals.

Ferrites for parallel bias

The general composition of the Philps Ferroxcube ferrites is $Me_\delta Zn_{1-\delta}Fe_2O_4$ where Me represents one of the divalent metals magnesium (Mg), manganese (Mn), or nickel (Ni). Ferroxcube materials starting with digit 2, 3, 4 have Me equal to Mg, Mn, Ni, respectively. We are interested principally in the series 3 (III) Ni-Zn ferrites. The original papers describing these materials and their properties were co-authored by Went and Gorter[75, 76]. However, the respective chemical compositions are not given because this is Philips proprietary commercial information. Although the Mn-Zn ferrites have permeability of order 10 times higher than Ni-Zn, the Mn-Zn varieties are not suitable because they have resistivity up to 10^4 times smaller resulting in dissipation due to eddy currents.

6.3.5 Tuning and shrinking

Actually, ferrite has two possible functions in an RF cavity: (i) to make the cavity tunable, and (ii) to shrink the cavity size (make it smaller or shorter) by inserting a volume of ferrite inside the cavity. This second use is particularly important at low RF (a few MHz or less). For a given oscillation frequency the wavelength in a material with high magnetic permeability is shorter than in free space (i.e. vacuum). The fundamental mode of an RF cavity resonator coincides with one quarter (or one half) wavelength fitting exactly inside the cavity. The frequency at which this occurs varies with permeability (and permittivity) of the material inside the cavity. Thus we desire materials with high permeability at RF frequencies. Soft/hard magnetic materials have high/low permeability. Although ferro-magnetic materials (such as iron, nickel, cobalt) have very high permeability, they are metallic; and the conduction electrons impede an EM wave from propagating within the material. Contrastingly, ferri-magnetic materials have large permeability and are insulators; and an EM wave may easily penetrate into the interior and propagate.

The basis for one method of cavity tuning is to vary the permeability of ferrite by applying a DC biasing magnetic field. Typically there is a region in the cavity where the peak (in time) electric field is largest, and another region where the peak magnetic field is largest; the ferrite is located in the latter. Ferrites constitute a large class of materials, but we focus on only two varieties. So-called nickel-zinc (Ni-Zn) ferrite has a spinel structure; it is a soft magnetic material suited both to tuning and to shrinking cavity size. Ni-Zn may be the only practical choice to make a small high-Q RF cavity in the range from 0.3-10 MHz. Ni-Zn ferrite is used across a large range of (parallel) bias and not toward saturation. The so-called yttrium-iron garnet ferrite (YIG) has a garnet structure. It is a less-soft magnetic material well suited to tuning, but the shrinkage of cavity size is less (only a factor 2 to 4) because the permeability is relatively small. YIG has the advantage of lower RF losses. So YIG becomes useful at higher frequency; say 30 MHz upward. The yttrium-garnet tuning uses the FMR that occurs at high magnetic bias.

6.3.6 FMR in a nutshell

The ferro-magnetic resonance (FMR) occurs expressly for materials in the saturated magnetic state, at the top or bottom of the B-H hysteresis curve, wherein all mechanisms for increased magnetization are exhausted except spin alignment and precession. When the bias, the spins and RF-magnetic field are parallel, the spins do not participate in the incremental magnetization; and so the relative permeability is exactly unity. When the the bias and RF-magnetic field are perpendicular, the relative permeability is greatly boosted by a resonance because the RF field exerts a periodic torque on the spins. The resonance frequency is set by adjusting the bias field. The permeability has a lossy component which is largest on resonance; and so the the RF of the EM wave is chosen near *and below* the FMR.

6.3.7 RF waves in media

The speed of a wave is equal to the product of frequency and wavelength. The wavelength of a cavity mode comes from that of the cavity (internal) dimensions. It would seem therefore, that the frequency (for fixed cavity size) can be lowered if the wave speed is reduced. The speed of an EM wave depends on the inverse square root of the product of dielectric and diamagnetic constants (that measure permittivity and permeability respectively) of the medium that the wave travels through. Thus, if either or both constants can be raised, the wave speed is slowed and the resonance frequency falls. This reasoning is correct, but an over simplification.

The wave is composed of photons. Being massless particles, photons always travel at the speed of light (in vacuum) - with no exception (because their speed is a property of space time). Actually the wave in a medium is a collective that slows down, even though its constituent photons do not. The photons are continuously absorbed and re-emitted by the atoms or molecules that make up the medium through which the wave travels, giving an appearance that the wave speed is slowed. The same effect can be derived from a Huygens' construction in which each atom scatters part of the wave; and when the parts recombine, the net wave-front moves more slowly. Feynman[70] explains in one of his famous lectures how the wave passage through a material is slowed down by the collective effect of all the atomic/microscopic fields. He describes the effect for a dielectric, but the explanation also holds for a diamagnetic. Of course, there are differences: dielectrics typically do not display hysteresis, and Feynman's exposition does not include electric or magnetic biasing (or amplitude dependence). In this simple case, the wave propagation speed is $c = 1/\sqrt{\mu_0 \mu_r \epsilon_0 \epsilon_r}$.

6.3.8 Relation of permeability to tuning range

Simplistically, the cavity resonance frequency $\nu \propto c/\lambda$ where λ is wavelength, and the wave speed is $c = 1/\sqrt{\mu_0 \mu_\Delta \epsilon_0 \epsilon_r}$ where μ_Δ is the incremental permeability, the permeability at RF in the presence of a bias field. Consider the initial and final values of ν before and after particle acceleration. The required range of incremental permeability is

$$\frac{\text{Max}[\mu_\Delta]}{\text{Min}[\mu_\Delta]} \;=\; \frac{\text{Initial}[\mu_\Delta]}{\text{Final}[\mu_\Delta]} \;=\; \frac{\nu^2_{\text{final}}}{\nu^2_{\text{initial}}} \;> 1\;. \tag{6.1}$$

Notice that the initial value is greater than the final value; and μ_Δ is a monotonic falling function of time during the particle acceleration. This has implications for the time variation of the bias H.

At each point on the DC hysteresis curve, the incremental permeability (for a minor loop) is different. Since H-field is generated by currents, one speaks of a bias current that is applied in order to shift the operating point to higher induction B leading to a lower incremental permeability and longer wavelength. In order for the wave to fit inside the cavity, the frequency must be raised. Hence rising bias field is associated with increasing cavity resonance frequency. This is true of both parallel and perpendicular bias. For the latter, raising the bias pushes the FMR further away from

the cavity drive frequency thereby moving the operating point into a region of lower incremental permeability.

6.3.9 Practicalities

A material with (relative) RF permeability range $\mu_\Delta = [1, 4]$ has exactly the same fractional tuning range as a material with permeability range $\mu_\Delta = [1, 4]\times 10^3$ if the material fills the cavity. However, the cavity volume is much less for the second material. Very large RF permeability is needed only when cavity shrinking is important. If tuning is the only requirement, then small values of RF permeability can be sufficient.

The length/diameter L of a vacuum-filled cube, sphere or quarter-wave-coaxial resonator is roughly $L \approx c/(4\nu)$ for the fundamental resonance frequency ν. For ν equal 100 MHz and above, the cavity size is under a metre, which is easily practicable; and there is no strong reason to shrink it; and a ferrite with $\mu_\Delta = [1, 4]$ would be adequate. Contrastingly for frequency below 1 MHz, the cavity size would be 100 metres which is impractical. Such a cavity has to be shrunk; it is filled with a high permeability ferrite $\mu_\Delta = [1, 4] \times 10^3$ (or similar).

In the intermediate regime of 5–50 MHz, one may choose to use smaller/larger volumes of high/low RF permeability ferrite, or use ferrites with moderate (relative) permeability a few tens or hundreds. In all cases, the choice is influenced by dissipation; ferrites are lossy and the energy absorbed in a cycle about a minor or major hysteresis loop is proportional to the area of the loop.

6.3.10 Measured dual dependence $\mu_\Delta(H, \nu)$

For accelerator applications, it is essential to make measurements $\mu_r(H, \nu)$ for the specific ferrite variety and intended bias and frequency range; and not to rely on the limited manufacturer's data. Ideally, the property is tabulated as a function of both variables. Further, the ferrite shape and bias arrangement of the test object should be the same as that in the final application so that they share the same geometry-dependent demagnetization factor. The dual dependence is measured by EM excitation of the ferrite, and sensing of the response as the AC or RF frequency is varied. Typically a network analyzer is used, and network theory used to extract μ_r from transmission and/or reflection measurements. If the procedure is repeated at different magnetic bias, the the dual dependence of incremental permeability $\mu_\Delta(\nu, H)$ may be constructed. Studies of this type, spanning small to large bias, are reported by Vollinger and Caspers[107, 111] for perpendicular, and by Klopfer[84] for parallel bias.

Another approach (post-dictive) is to build a mock-up[1] or prototype of the cavity and perform signal level measurements in which the cavity resonance frequency and quality factor are measured as a function of bias field. Measurement of the resonance with the ferrite removed allows to infer the permeability contributed by the ferrite.

6.3.11 Calculating bias field from frequency

The cavity drive frequency must be perfectly matched to an integer multiple of the charged particle revolution frequency around the synchrotron. If the particles accelerate, there will be a programme of values drive-frequency versus time called a *frequency law.* The magnetic bias field must track a corresponding program of values. Thus we wish to find the bias field (law) that makes the cavity resonance frequency $\omega_{\rm res}$ and drive frequency equal. Now $\omega_{\rm res}$ is a function of the incremental permeability, which in turn is a function of the resonance frequency and DC bias. This recursive relationship has to be found/solved self-consistently. We shall illustrate by a crude example. Suppose ω_c is the RF cavity resonance frequency without ferrite. If filled with ferrite, the frequency

[1] This could be plywood or stiff cardboard covered in copper sheets.

becomes:

$$\omega_{\rm res} = \omega_c / \sqrt{\mu_\Delta[H, B(H), \omega_{\rm res}]} \tag{6.2}$$

This is a nonlinear equation that is solved iteratively for bias as a function of frequency, $H(\omega_{\rm res})$. The magnetisation is a function of the bias and material history given by the DC hysteresis curve (B, H), or equivalent DC permeability curve, for a defined history. For compactness, we drop the subscript "res", and simply write ω.

Eq. 6.2 expresses a relationship between ferrite geometry, biasing field and resonance frequency. If the ferrite fills a small fraction of the cavity volume, and the in-vacuum cavity fields are known, then perturbation theory and Slater's theorem may be used to give an improved estimate.

6.4 Magnetic biasing

Suppose DC bias and RF magnetic fields are applied to a ferrite material; these fields penetrate to the interior. In addition there is an interior field due to magnetization of the ferrite. Suppose the DC bias magnetic field and that of the applied RF electromagnetic wave have the same orientation in space; this is called parallel bias. Contrastingly if the RF magnetic field is orthogonal to the DC bias, this is called perpendicular bias. Usually it can be assumed that the magnitude of the bias is much larger than that of the RF field. In the context of tuning an RF cavity resonator as follows. For parallel biasing, we use the properties of the B-H hysteresis curve and incremental permeability that occur well below saturation. For perpendicular biasing, we use the dynamical properties of the ferrite that occur on the B-H hysteresis near (or at) saturation. Parallel biasing and the properties of spinel-ferrite limit their use to the frequency range around 0.1-10 MHz, appropriate to synchrotrons with low harmonic number. Perpendicular biasing and the properties of garnet-ferrites limit their use to frequencies above 30 MHz. The upper limit is in the GHz range, because the FMR is moved by the bias. However, the demand for tunable cavities above 100 MHz is limited. The transit time factor implies that high frequency can only be employed for relativistic particles, for which no frequency swing is needed.

6.4.1 Bipolar versus unipolar bias current supply

The choice of bias current supply and major hysteresis loop go hand in hand. The tuning range achieved under parallel bias relies on the large incremental permeability that occurs far from saturation. Unfortunately, this happens to be the region where the ferrite is most lossy; the energy dissipation is much reduced in saturation. The largest range of permeability occurs when the ferrite is exercised between the full negative and positive saturation; and demands a bipolar current source. For synchrotrons with a relatively low injection energy, such as those described by Brockman[77], this bipolar cycle may be a necessity. However, an acceptable range of permeability may result from cycling B-H (in a single quadrant) between the remanent and saturated inductions; and this may be achieved with a unipolar current source - which is simpler and less expensive. Klingbeil[81] advocates for this type of B-H cycle. In this case, a lower remanent field is an advantage. Modern machines, having higher energy injection (linear accelerators), can perform adequately with a unipolar source. In either case, uni- or bi-polar, passing through saturation is essential to making the B-H cycle repeatable. For the bi-polar case, the requirement for $\partial B/\partial H$ to be monotonic increasing, implies the particle acceleration occurs above the coercive value H_c.

The tuning range achieved under perpendicular bias relies on the FMR, which occurs near and at saturation. The saturated portion of the B-H curve differs very little whether a uni-polar or bi-polar current source drives the bias field. Economy suggests to use the uni-polar source.

Although only a portion of the B-H curve is used to tune the cavity while the charged particles are accelerated, nevertheless the ferrite must be exercised through the entire B-H loop in order to prepare the initial condition for the next acceleration period. This has two implications: (i) the

bias current supply must be capable to source the entire range of H; and (ii) the ferrite variety is chosen to have a sufficiently small saturation value of H that excessive demands are not placed on the bias current source.

The current carrying coils and windings that produce the bias field and the ferrite cores comprise large inductances. There is a back-e.m.f $V = LdI/dt$ that opposes changes of the bias field. Whether or not the current variation is bipolar, the over-voltage from the power supply must be bipolar because the field is made to rise and then to fall. In the case of fast-cycling booster synchrotrons, with tens of Hz repetition frequency, the demands for over voltage can be challenging.

6.5 Theory of parallel bias tuning

The mathematical analysis of cavity tuning with parallel bias is model dependent. Moreover, there is no simple model for the major hysteresis loop when the bias winding is driven by a uni-polar current source. Therefore, we cannot state a generalised theory. Instead, we have an illustrative example that relies on a symmetric bipolar current source.

We assume that the vacuum-filled RF cavity has resonance angular frequency ω_c. We now suppose that the cavity volume is filled with ferrite, and that we wish to find the H-field that will give the new resonance frequency $\omega < \omega_c$. In the regime of parallel bias, we may approximate the permeability by the product of the bias dependence (at low frequency) and the frequency dependence (at zero bias) from DC to a few MHz. We take the frequency dependence to be linear: $\mu_r(\omega)/\mu_r(0) = [1 - \beta\omega/\omega_c]$ where $0 < \beta < 1$ is a normalised dimensionless variable. $\beta = K/(\mu_r(0)/\omega_c)$ where $K = (\partial\mu_r/\partial\omega)$ is the ferrite material property as $\omega \to 0$. For the magnetic bias, we assume operation on the major hysteresis loop cycled by a bipolar current source between full negative and positive saturation. The charged particle acceleration takes place while the ferrite magnetization is in the the upper-right quadrant of the B-H curve. The dependence of permeability on bias field is modeled by the B_1 type, F_2 variety mathematical model of Sec. 1.5.5, namely:

$$B_1/\mu_0 = M_s(2/\pi)\arctan[(\pi/2)a(H/Hc\ -1)]\ + (H - H_c)\ . \tag{6.3}$$

M_s is the saturation magnetization. The value of a adjusts the remanent field $B_r/\mu_0 = \pm[H_c + M_s(2/\pi)\arctan(a\pi/2)]$. F_2 is chosen because it has a simple derivative. The incremental permeability is

$$\mu_\Delta = \frac{1}{\mu_0}\left(\frac{\partial B}{\partial H}\right)(1 - \beta\,\omega/\omega_c) = \left[1 + \frac{aM_s/H_c}{1 + (a\pi/2)^2(H/H_c\ -1)^2}\right](1 - \beta\,\omega/\omega_c)\ . \tag{6.4}$$

Eq. 6.4 is substituted into Eq. 6.2, and solved for the drive field H in terms of the resonance frequency which we shall write in the form $\omega = \alpha\omega_c$. The equation is a quadratic in H with solution:

$$\frac{H}{H_c} = 1 + \frac{2}{a\pi}\sqrt{-1 + \left(\frac{aM_s}{H_c}\right)\left[\frac{\alpha^2(1-\alpha\beta)}{1-\alpha^2(1-\alpha\beta)}\right]}\ . \tag{6.5}$$

The radicand, the contents of the square root operation, must be greater than or equal zero for real solutions. If the frequency dependence is small, $\beta \ll 1$, we may find the limits on the tuning range:

$$\sqrt{\frac{H_c}{H_c\ + a\,M_s}}\ \leq\ \alpha\ <\ 1\ . \tag{6.6}$$

Evidently, the range is large if $a \times M_s \gg H_c$. This implies two desirable conditions: first $M_s \gg H_c$, and second that the remanent field B_r/μ_0 is a large fraction of M_s, because a and B_r are related. In fact, this is not surprising - because if B_r is large, the initial permeability is larger.

The shape of the curves $H(\alpha)$ changes from concave to convex according to the value of β. The gradient $\partial H/\partial\alpha$ is zero at $\alpha = 2/(3\beta)$. This stationary point may be moved outside of the range $\alpha = [0, 1]$ by selecting $\beta < 2/3$. If β exceeds this value, then $H(\alpha)$ becomes dual valued.

Ferrite fractional filled cavity

If the ferrite fills only a fraction $0 \leq F \leq 1$ of the cavity volume, the tuning equation becomes $\omega_{\rm res} = \omega_c/\sqrt{(1-F) + F \times \mu_\Delta(\omega_{\rm res})}$. Again we substitute Eq. 6.4, and solve for the required bias field:

$$\frac{H}{H_c} = 1 + \frac{2}{a\pi}\sqrt{-1 + \left(\frac{a\,F\,M_s}{H_c}\right)\left[\frac{\alpha^2(1-\alpha\beta)}{1-\alpha^2(1-\alpha\beta\,F)}\right]}\,. \tag{6.7}$$

When $\beta \to 0$, the tuning range becomes Eq. 6.6 with aM_s replaced by aFM_s.

6.5.1 Example

Suppose that we wish to both tune an RF cavity and shrink its size. Suppose the tuning range is $1-2$ MHz. Further suppose there is an existing geometry for a relatively compact vacuum-filled cavity with 10 MHz resonance frequency. We intend to load the interior volume, excluding the vacuum/beam pipe, with ferrite to achieve a ten times lower resonance frequency. Imagine there are seven types of ferrite available with $\gamma \equiv M_s/H_c$ values ranging from 50 to 3200. Which of these ferrites is acceptable? The left-hand plot in Fig. 6.1 shows the result of evaluating formula 6.5 for $a = 1, \beta = 0.1$ as a function of $\alpha = \omega/\omega_c$ for seven values of γ. Focus on the range $\alpha = [0.1, 0.2]$. 1 MHz can be achieved for $\gamma \geq 200$. However, some of the H/H_c values are very close to one; which corresponds to zero magnetic induction. Such an operating point is subject to slight variability, cycle to cycle, and to stray magnetic fields from other sources. Therefore, a larger value of H/H_c is required, suggesting $\gamma \geq 10^3$.

The choices $a = 1$ and particularly $\beta = 0.1$ were somewhat arbitrary. Greater realism can be introduced for β. From Snoek's law, we know that the knee frequency (signalling steep decline) is inversely proportional to the static permeability, which in turn is roughly proportional to $\gamma = M_s/H_c$. Hence we may construct $\beta(\gamma)$. Using realistic material properties for the range 0-10 MHz, $\beta(\gamma) \simeq 2.6 \times 10^{-4}\gamma$. The right-hand plot in Fig. 6.1 shows the result of evaluating formula 6.5 for $a = 1, \beta(\gamma)$ as a function of α for the seven values of γ. It does not change the previous conclusion to adopt a ferrite with $\gamma \geq 10^3$. However, it does suggest that the required bias range H/H_c is slightly smaller. The effect would be more important if we had selected a 1-4 MHz (or higher) tuning range. Incidentally, it is noted that $\beta(\gamma = 3200) = 0.8364$ which exceeds the critical value $\beta = 2/3$, above which $H(\alpha)$ back-bends into a convex arc.

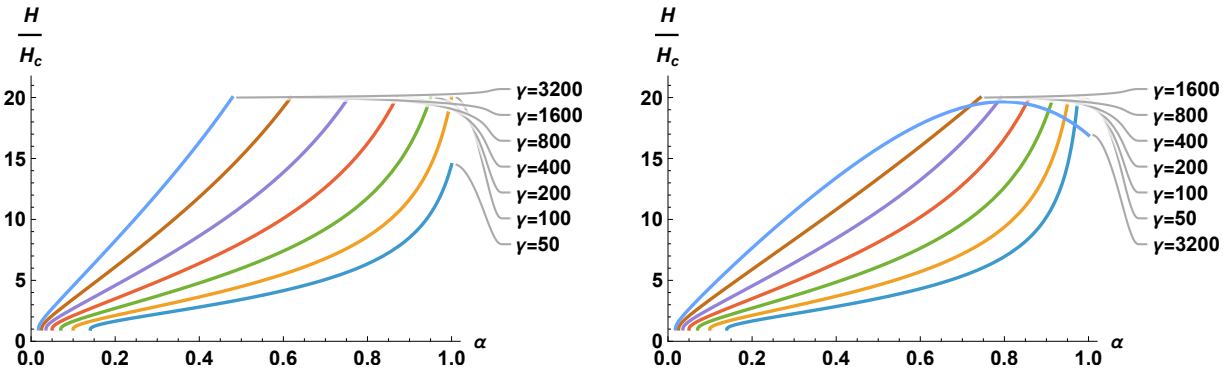

Figure 6.1: Parallel bias tuning program H/H_c versus fractional frequency $\alpha = \omega/\omega_c$ for a variety of $\gamma \equiv M_s/H_c$. Left: Adjustable constant $\beta = 0.1$. Right: Linear frequency coefficient $\beta = \beta(\gamma)$.

6.6 Theory of perpendicular bias tuning

In the particular regime of perpendicular bias, we may appeal to the LLG equation to give the frequency dependence of $\mu_\Delta = 1 + \Re[m_y/h_y]$. We remind the reader that the LLG equation and the form of the effective field $H_{\rm eff}$ used here assumes that the material is near saturation (M almost independent of H) and that the static values H_z and M_z are mutually self-consistent. Note also that the ratio of M_z/H_z is different for an H up-sweep towards saturation versus an H down-sweep away from saturation; the latter is larger because M_z lags. In Chap. 4.5.3 we encountered the (linearized) incremental susceptibility for a cylinder or sphere aligned with H_z. The formulae are:

$$\begin{aligned} \text{Inphase}[m_y/h_y] &= \Re[\chi_{yy}] = g^2 M_z H_z[\omega^2(-1+\delta^2) + g^2 H_z^2(1+\delta^2)^2]/D & (6.8)\\ \text{Quadrature}[m_y/h_y] &= \Im[\chi_{yy}] = g M_z \omega\delta[\omega^2 + g^2 H_z^2(1+\delta^2)]/D & (6.9)\\ D &= \omega^4 + 2(gH_z\omega)^2(-1+\delta^2) + (gH_z)^4(1+\delta^2)^2\ . & (6.10)\end{aligned}$$

Here H_z is the effective field including the demagnetization factor. Even though the LLG equation was formulated to explain a resonance at multi-GHz frequencies, the formulae work quite well down into the kHz range. $\mu_\Delta \to 1 + M_z/H_z$ as $\omega \to 0$. This may be larger than the initial permeability μ_i because μ_i is taken on the virgin magnetization curve in the vicinity of $(B,H) = (0,0)$ rather than on a major loop passing through $(-B_r, 0)$ and $(0, +H_c)$.

Eq. 6.8 is substituted into Eq. 6.2. In principle, this leads to a quartic equation for the bias $H_z(\omega)$. We know that $\delta \ll 1$. Suppose for the moment that we set $\delta = 0$. The bias equation simplifies to a quadratic:

$$\frac{\omega}{\omega_c} = \left[\frac{H_z(H_z+M_z) - (\omega/g)^2}{H_z^2 - (\omega/g)^2}\right]^{-1/2}\ . \qquad (6.11)$$

Remember that $g \times H$ has the dimensions of angular frequency. We could rewrite the field values in terms of equivalent frequencies; but it is better to express the frequency in terms of an equivalent H-field value. The natural reference for frequency is ω_c, and for field it is M_z. Choosing the cavity frequency as a reference leads to M_z becoming a variable. But the saturation magnetization is a material property, a constant. So M_z is taken as the "standard unit". We set $\omega = \alpha\omega_c$ and $\omega_c = \beta \times (gM_z)$. The ferrite loaded value is less than the vacuum-filled value; and so $0 < \alpha < 1$. The solution of the quadratic is:

$$\frac{H_z}{M_z} = \frac{\alpha^2[1 + \sqrt{1 + 4(1-\alpha^2)^2(\beta/\alpha)^2}]}{2(1-\alpha^2)}\ . \qquad (6.12)$$

The cavity operation frequency must be below the gyromagnetic frequency, and so $\alpha\beta M_z < H_z$; this implies $\alpha < 1/\sqrt{2}$. Suppose there is an upper limit on the bias $H_z < \gamma M_z$ where $0 < \gamma < 1$. We may find an upper limit on the vacuum-filled cavity frequency $\omega_c = (gM_z)\beta$.

$$0 < \alpha < \frac{1}{\sqrt{2}} \quad \text{and} \quad 0 < \beta < \sqrt{\gamma\left[\frac{1}{\alpha^2 - 1} + \frac{\gamma}{\alpha^2}\right]}\ .$$

The tuning range is progressively limited to smaller values of α as β rises or γ falls. The properties of ferrite imply $\gamma \ll 1$.

Ferrite fractional filled cavity

If the ferrite fills only a fraction $0 \le F \le 1$ of the cavity volume, the tuning equation becomes $\omega_{\rm res} = \omega_c/\sqrt{(1-F) + F \times \mu_\Delta(\omega_{\rm res})}$. Again we substitute Eq. 6.8, and solve for the required bias field:

$$\frac{H_z}{M_z} = \frac{\alpha^2 F[1 + \sqrt{1 + 4(1-\alpha^2)^2\beta^2/(\alpha F)^2}]}{2(1-\alpha^2)}\ .$$

Suppose there is an upper limit on the bias $H_z < \gamma M_z$. The upper limit on the vacuum-filled cavity frequency, $\omega_c = (gM_z)\beta$, is given by

$$0 < \alpha < \sqrt{\frac{\gamma}{F+\gamma}} \quad \text{and} \quad 0 < \beta < \sqrt{\gamma\left[\frac{F}{\alpha^2-1} + \frac{\gamma}{\alpha^2}\right]}\,.$$

6.6.1 Magnetic quality factor

The magnetic quality factor Q_m of the ferrite material is the per cycle energy stored divided by the energy dissipated; and is given by

$$Q_m = \frac{\mu'}{\mu''} = \frac{1+\Re[\chi_{yy}]}{\epsilon+\Im[\chi_{yy}]} \approx \frac{[(gH_z)^2-\omega^2][g^2H_z(H_z+M_z)-\omega^2]}{\epsilon\times[(gH_z)^2-\omega^2]^2 + gM_z[(gH_z)^2+\omega^2]\omega\delta}\,. \tag{6.13}$$

Strictly speaking $\epsilon \equiv 0$; however, the need for it will be come apparent. Q_m evaluated in the DC limit $\omega \to$ becomes $(1+M_z/H_z)/\epsilon$. Thus ϵ regularizes Q_m to evade the singularity at $\omega = 0$. In practise, the ratio of measured values of μ', μ'' at low frequency is very large; and therefore $\epsilon \ll 1$ and can be omitted (set to zero) when Q_m is evaluated in the MHz range and above. The quality factor becomes zero at two values of angular frequency ω equal gH_z and $g\sqrt{H_z(H_z+M_z)}$.

6.6.2 Example

Suppose we employ a garnet ferrite with saturation magnetization 800 Oersted (63662 A/m). The equivalent frequency $gM_z/(2\pi)$ is 2.24 GHz. Suppose that we wish to use a vacuum-filled cavity with 200 MHz resonance frequency. The equivalent field is $H_c = 71.4$ Oersted (5682 A/m). Suppose that we fill the cavity with ferrite, and wish operate it over the range 40-100 MHz. What is the range of bias field required? We evaluate Eq. 6.12 with $\beta = H_c/M_z = 0.08925$ and α ranging over $[0.2, 0.5]$. The results are plotted in Fig. 6.2.

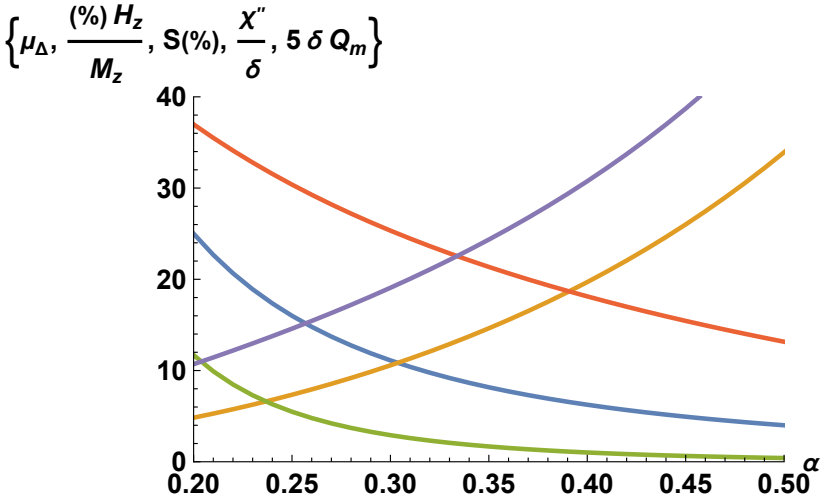

Figure 6.2: Perpendicular bias tuning program versus fractional frequency $\alpha = \omega/\omega_c$. μ_Δ shown blue; H_z/M_z as percentage shown gold; $S = \alpha\beta/(H_z/M_z)$ as percentage shown coral; $\chi''_{yy}/(\delta)$ shown green; and $5 \times Q_m\delta$ shown purple.

The parameter S was introduced in Chap. 4.5.3. For values $S < 1/2$ the real component of the complex susceptibility χ is almost independent of the loss parameter $\delta = \alpha_G \times (M_z/M)$ where α_G is the Gilbert damping factor. Thus the calculation has been self-consistent: we presumed $\delta = 0$, and we have found a solution regime where a non-zero value of δ would make no difference to the

solution values. This is always the case when $\beta \ll 1$. Contrastingly, if $\beta \simeq 1$ or larger, as is the case if we had chosen a large value for ω_c, the permeability, bias field and S-values and FMR power losses all grow to large values.

It is noteworthy that the magnetic quality factor appears to rise with cavity resonance frequency. Contrastingly, at fixed bias field, we know Q_m to be largest at low frequency. The explanation is that we have plotted $Q_m(\alpha, H_z)$; and both α and $H_z(\alpha)$ vary in order to satisfy Eq. 6.12.

6.7 Geometry of ferrite and bias current conductors

Suppose the cavity resonator is of the coaxial type formed of concentric metallic cylinders with disc shaped end plates. The length of the cylinder is a quarter wavelength. The charged-particle beam travels through/along the inner cylinder. The inner cylinder stops before one end plate leaving a (accelerating) gap where the electric field is largest. The magnetic field encircles the inner metallic tube. The concentric ferrite load is usually made up from several cores[2]. Ferrite cores (dough-nut shape) encircle the inner cylinder and are immersed in the EM-field. The cores look like thick discs penetrated by a central hole. The cavity geometry and ferrite load is sketched in Fig. 6.3.

Current-carrying conductors generate a DC magnetic field which biases the cores. For parallel bias, the conductor links through all the cores and is wound about them forming a toroidal surface. This configuration drives an azimuthal magnetic field which encircles the inner metallic tube; this field is parallel to the RF magnetic field. Contrastingly, for perpendicular bias the conductor is circumferential about the core (as in Fig. 6.4) and drives a DC magnetic field that is parallel to the beam-tube axis, and is perpendicular to the (azimuthal) RF magnetic field.

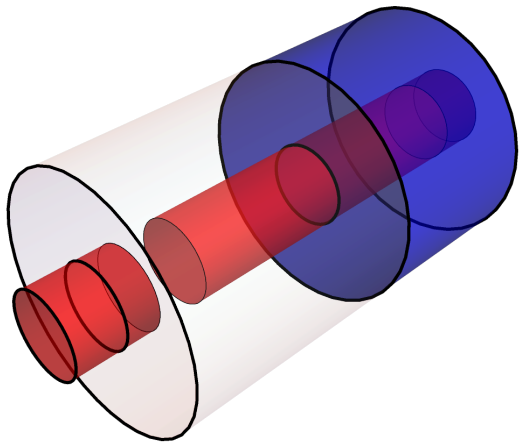

Figure 6.3: Coaxial Cavity with ferrite loading. The metallic, evacuated pipe is shown red with an acceleration gap. The concentric ferrite load is show blue. The remainder empty interior volume is shown grey. Depending on the application, the ferrite may fill the cavity volume.

6.7.1 Parallel bias of concentric core

As described above, the metallic cavity is concentric with the (metallic) vacuum pipe that transports the charged particles. The ferrite volume (within the cavity) is an annular region also concentric about the pipe. By far the simplest way to bias the ferrite is to wrap turns of a current-carrying conductor about the annular ferrite cores. In consequence of this, the bias field is azimuthal. It is desirable that there not be too many turns, otherwise the RF wave is impeded (by the conductor)

[2]It is difficult to maintain material uniformity in a single large disk. Further, the subdivision into cores provides the opportunity to introduce cooling.

from entering into the ferrite interior. Fortunately, as demonstrated in Chap. 2, even a relatively small number of turns (roughly 6, or more, equally spaced) is sufficient to confine the bias field within the annulus. This has two beneficial consequences: (i) the bias field does not extend into the vacuum pipe, and cannot deflect the charged particles; and (ii) the DC azimuthal demagnetizing factor can be made nearly zero. In practise, the bias electrical current tends to be very large and so more turns are used. In the cavity fundamental EM resonance mode, the electric field is parallel to the cavity cylinder axis, and the magnetic field is azimuthal about the cylinder axis. Hence, it is automatic that the RF magnetic field is parallel to the bias field.

6.7.2 Perpendicular bias of concentric core

The implementation of perpendicular bias demands far greater technological complexity than parallel bias. Fig. 6.4 sketches the geometry. A ferrite core encircles the vacuum pipe. The core (or cores) are encircled by azimuthal current carrying coils that drive a solenoidal bias H-field through the ferrite. There result north and south poles on the end faces of the ferrite. The magnetic circuit is completed by an iron yoke that encloses the ferrite and that is contact with ferrite poles. In practise[99], the configuration is complicated by the need to cool both the ferrite and the conductors; so there are cooling tubes with coolant flowing. Further, electrical connections to the conductors must pass out of the yoke. If the bias current is changed rapidly, to follow the frequency program of a fast cycling synchrotron, there will be eddy current heating of the yoke - requiring additional cooling. Eddy-current heating in the ferrite itself is negligible because of the very high resistivity.

Despite the yoke, a small fraction of the magnetic flux will escape from the ferrite; so there will be a solenoidal magnetic within the vacuum pipe (that transports the charged particles). The field component parallel to the cylinder axis has zero effect (because the velocity and field are parallel), but the radial component at the ends imparts an azimuthal rotation. The impulses at either end are oppositely directed, and almost cancel. But the residual field error cannot be forgotten, because the particles pass repeatedly through the cavity; and there may be a resonant effect. This is suppressed if cavities are placed at locations of relative π phase advance of the transverse betatron oscillations. Alternatively, the particle-beam dynamics effect is completely eliminated if the tuner is moved off-axis via a transmission line connection.

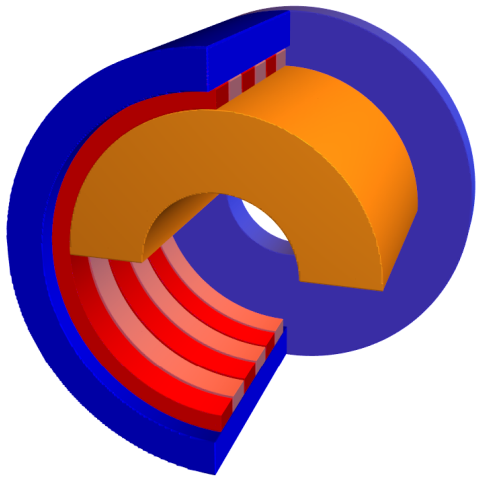

Figure 6.4: Cut-away view of ferrite tuner with perpendicular bias. The upper half of the ferrite core is show yellow. The concentric conductors are shown red and pink. The rear half of the magnetic yoke is shown blue, and one of the end-disc poles is shown complete. The other yolk end-disc pole is omitted in order to show the interior of the tuner.

6.8 Parallel or perpendicular, Ni-Zn or YIG?

At low frequency and without magnetic bias, Ni-Zn and YIG have dissimilar but overlapping properties. Nickel-zinc ferrite is magnetically softer and more lossy. Yttrium-iron-garnet (YIG) is a harder magnetic material, that is much less lossy. Ni-Zn ferrites have very large permeability ($\simeq 1000$) upto a few MHz; this drops rapidly at a few tens of MHz; and over the same region the material becomes rather lossy. The precipitous drop is due to domain wall vibration. Yttrium-Iron-Garnet (YIG) has large permeability ($\simeq 100$) upto 10 MHz; this drops to ten at around 100 MHz; over the same region the material becomes lossy - but much less so than Ni-Zn.

Both Ni-Zn and YIG may be parallel biased. But in the niche range of frequency upto a few MHz, shrinking cavity size is a major consideration; and this makes large μ_Δ very desirable. The larger $\partial B/\partial H$ associated with $\mu_\Delta(\nu = 0)$ gives a clear advantage to Ni-Zn despite it being more lossy. If there were applications in the region 10-20 MHz, and cavity size was less important, YIG could be useful in that range.

When parallel biased and driven to magnetic saturation, the incremental permeability of Ni-Zn and YIG is unity (the same as free space). When perpendicular biased, the behaviour in saturation is completely transformed. Spinel and garnet ferrites both display the ferro-magnetic resonance, leading to a large complex permeability. Both Ni-Zn and YIG may be perpendicular biased. But in the band of frequency 30-110 MHz, the low RF power loss properties of the YIG garnet are superior to the Ni-Zn spinel.

6.9 Parallel biased Ni-Zn ferrite

Low RF applications requiring the most dramatic reduction of RF cavity size employ Ni-Zn ferrite. We suppose the B-H major loop includes saturation, and that the material has previously been driven (i.e. biased) into saturation; this guarantees reproducibility. Prior to acceleration, the operating point is moved toward $B(\simeq H_c) > 0$ for bi-polar bias, or toward $B_{\rm rem} > 0$ for uni-polar bias. If an RF magnetic field $\pm\Delta H$, small compared with the bias, is now introduced, the magnetization will follow a local, minor hysteresis loop; as explained in Fig. 1.3. The minor loop has the incremental permeability given by $\mu = \Delta B/\Delta H$. This value is (potentially) much larger than the free-space value; and so the EM wave is slowed down in the ferrite and the wavelength is shortened leading to resonanant excitation of the cavity. As the particles accelerate, so the resonance frequency and bias rise in unison.

6.9.1 Literature Survey

The literature of parallel-biased RF cavities spans from the mid 1950's to the present time.

Brockman

The primary reference for Ni-Zn ferrite loaded RF cavities is Brockman, van der Heide and Louwerse[77]. This comprehensive article from 1969 celebrates the triumph of Philips Feroxcube utilised in six proton synchrotrons at national laboratories in the US and Europe. These machines were constructed between 1959 and 1963, and were operated with RF ranging over 1-10 MHz. The companion article by Gouiran[78] describes the design, technology and construction of these accelerators. Brockman begins with a lucid account of the magnetic properties of ferrite, including the incremental permeability and frequency dependence of the complex permeability. There are many types of Ni-Zn ferrite with varying composition and properties. For example, the original Ferroxcube types have chemical formula $\mathrm{Ni}_{(1-x)}\mathrm{Zn}_x\mathrm{Fe}_2\mathrm{O}_4$ with x ranging from 0 to 0.64. A ferrite with the highest permeability is not necessarily the best material. The magnetically softer varieties have higher permeability and also losses; their properties also vary more quickly with bias

and frequency than the magnetically harder varieties. The Curie temperature, that at which the permanent magnetization disappears, is significantly higher for the magnetically harder materials. Brockman discusses the factors (and compromises) leading to the best choice of ferrite variety for a particular application, using five synchrotrons as examples. Thermal management, heat dissipation and cooling are an important consideration. Brockman also discusses the role of the current supply for the bias field: whether it is bipolar (and able to cycle through the complete B-H loop); or unipolar (capable to cycle only between $B_{\rm rem}$ and $B_{\rm sat}$ in the upper-right quadrant); or a specialist current source[3] that can supply large positive and small negative values. This has a strong influence on the range μ_Δ. Brockman's Fig. 14b is in error; it shows the derivative $\mu_r \propto \partial B/\partial H$ to be continuous at the remanent field. However, this is a recoil point; so the differential permeability differs between the branches at $H = 0$. The correct variation is shown in Fig. 5.2.

Kerns

The article by Kerns[82] *et al* (1965) describes preparatory design for the Ferrmilab Main Ring RF cavities[83] that began operation in 1971. The cavity is a $\lambda/2$ structure with two accelerating gaps. Between 1965 and 1969, the design was revised: moving the gaps from the ends to the centre. Significantly, these are 53 MHz cavities, a departure from previous designs; and that benefit from the experimental fact that the product $\mu_\Delta Q\nu$ rises with frequency ν to a peak in the region 20-50 MHz. The tuning range is small: $\nu_f - \nu_i = 0.3$MHz. Kerns presents a systematic design procedure for this new frequency regime. For similar cavity dimensions, but higher RF, a much smaller volume of ferrite is required; and in this design the two tuners are side-coupled and pushed off the cylinder axis. In this application, the ferrite is primarily used for tuning the resonance frequency; and not shrinking the cavity size. Kerns states "the use of salient ferrite parameters are (among) the prime considerations of the design example" and graphs measured values of μ_Δ and ferrite Q versus bias magnetic field at the operating frequency 50 MHz. No description is given of the measurement procedure. However, it appears that the tuner alone is modeled as a ferrite-loaded transmission line terminated in a short, and that network theory is used to calculate μ_Δ from network measurements.

Gardner

There are more modern articles by Gardner[79] (1991) and Klingbeil[81] (2010). Both draw heavily on Brockman and reproduce some of his ferrite property graphs. Gardner[4] illustrates the ferrite applications with more modern synchrotrons, and ferrite varieties from Philips and Toshiba. Gardner concludes with technical descriptions (including the bias windings) of the accelerating stations at the CERN PS, Fermilab Booster, PS Booster and CERN LEAR. These illustrate quarter-wave and half-wavelength structures, and also a side-coupled off-axis ferrite load. The article by Gardner was updated and expanded by Schnase[80] in 2005.

Klingbeil

After introducing incremental and complex permeability, Klingbeil[81] develops the simple mathematical model, summarised in Sec. 5.6.1, for the resonance property of a ferrite-loaded quarter-wave cavity. The impedance, quality factor and filling time are derived. There follows engineering aspects such as RF power amplifier, cooling, biasing, etc. Klingbeil concludes the CAS article with a technical description of the SIS18 ferrite cavity[85] at the GSI Helmholtz Centre for Heavy Ion Research in Darmstadt Germany.

[3]Such as that designed (PPAD-464-D) by Graham Rees in 1962 for the Princeton-Pennsylvania Accelerator. Many years later, Dr Rees was my mentor at Rutherford Appleton Laboratory UK.

[4]Ian S.K. Gardner designed and constructed the 2nd harmonic and main/fundamental accelerating cavities for the Rutherford Laboratory Nimrod and ISIS proton synchrotrons.

Klopfer & Klingbeil

The three preceding references are all reviews. The most modern article, by Klopfer et al[84], present measured properties of the specific ferrite used for the parallel-bias tuning of RF cavities at the SIS-18 and SIS-100 synchrotrons at the FAIR complex at GSI. The material is a Ni-Zn ferrite (Philips Ferroxcube). The frequency dependence of the complex permittivity is experimentally investigated (and graphed) for several values of the biasing field that span the operation range. The toroidal ferrite cores, in addition to the bias winding, are wound with a primary coil for RF excitation and a secondary coil for sensing/pick-up allowing to perform transmission and reflection measurements. The bias and RF fields are necessarily parallel. The Klingbeil series-LCR model is analytically inverted for μ' and μ'' in terms of the input impedance of the network (electrical circuit) and excitation frequency. The Polder tensor for partially saturated ferrite is very difficult to calculate. Using a fit to data, the authors propose a simple empirical model for the excitation-parallel-to-bias component of the tensor. Notably, in the working cycle of the GSI SIS 18 cavity, the bias current is varied only in the range from zero to its maximum value without changing its polarity. The reversible permeability[5] is tabulated as a function of bias field for a fixed 0.5 MHz RF.

In contrast to Brockman who favoured bi-polar current supplies and four-quadrant hysteresis curves, Klingbeil[6] advocates convincingly for uni-polar supplies and a single-quadrant hysteresis major loop.

> In my [Klingbeil] opinion, the unipolar supply (even though it is technically simpler) has some practical advantages: In this case, the minor hysteresis loops are always located on the upper path in the first quadrant. Therefore, the incremental permeability should be rather reproducible (compared to bi-polar supplies). And if I take the SIS18 ferrite cavity as an example, it nevertheless allows large tuning ranges. The maximum resonant frequency is about 5.4 MHz, the minimum about 0.8 MHz. Therefore, the tuning range is almost a factor of 7 in spite of the unipolar supply. The monotonic dependency of the incremental permeability/the resonant frequency on the bias current furthermore makes the closed-loop resonant-frequency control less complicated.
>
> Because we regarded the old SIS18 solution as a very reliable and robust one, our new accelerating cavities[86] for the FAIR synchrotron SIS100 (with a smaller tuning range) are based on almost the same ferrite material and on the same unipolar supply operating principle.

6.10 Perpendicular biased YIG ferrite

6.10.1 Influence of bias orientation on tuning

As early as 1956, researcher C.E. Fay[42] made an exploratory comparison of bias orientations. He took a closed (air-filled) rectangular waveguide TE_{101}-mode cavity, with mode frequency ν_c. A slab of Ferramic[7] was placed inside the waveguide, and the resonance frequency ν_r and quality factor in the X-band measured as a function of the bias field strength. The ferrite occupied $\simeq \frac{1}{10}$ of the cavity volume. His Fig. 3 shows the results for perpendicular bias. When the spin-precession frequency ν_0 is close to ν_c, the resonance frequency is raised above ν_c and the quality factor drops by a factor $\simeq 3.7$. The conditions correspond to negative susceptibility as occurs when $\nu_r > \nu_0$. (This condition is not suitable for cavity tuning in a charged particle accelerator.) The RF field

[5] The limit of zero amplitude. i.e. signal level.

[6] Personal communication 2025.

[7] Trade name (in the 1950's) for an iron-magnesium ferrite purchased from the General Ceramics and Steatite Corporation. Incidentally, steatite (also known as soapstone) is a talc-schist type of metamorphic rock. Steatite is used industrially to make electrical insulators.

excitation vector was held fixed, while the bias orientation was changed. His Fig. 4 shows results for parallel bias: the resonance frequency falls below ω_c and the quality factor falls by a factor $\simeq 4.4$. The falling frequency under parallel bias is not consistent with the FMR.

6.10.2 Literature survey

The review by Poirier[88] in 1993 lists the literature on particle accelerator applications of perpendicular biased ferrite. As was mentioned above, the influence of perpendicular bias on a ferrite loaded waveguide resonator was observed as early as 1956. But a laboratory bench experiment is far from a technological realization.

LANL-TRIUMF-SSCL

In 1982-83 Earley[92] and collaborators made a crucial observation that has been influential until the present time. He proposed to perpendicular bias the ferrite and set the bias-field such that the FMR is above the RF cavity frequency. The incremental permeability is large[8] at frequency close to the FMR resonance, and the power losses are also large; see Fig. 4.1. RF electromagnetic energy is transferred to the electron spins and dissipated through (partially understood) mechanisms that are described phenomenologically by the Gilbert damping. Both the permeability and losses decline steeply either side of the resonance, but less so the permeability. This results in a regime where the permeability has a useful value, and the losses are negligible. Indeed, the ferrite losses are so small that the cavity quality factor is dominated by the ohmic loss in the copper cavity walls. The idea was demonstrated[92] in a quarter-wave cavity loaded with Ni-Zn or Mn-Zn or Ca-Va garnet ferrite. The ferrite occupied roughly 1/6 of the volume of the resonator. For all the materials, variation of the DC bias resulted in a tuning range of about 4 MHz about 50 MHz. For all the materials, the power loss in the ferrite became negligible above 49 MHz.

The LANL collaborators of Earley were determined to build a 50 MHz cavity with a 10 MHz tuning range and high accelerating voltage suitable for a rapid-cycling booster synchrotron. The watershed paper[96] by Smythe *et al* in 1985 contains several advances. Using a quarter wave cavity with dual-orientation magnetic bias, they demonstrate the dramatic reduction of ferrite power loss, and enhancement of quality factor, that arises when the bias is switched from parallel to perpendicular. They report the magnetic Q versus permeability μ_Δ for three type of Mg-Mn-Al spinel ferrite and three types of Y-Fe garnet. In the range $\mu_\Delta = [1, 4]$ all have Q in the range 10^4–10^3. The TDK Y1 type garnet[9] was the most promising. They present a prototype 50 MHz cavity design, that became the basis for more than a decade of development. The tuner is coaxial with a quarter-wave cavity, and the power tetrode is capacitively coupled to the inner cylinder of the coax. The tuner cores, azimuthal conductors and iron yoke are all coaxial. In 1987 the engineering prototype demonstrated[98] gap voltages between 130 and 140 kV over a tuning range of 50 to 60 MHz.

Deriving from the booster ring, the LANL team began work on a prototype Main Ring (MR) cavity design with higher gap voltage and much smaller tuning range (1 MHz). At this time TRIUMF (Canada) adopted the LANL booster and MR cavity designs for its KAON Factory proposal. In 1989 LANL and TRIUMF collaborators presented[100] the MR design: a half-wave structure with the tuner taken off axis. The LANL booster cavity was transferred to TRIUMF, equipped with a ramping bias supply, a power tetrode, and rudimentary RF controls; and in 1991 the TRIUMF team demonstrated[101] a tuning range 46-61 MHz, upto 65 kV gap voltage, and rapid cycling (50 Hz) of the complete system. In 1991 the Superconducting Super-Collider Laboratory (SSCL) adopted the LANL/TRIUMF design for their booster RF cavity. In 1992 work ceased at LANL & TRIUMF, and was transferred to SSCL along with the prototype booster cavity. In 1993

[8] Possibly extremely large if the Gilbert factor α is sufficiently small $\alpha < 0.01$.

[9] The chemical composition is not given.

Friedrichs[102] and Goren[103] reported high-power tests of the booster cavity with large amplitude RF, including its nonlinear behaviour as a hardening resonator. Work was abandoned in 1995 when the SSC project was cancelled. There followed a hiatus.

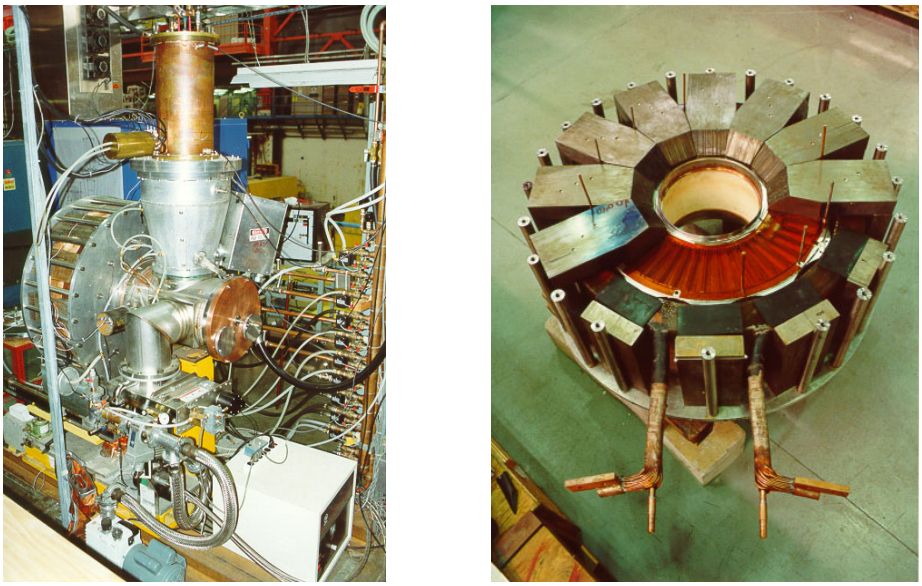

Figure 6.5: TRIUMF Booster cavity test stand (to the left) and ferrite tuner with bias coils and steel yoke visible (to the right). Photographs courtesy of Roger Poirier.

CERN & DESY

The response of the accelerator community to Earley's 1983 paper was immediate. The CERN PS designs[10] and constructs[93] a 114 MHz cavity with an off-axis perpendicular-biased tuner. The AECL-DESY collaboration builds 52 MHz RF systems for HERA[94] and PETRA-II[95]; the cavities are tuned by-off-axis perpendicular-biased ferrite. In both examples, the tuning range and volume of ferrite is small.

Renewed interest in perpendicular biased ferrite arose at the CERN in 2012-2015. The CERN studies led by Vollinger[107] and Caspers were directed toward a booster cavity with high quality factor and large tuning range: 20-40 MHz. A continuing theme was the development and perfection of RF transmission and reflection measurements to quantify the complex permittivity as a function of frequency (0–100 MHz) and of perpendicular bias field (0.01–0.1 Tesla). The first step[107] was the selection of a YIG ferrite, G-510 manufactured by Trans-Tech, followed by refinements[108, 109] of the measurement techniques (in particular the 1-port reflection), and leading toward a design[110, 111] for a quarter-wave coaxial resonator with coaxial ferrite load and orthogonal bias. Although the frequency could be swept from 18 to 40 MHz, the quality factor is large (upto 5000) only above 30 MHz. The small magnetic quality factor occurs because the large μ' needed to achieve lower resonance frequency is associated with large μ'' due to the energy dissipated in driving the electron spin precession. This effect is evident in Figs. 4.1 and 6.2.

FNAL

There was also strong interest in perpendicular biased ferrite at the FNAL in 2014-2018. The FNAL studies[112] were directed toward replacing the aging RF cavities in the Booster ring and the addition of second-harmonic cavities. The LANL/TRIUMF/SSCL cavity was modeled in the

[10] See CERN-PS-RF-Note-85-3 A ferrite tuner for the 114 MHz Cavity.

CST[11] computer software. No details of μ_r are provided. During 2015-2018 the FNAL Collaborators focused on the 2nd harmonic cavity, whose tuning range is 77-105 MHz. Significant attention has been paid to the precise material properties of the AL800 garnet ferrite rings that form the tuner. The DC permeability as a function of H-field was measured[113] in 2015-2016 in order to supply self-consistent values for the ratio of saturated magnetization to driving field M_z/H_z. Further, the incremental permeability was measured in 2017-2018. Construction of the FNAL prototype cavity was completed[114] in 2018.

6.11 RF hardening resonator

The six chapters of this text were inspired by the desire to understand Vloden Shapiro's explanation of why the LANL/TRIUMF/SSCL prototype booster-ring RF cavity behaves as a hardening resonator. That the work was inspiring does not imply the analysis is wholly correct. Nevertheless, Shapiro[61] identifies all the factors involved: the ferrite in a near saturated state behaves almost as a single domain; the weakly damped FMR described by the LLG equation; damping is needed for the spins to relax into alignment with the bias; the importance of ferrite shape and demagnetization factors; that neither the bias or the RF field are uniform across the entire ferrite; and that other processes may be present, such as spin waves. As noted in the introduction, the physical phenomena involved are not the usual province of accelerator physics; and so they were outlined in the preceding five chapters.

The sinusoidally driven anharmonic oscillator[116] has the equation of motion

$$\ddot{x} + \dot{x}\delta + x\alpha + \beta x^3 \;=\; \gamma \cos\phi(t) \; .$$

Here $\alpha, \delta > 0$. For such an oscillator, the resonance curve has a different shape for each value of the drive amplitude γ. If $\beta > 0$, then the resonance frequency rises with $|\gamma|$ and the system is described as a hardening resonator. If $\beta < 0$, the system is a softening resonator. In either case, above a threshold value of γ which depends on β, δ, the resonance curve becomes triple-valued. Over a certain range of excitation frequency, there are three distinct values for the amplitude of the steady state response; but only one of them is stable (at a particular frequency) for small perturbations. Hence the system may jump from one state to another as the drive frequency is swept up or down. Friedrichs[102] and Goren[103] reported observing this hardening-resonator instability in 1993. Suppose the RF permeability is known as a function of the DC bias, $\mu_\Delta(H_z)$, from signal-level measurements. Then for large amplitudes, Friedrichs states the cavity resonance frequency behaved as if the permeability were $\mu_\Delta(\sqrt{H_z^2 + h_y^2})$. Friedrichs shows a resonance curve calculated from that relation, while Goren shows the experimental curve from oscilloscope traces taken at 7kV and 70kV voltages on the accelerating gap.

Suhl

This was not the first time nonlinear behaviour was reported for perpendicular bias. Suhl[43] proposes a mechanism by which the FMR is weakened and broadened at larger drive amplitudes. The resonance peak is the manifestation of the imaginary (dissipative) part of the susceptibility ξ'', and Suhl argues it may behave as a softening resonator with respect to variation of the bias H_z. However, the RF cavity resonance frequency is not the FMR frequency! So we must look elsewhere for the explanation.

[11] CST Studio Suite is a high-performance 3D EM analysis software package for designing, analyzing and optimizing electromagnetic (EM) components and systems.

Rakowsky

Rakowsky[115] reports the behaviour of a parallel-biased RF cavity as a softening resonator at the Brookhaven AGS in 1969. The Ferroxcube ferrite loads were replaced by high-Q ferrite (unspecified) from Toshiba, enabling the cavity to be driven at high RF power. The AGS operated over the frequency range 1.4–4.5 MHz. The frequency program varies very slowly. So we may consider the cavity frequency response (resonance curve) over a small range ($\pm 5\%$) about a fixed centre frequency. In such a small range ($\simeq$ 0.1 MHz) the variation of permeability versus frequency (Snoek's law) is insignificant. At small RF amplitude the incremental permeability follows the differential $\partial B/\partial H$ as a function of bias field. Suppose the ferrite is near the saturated region. The RF excitation extends over $\pm\Delta H_y$. At larger amplitudes, the negative value $-\Delta H_y$, pulls the magnetization increment away from saturation; leading to a larger increment $-\Delta B_y$; and hence the incremental permeability becomes greater at larger amplitude. This means the resonance frequency will fall. Of course, this mechanism does not apply to a perpendicular-bias hardening resonator.

Goren

Goren[103] attempted to explain the hardening resonator behaviour in 1993. Despite the cylindrical symmetry of the tuner, Goren uses Cartesian coordinates[12] as if it were a cube. Goren takes the Landau-Lifshitz equation without damping, and uses the principle of harmonic balance to find a steady state solution for the fundamental component of the magnetization amplitude m_y in response to an RF drive h_y and DC bias H_z. Little or no account is taken of the DC component of magnetization, of other frequency components, or of cross-coupling due to the demagnetization factors. The susceptibility χ', the ratio m_y/h_y, is found to contain an additional term proportional to $-h_y^2/H_z^3$ such that the permeability ($\mu_\Delta = 1 + \chi'$) falls and the resonance frequency ($\propto 1/\sqrt{\mu_\Delta}$) rises with RF amplitude. Despite the gross simplifications, the notion that the permeability falls because the incremental magnetization m_y does not rise in proportion to h_y is correct. This is an indirect way of saying the ferrite saturates.

Shapiro

Shapiro[61] is critical of the shortcomings in Ref.[103], and addresses them all. The Gilbert loss factor α quantifying the FMR resonance width is restored. Non-uniformity of the DC and RF magnetic fields is accounted for by a range of FMR frequencies that further broadens the peak. The cylindrical tuner and LLG equation are taken in cylindrical coordinates. [The form of the LLG equation does not change; because each spin precesses about a point in space without performing any translation.] Shapiro takes the ferrite tuner to be composed of several thin discs, each with a longitudinal demagnetization factor $N_{zz} \approx 1$ and transverse factors equal to zero. Although this is correct for a single, isolated[13] disc, it is not clear that this continues to be so when the discs are closely spaced in a stack. Nevertheless, the disc model is used. The DC and RF demagnetization factors are taken equal $N_{zz} = n_{zz}$, leading to additional mathematical simplification. Shapiro finds an approximate solution of the nonlinear LLG equation (for the magnetization components) by time averaging over the fast varying Fourier harmonics. The susceptibility m_y/h_y is found to be M_z/H_z plus a term quadratic in the magnetizations m_x and m_y. Later he writes $m_y \propto h_y$ and hence the permeability is quadratic in the RF amplitude; similar to Goren's conclusion. Surprisingly, Shapiro does not identify this effect as exhaustion of the supply of electron spins (i.e. saturation).

Shapiro reports data for Q_m and μ_Δ versus cavity resonance frequency, from the LANL-TRIUMF-SSCL prototype. The values are inferred (by calculation) by Smythe and other authors from other measured quantities. The trend is that Q_m rises and μ_Δ falls. Shapiro expects μ_Δ to

[12] He seems not to understand that the SMM equation does no change form when expressed in cylindrical or other orthogonal coordinates.

[13] The derivation assumes the body is immersed in an infinite vacuum medium with no other bodies present.

fall, and Q_m to be roughly constant; and he concludes that there must be another energy loss mechanism at play at lower frequency. Shapiro proposes to solve this (supposed) mystery by making the Gilbert damping factor frequency dependent, say $\alpha \propto 1/\omega$. However, the reasoning is in error. There is a hidden variable: the bias field. The joint variation of the resonance frequency and bias field, according to Eq. 6.12, cause the magnetic quality factor to rise. Therefore, the Gilbert factor α is constant over the tuning range. The true resolution of the mystery is manifest in Fig. 6.2. Moreover, measured permeability spectra shown in Figs. 5.4 and 5.5 is supportive of there being no additional magnetic energy loss at low frequency. After the $\alpha(\omega)$ detour and remarks concerning the relation between cavity and magnetic Q, Shapiro goes on to describe several ferrimagnetic processes that may occur around the cavity resonance frequency and compromise its performance.

Koscielniak

In Chap. 4 of the present work, the author has solved the nonlinear LLG equations for biasing of a cylindrical[14] body into a magnetized state near saturation, and application of a RF magnetic field (a) parallel and (b) perpendicular to the bias. The mathematics is complicated, but the results are simple to understand. In case (a), a spectrum of response frequencies emerges. In case (b), the incremental magnetization with respect to the RF field eventually saturates. The latter behaviour is illustrated in Figs. 4.2 to 4.4. The effect is most dramatic when the EM wave frequency is equal to the Larmor frequency, as in Fig. 4.3, but also prevalent when the Larmor frequency (also called FMR frequency) is above the RF drive (Fig. 4.2) or below the RF drive (Fig. 4.4). In the favoured cavity tuning scenario, the RF drive is below the FMR frequency, as in Fig. 4.2.

There is no need to solve for the detailed EM-field geometry/distribution within the cavity to conclude that the cavity must behave as a hardening resonator. After all of the electron spins have become aligned, there can be no further change in the incremental magnetization. This being so, the permeability deviates from the linear, Polder theory and tends to unity. Consequently, the resonance frequency of the cavity must rise with the amplitude of the applied RF field. Unlike the Duffing resonator, this system will not display a strong third harmonic of the RF drive. Low harmonics of the cavity fundamental resonance are absent because they do not receive a permeability boost from the FMR and therefore do not fit inside the cavity. In this chapter, Sec. 6.6, the author reports a simple theory of perpendicular-bias cavity-tuning that explains the apparent dependence of quality factor on the operation frequency. There is no need to invoke a fictitious dependence of the Gilbert loss parameter on frequency.

Thermal limitation on observing nonlinearity

In principle, the hardening resonator behaviour could be observed in cavities loaded with either YIG or Ni-Zn ferrite. However, there is a crucial question: "can the system survive strong dissipation?" If the material is thermally stressed beyond what the cooling can take away, then you might not be able to access the strong nonlinear regime. The Ni-Zn ferrites have an intrinsically lower magnetic quality factor (than YIG); material heating and insufficient cooling (or impractical cooling requirements) may prevent observation of the rise of resonance frequency with amplitude or "snapback" behaviour when Ni-Zn (and perpendicular bias) is employed.

6.12 Conclusion

These chapters have pedagogic and research components.

[14]Technically the ferrite load in an RF cavity is not a simple cylinder; rather it is a hollow cylinder. Nevertheless, the same mechanism of saturation will apply.

6.12.1 Pedagogy

In Chap. 1 we introduced the classical explanation of magnetism: Ampèrian current loops. These currents do not participate in conduction. We also attempted to de-mystify the de-magnetizing factor. In Chap. 3 we introduced the quantum explanation of magnetism: electron spin magnetic moments. In certain materials, the uncanny and bizare exchange interaction aligns these spins parallel. Of all the chapters, Chap. 2 is the most pedagogic in flavour; in it we emphasized aspects of cylindrical arrangements of current carrying wires not usually addressed, and the connection between line currents and two-dimensional fields and complex functions. In Chap. 5 we discussed (at length) the many dependencies of incremental permeability. In Chap. 6 we gave an account of the use of ferrites for cavity frequency-tuning and size-shrinking, including literature surveys for parallel and perpendicular bias variants.

6.12.2 Research

The derivation of the symmetry properties of the elements of the demagnetization tensor for a solid cylinder, Eq. 1.18, is the authors own. In Sec. 1.5.5 we critiqued toy models of hysteresis branches, pointing out the discontinuity in value or derivative. In Chap. 2 we discussed toroidal windings mounted on an annular solenoid. Contrary to text book accounts, we emphasized in Secs. 2.2 to 2.5 that the magnetic field is not uniform and that the azimuthal variation depends on the number and symmetry of the windings. In passing, Sec. 2.4, we emphasized the deep connection between Ampère's circuit law and the Biot-Savarat law of field from a conductor. Chap. 4 was written before all other chapters. In Chap. 4 we discussed the Landau-Lifshitz-Gilbert equations for the precession of spin magnetic moments. Here (for the first time) the LLG equation is solved analytically in the strong nonlinear regime to give dependence of permeability on RF amplitude. For RF parallel to bias, a spectrum of response frequencies emerges. For RF perpendicular to bias, magnetic saturation occurs. In Sec. 5.4.1 we introduced phenomenological functions that satisfy Snoek's empirical law for RF permeability of ferrites. In Secs. 6.5 and 6.6 we introduced (for the first time) simple mathematical models to calculate magnetic bias field from cavity resonance frequency. The former uses the dual-dependence model $\mu_\Delta(H,\nu)$ appropriate to parallel bias. The latter uses the FMR, appropriate to perpendicular bias, and explains the apparent fall of magnetic quality factor at lower frequency. This effect is reported by Smythe[96] Fig. 2, and Shapiro[61] Fig. 3, and Vollinger[110] Fig. 5. In Sec. 6.11 we use the results of Chap. 4 to explain why the perpendicular-biased cavity behaves as a hardening resonator at large RF amplitude: magnetic saturation of the ferrite causes the resonance frequency rises with amplitude leading to the hardening oscillator "snap-back" instability.

6.12.3 Unresolved

It is an open question whether Kittel's assumption, that the DC and RF demagnetization factors are equal, is correct; and further if Brown's theorem for the trace of the demagnetization matrix is unchanged when the magnetizing field oscillates rapidly. These questions could be investigated both by mathematical analysis (starting from Maxwell's equations and the vector potential) and by experiment. A related question concerns "what are the radial and azimuthal demagnetizing factors?" for oscillating EM fields. These are complicated questions.

Bibliography

[1] James Clark Maxwell: A Treatise on Electricity and Magnetism, Clarendon Press, Oxford, 1873.

[2] Josiah Willard Gibbs: Vector Analysis: a text-book for the use of students of mathematics and physics. Publishers: Charles Scribners New York N.Y. and Edward Arnold London U.K., 1901.

[3] See Vol. II. Chap. IV Induced Magnetization, and Chap. V Problems In Induced Induction in Ref.[1]. In particular the articles #431 Hollow Spherical Shell; #435 Crystalline Sphere (in which magnetization coefficients depend on direction); #437 Ellipsoid; #439 Cylinder.

[4] John C. Slater and Nathaniel H. Frank: Electromagnetism, McGraw-Hill Book Company, 1947. In particular, Chap. 6 Magnetic Materials, Secs. 1-4.

[5] Wolfgang Panofsky and Melba Phillips: Classical Electricity and Magnetism: Addison-Wesley Publishing Co., 1955.

[6] Paul Lorrain and Dale Corson: Electromagnetic Fields and Waves, W.H. Freeman and Co., San Francisco, 1962.

[7] John David Jackson: Classical Electrodynamics, John Wiley & Sons, New York NY, 1962.

[8] S. Simons: Vector Analysis - for Mathematicians, Scientists and Engineers, Pergamon Press, 1970.

[9] William J. Duffin: Electricity and Magnetism, McGraw-Hill Book Co, United Kingdom, 1973.

[10] B.I. Bleaney and B. Bleaney: Electricity and Magnetism: Oxford University Press, 1976.

[11] D.J. Griffiths: Introduction to Electrodynamics, Prentice-Hall, 1981.

[12] Constantine A. Balanis: Advanced Engineering Electromagnetics, John Wiley & Sons, 1989. In particular Sec. 2.8.3 Ferrites.

[13] Andrew Zangwill: Modern Electrodynamics, Cambridge University Press, 2012.

[14] P.A.M. Dirac: The Principles of Quantum Mechanics: Clarendon Press Oxford, 1947. In particular Chap. XI Relativistic Theory of the Electron.

[15] A.A. Mirin, M.F. Uman, C.W. Hartman, J. Killen: An Analytic Representation of Fields Resulting From Currents on a Torus, UCRL-52069, 1976. (Lawrence Livermore Laboratory Report).

Authors use the Green's function in toroidal coordinates to find the vector potential due to toroidal surface current density. They form the curl to find the interior magnetic field. Finally, the focus on the case of a helical current winding.

[16] G. Mörée, and M. Leijon: Review of Hysteresis Models for Magnetic Materials. Energies 2023, 16,3908.

https://doi.org/10.3390/en16093908

[17] D.C. Jiles, D.L. Atherton: Theory of ferromagnetic hysteresis, Journal of Applied Physics Vol. 55 p. 2115 (1984).

[18] J.A. Osborn: Demagnetizing Factors of the General Ellipsoid, Physical Review Vol.67, Issue 11-12, p. 351-357 (1945).

[19] Edmund C. Stoner: The demagnetizing factors for ellipsoids, The London, Edinburgh, and Dublin Philosophical Magazine and Journal of Science, Series 7, Vol. 36, Issue 263, p. 803-821 (1945).

[20] Dan Wei: Micromagnetics and Recording Materials, Springer Briefs in Applied Sciences and Technology (2012).

[21] M. Satoh and Y. Ishii: Simple and approximate expressions of demagnetizing factors of uniformly magnetized rectangular rod and cylinder, J. Appl. Phys. Vol. 66, pp. 983–985 (1989).

Authors find that exact and complicated expressions for demagnetizing factors (developed by other previous authors) are well approximated by simple formulae.

[22] Du-Xing Chen, James A. Brug and Ronald B. Goldfarb: Demagnetizing Factors for Cylinders, IEEE Trans. On Magnetics, Vol. 27 No.4 pp. 3601-3619 (1991).

[23] Masanori Kobayashi and Yoshifumi Ishikawa: Surface Magnetic Charge Distributions and Demagnetizing factors of Circular Cylinders, IEEE Trans. on Magnetics, Vol. 28, No. 3 pp. 1810-1814 (1992).

The authors use numerical methods to calculate and tabulate magnetization properties, such as axial demagnetization factor, of a cylinder as a function os aspect ratio and permeability.

[24] M. Kobayashi, Y. Ishikawa, S. Kato: Magnetizing Characteristics of Circular Cylinders in Peperpendicular Applied Magnetic field, IEEE Trans. On Magnetics Vol. 32 No. 1 pp. 254-258 (1996).

The authors use numerical methods to calculate and tabulate magnetization properties, such as transverse demagnetization factor, of a cylinder as a function os aspect ratio and permeability.

[25] Du-Xing Chen, Enric Pardo, Alvaro Sanchez: Fluxmetric and magnetometric demagnetizing factors for cylinders, Journal of Magnetism and Magnetic Materials Vol. 306 pp. 135-146 (2006).

Authors use numerical methods to calculate axial magnetisation properties for variety of aspect ratio and permeability.

[26] Gary M. Wysin: Demagnetization Fields (of cylinders, and bars of square cross-section). Department of Physics, Kansas State University, 2012.

This is an introductory tutorial. Compared with Eq. 1.7, Wysin omits the volume integral because the magnetization is assumed uniform within the cylinder; such that $\nabla \cdot \mathbf{M} = 0$. There is an azimuthal surface bound-current density $\mathbf{J}_b$ on the cylindrical side walls, and an axial surface bound-current density $\mathbf{J}_f$ on the disc-shape end walls. The surface integral over the cylindrical side walls, which is omitted, leads to the transverse demagnetization factors $N_{x,y}$. The surface integral over the end-discs leads to the axial demagnetization factor N_z.

`https://www.phys.ksu.edu/personal/wysin/notes/demag.pdf`

[27] Alessio Caciagli, Roel J. Baars, Albert P. Philipse, Bonny W.M. Kuipers: Exact expression for the magnetic field of a finite cylinder with arbitrary uniform magnetization, Jnl. of Magnetism and Magnetic Materials, Vol. 456 pp.423-432 (2018).

Authors develop the scalar magnetic potential for external field applied transverse to a cylinder, and the corresponding demagnetization factors. Combining the transverse case with previously known expressions for the longitudinal (i.e. axial) case, they find the demagnetization factor for arbitrary orientation of the cylinder with respect to the applied field.

[28] Du-Xing Chen, Enric Pardo, Alvaro Sanchez: Radial Magnetometric Demagnetizing Factor of Thin Disks, IEEE Trans. On Magnetics, Vol. 37, No.6, pp. 3877-3880 (2001).

Authors adopt cylindrical polar coordinates in an attempt to find a radial demagnetizing factor. They claim that a vector potential $\mathbf{A} = [A_r, A_\theta, A_z] = [0, A_\theta(r,z), 0]$ yields a radial magnetic field that satisfies Maxwell's equations. However, we disagree. In the case of magneto-statics, and when there are no free currents, the field generated by the vector potential does not differ from that due to the scalar potential. The latter is not consistent with fields that diverge from a point, because there are no magnetic monopoles.

[29] Marco Beleggia, D. Vokoun, Marc De Graef: Demagnetization factors for cylindrical shells and related shapes, Jnl. of Magnetism and Magnetic Materials Vol. 321, pp. 1306–1315 (2009).

Authors present analytic results for the demagnetization factor $N_{x,y,z}$ for cylindrical transformer cores when Cartesian axes are aligned with principal axes of the cylinder.

[30] Marco Beleggia, Marc De Graef and Yonko T. Millev: Magnetostatics of the uniformly polarized torus, Proc. Royal. Society. A, Vol. 465, pp. 3581–3604 (2009).

Authors make the first analytic treatment of the axial demagnetization factor for a variety of tori. They start from the Green's function Eq. 1.7, and proceed to express this in toroidal coordinates. There are many excellent references provided in their introduction.

[31] Manfred E. Schabes and Amikam Aharoni: Magnetostatic Interaction Fields for a Three-Dimensional Array of Ferromagnetic Cubes, IEEE Trans. On Magnetics, Vol. 23 No.6 pp. 3883-3888 (1987).

[32] Amikam Aharoni: Demagnetizing factors for rectangular ferromagnetic prisms, Jnl. Applied. Physics Vol. 83 p. 3432. (1998) Cuboid (aka rectangular brick) $2a \times 2b \times 2c$.

[33] Du-Xing Chen, Enric Pardo, and Alvaro Sanchez: Demagnetizing Factors of Rectangular Prisms and Ellipsoids, IEEE Trans. On Magnetics, Vol. 38, No. 4, pp. 1742-1752 (2002).

The authors reproduce previously derived formulae for cuboids with dimensions a, b, c, and tabulate the demagnetizing factors for a wide variety of the aspect rations between a, b, c.

[34] F.Slanovc, M.Ortner, M.Moridi, C. Abert, D. Seuss: Full analytical solution for the magnetic field of uniformly magnetized cylinder tiles, Jnl. of Magnetism and Magnetic Materials Vol. 559 (2022).

Cylinder tiles are sector-like partial objects that can be assembled to make general cylindrical shapes suitable for finite element analysis.

[35] William Fuller Brown: Single-Domain Particles: New Uses of Old Theorems, Amreican Journal of Physics, Vol. 28, pp. 542-551 (1960).

[36] Hendrik Antoon Lorentz: The theory of electrons and its applications to the phenomena of light and radiant heat, Article 117. Published by G.B. Teubner Leipzig Germany 1909; Dover Publications New York N.Y. 1952.

[37] Philip Morse & Herman Feshbach: Methods of Theoretical Physics, McGraw-Hill Book Co., New York N.Y., 1953.

[38] C. Lester Hogan: Introduction to the Ferrites Issue, Proc. of the Institute of Radio Engineers (IRE), Vol. 44 No. 10 p. 1233, Oct. 1956.
The entire Issue No.10 is dedicated to Ferrites.
"Proceedings of the Institute of Radio Engineers" was the magazine of that organization which began in 1913. The Institute of Radio Engineers was formed on May 13, 1912 from two groups that had met earlier in the century in New York and Boston. In 1930, the IRE began publishing its Proceedings on a monthly basis. The IRE was a professional organization which continued until it merged with the American Institute of Electrical Engineers (AIEE) in 1963 to form the Institute of Electrical and Electronics Engineers (IEEE).

[39] J. H. Van Vleck: Fundamental Theory of Ferro- and Ferri-Magnetism, Proc. of the Institute of Radio Engineers (IRE), Vol. 44 No. 10 p. 1248, 1956.

[40] Nicolaas Bloembergen: Magnetic Resonance in Ferrites, Proc. of the Institute of Radio Engineers (IRE), Vol. 44 No. 10 p. 1956, Oct. 1956.

[41] C. Dale Owens: A Survey of the Properties and Applications of Ferrites Below Microwave Frequencies, Proc. of the Institute of Radio Engineers (IRE), Vol. 44 Issue No. 10 p. 1234, 1956.

[42] Clifford E. Fay: Ferrite-Tuned Resonant Cavities, Proc. of the Institute of Radio Engineers (IRE), Vol. 44 No. 10 p. 14446, 1956.

[43] Harry Suhl: The Nonlinear Behavior of Ferrites at High Microwave Signal Levels, Proc. of the Institute of Radio Engineers (IRE), Vol. 44 No. 10 p. 1270, Oct. 1956.

[44] Stephen Gasiorwicz: Quantum Physics, John Wiley & Sons, New Yor N.Y., 1974. See in particular Chap. 8: N-Particle Systems.

[45] Landau, L.D. and Lifshitz, E.M.: On the theory of the dispersion of magnetic permeability in ferromagnetic bodies. Physikalische Zeitschrift der Sowjetunion Vol.8: p. 153–169 (March, 1935). In Landau, L.D. (1967). Collected Papers (ed. D. ter Harra), 101–117. New York: Gordon and Breach.

[46] For an excellent review of domain structure and copious references on the related topics, see Kittel, C., "Physical Theory of Ferromagnetic Domainis." Reviews of Modern Physics, Vol. 21 (October, 1949), p. 541.

[47] Néel, L: Properiétés magnétiques des ferrites: Ferrimagnétisme et antiferromagnétisme (Magnetic properties of ferrites: Ferrimagnetism and antiferromagnetism). Annales de Physique (Paris) Vol. 3: p.137–198 (March, 1948).

[48] J. H. E. Griffiths: Anomalous High-frequency Resistance of Ferromagnetic Metals, Nature, Volume 158, Issue 4019, pp. 670-671 (1946).

[49] Dirk Polder, "On the phenomenology of ferromagnetic resonance, Physical Review, Vol. 73, No. 9, p. 1120, 1948.

Although the permeability/susecptibility tensor is usually credited to Polder, the equations leading to the tensor are those of Kittel[51, 52].

[50] Dirk Polder, "On the theory of ferromagnetic resonance", The London, Edinburgh, And Dublin Philosophical Magazine And Journal of Science, Vol. 40, Issue 300, No. 2, pp. 99–115, 1949.

Kittel's classical theory of resonance in a magnetized ferromagnetic material is generalized; a phenomenological theory is obtained in which the dependence on the shape and the dimensions of the specimen no longer occurs. As an application the propagation of a plane electromagnetic (micro-) wave in a magnetized ferromagnetic medium is discussed. A quantum theory of the resonance phenomenon is given on the basis of a generalized Bloch spin-wave theory. An ambiguity in the use of the term gyro magnetic ratio is pointed out. It is suggested that the anomalous g-value found by resonance experiments may be explained by the combined effect of an electric crystal field and spin-orbit interaction.

[51] Charles Kittel: Interpretation of Anomalous Larmor Frequencies in Ferromagnetic Resonance Experiment, Physical Review, Vol. 71, p. 270, (1947). Introduces demagnetization field into the DC magnetic field to explain experimental data; there is no damping term in the LLG equation.

[52] Charles Kittel: On the Theory of Ferromagnetic Resonance Absorption, Physical Review, Vol. 73, p. 155, (1948). Introduces a demagnetization field into both the DC and the RF magnetic field. Further, Kittel assumes that the DC and RF tensor values are the same. No discussion, rather it is an assertion. There is no damping term in the LLG equation used by Kittel. The paper treats other topics, such as crystal anisotropy, etc.

[53] Felix Bloch: Nuclear Induction, Physical Review, Vol. 70, No. 7&8, pp. 460-474, 1946.

The title refers to Nuclear (Spin) Magnetic Resonance (NMR) in a crystal lattice, and the voltage induced in a coil by the precession of nuclear magnetic moments. The nuclear spin equation of motion is essentially the same as that of an electron spin. NMR spectroscopy was later used to determine molecular structue. NMR is also an important medical diagnostic. In deference to patient anxiety over the word *nuclear*, the method is called Magnetic Resonance Imaging (MRI).

[54] Benjamin Lax and Kenneth J Button: Microwave Ferrites and Ferrimagnetics, McGraw-Hill, New York, 1962. In particular Chap. 4.3 Internal DC Magnetic Field.

[55] Vincent G. Harris (editor): Modern Ferrites: Basic Principles, Processing and Properties, Volume 1, Wiley (2022).

[56] A. Koper, A. Lehmann-Szweykowska, R. Wojciechowski and M Mucha: An analysis of the magnetic ground state in yttrium iron garnets, Journal of Physics: Condensed Matter, Vol.7 No.7 p. 1391 (1995).

[57] Thomas L. Gilbert: A Lagrangian Formulation of the Gyromagnetic Equation of the Magnetization Field, Physical Review D. Vol. 100, p. 1243 (1955).

This, in fact, is not a paper. Rather it is the abstract for a session in the Conf. Magnetism and Magnetic Materials, Pittsburgh, PA, June 14–16, 1955. [Abstract only; full report, Armor Research Foundation Project No. A059, Supplementary Report, May 1, 1956]

D6. A Lagrangian formulation of the gyromagnetic equation of the magnetization field. T. L. Gilbert, Armour Research Foundation of Illinois Institute of Technology. –The gyromagnetic equation, $d\mathbf{M}/dt = \gamma\mathbf{M} \times \mathcal{G}$, for the motion of the magnetization field $\mathbf{M}(r)$, in a ferromagnetic material can be derived from a variation principle, as first shown by Doering[1]. Here $\mathcal{G}$ is the effective internal field, including the magnetic field and contributions from exchange, anisotropy, and magnetoelastic effects. Using the variational principle, the equations of motion can be recast into a Lagrangian form. This makes possible a consistent derivation of the equations of motion of the magnetization field and other fields to which it may be coupled (e.g., the displacement field of the lattice and the electromagnetic field). It also permits

the introduction of viscous damping effects in a consistent manner using the Rayleigh dissipation function. It is shown that viscous damping of the magnetization fields leads to an equation of motion which reduces to the Landau-Lifshitz equation only when the damping is small. It is also shown that this Lagrangian formalism permits the introduction of damping due to disaccomodation in a consistent and very general way.

1: W. Doering, Z. Naturforsch. 3a, 374 (1948)

[58] Thomas L. Gilbert: A Phenomenological Theory of Damping in Ferromagnetic Materials, IEEE Trans. On Magnetics, Vol. 40, No. 6, pp. 3443-3449, Nov. 2004.

This work is a condensed version of chapters I-III of Gilbert's Ph.D. thesis, Illinois Institute of Technology (1956), and was published in the "Classics in Magnetics" series of IEEE Trans. This is essentially the content of Ref.[57] in the only accessible form.

[59] V. G. Bar'yakhtar; B. A. Ivanov: The Landau-Lifshitz equation: 80 years of history, advances, and prospects. Low Temperature Physics Vol. 41 No.9, pp. 663–669 (2015)

[60] M. Lakshmanan: The fascinating world of the Landau–Lifshitz–Gilbert equation: an overview. Philosophical Transactions of Royal Society A, Vol. 369, pp. 1280–1300 (2011).

[61] V.E. Shapiro: Magnetic Losses and Instabilities In Ferrite Garnet Tuned RF Cavities For Synchrotrons, Jnl. of Particle Accelerators, Vol. 44(1), pp. 43-63 (1994).

[62] Zhenlin Jia, Shuchen Wang, Tong Li, Zenan Zhang, Xiaowei Jin, Desheng Xue: Power dependence of electron paramagnetic resonance: Analytical solution of Landau–Lifshitz–Gilbert equation, Journal of Applied Physics, Vol. 137, 123901 (28 March 2025).

[63] Robert E. Collin: Foundations of Microwave Engineering, McGraw-Hill Book Company, New York, 1965. In particular Sec. 6.6 Microwave propagation in ferrites.

[64] Simon Ramo, John Whinnery, Theodore Van Duzer: Fields and Waves in Communication Electronics: John Wiley & Sons, New York, 1965. In particular Sec. 9.13 Tensor Permeability of Ferrites.

[65] Richard A. Baartman: Microwave Studies of an Amorphous Ferromagnet. MSc. Thesis, Dept. Physics, Simon Fraser University, Canada, 1981. In particular, Sec. 2.1.6.

[66] Jacobus Louis Snoek: Non-Metallic Magnetic Materials for High Frequencies, Philips Technical Review, Vol. 8 (December, 1946), pp. 353-360.

Article includes a graph of a Ferroxcube ferrite from DC to 1 MHz.

[67] J.L. Snoek: Dispersion and absorption in magnetic ferrites at frequencies above one Mc/s, Physica, Volume 14, Issue 4, May 1948, Pages 207-217.

[68] Chihiro Ohmori *et al*: High Field-Gradient Cavities Loaded with Magnetic Allos for Synchrotrons, Proc. 1999 Particle Accelerator Conference, New York, pp. 413-417.

[69] Mauro M. Paoluzzi *et al*: The LEIR RF System, Proc. 21st IEEE Particle Accelerator Conference, Knoxville, TN, USA, 16 - 20 May 2005, pp.1619.

[70] Richard Feynman: Vol.1 Chap 31: The Origin of the Refractive Index.

`https://www.feynmanlectures.caltech.edu/I_31.html`

The speed of light only *appears* to slow down in a medium because it is constantly absorbed and re-emitted by the atoms or molecules that make up the medium. For example, Feynman gives a simplified (for a general audience) account of the refractive indsex of glass in Chap. 3 of "QED: the strange theory of light an matter", Princeton University Press, 1985.

[71] Philips Data handbook: Components and materials, Book C4: Ferroxcube potcores, square cores & cross cores (1986).

[72] Philips Data handbook: Components and materials, Book C5: Ferroxcube for power, audio/video & accelerators (1986).

[73] Philips Data Handbook Soft Ferrites and Accessories.

`https://ferroxcube.home.pl/appl/info/HB2009.pdf`

The "handbook" is not useful for particle accelerator cavity tuning. The data for initial-permeability and amplitude-permeability is intended for other applications.

[74] Philips Technical Review. The Philips Technical Review was a journal published by N.V. Philips' Gloeilampenfabrieken of Eindhoven, Netherlands from 1936 to 1988.

`https://www.worldradiohistory.com/Philips_Technical_Review.htm`

[75] J. J. Went and E. W. Gorter: The Magnetic and Electrical Properties of the Ferroxcube Materials, Philips Technical Review, Vol. 13 No. 7; pp. 181:208 January 1952.

`https://www.worldradiohistory.com/Archive-Company-Publications/Philips-Technical-Review/50s/Philips-Technical-Review-1951.pdf`

[76] J.J. Went, G.W. Rathenau, E.W. Gorter, G.W. van Oosterhout: Ferroxcube, a class of new permanent magnet materials, ibid pp. 194:208.

[77] F. G. Brockman, H: van der Heide and M. W. Louwerse: Ferroxcube for proton synchrotrons, Philips Technical Review, Vol. 30. No. 11/12 (1969) p. 312-329.

`https://www.worldradiohistory.com/Archive-Company-Publications/Philips-Technical-Review/60s/Philips-Technical-Review-1969.pdf`
or
`https://pearl-hifi.com/06_Lit_Archive/02_PEARL_Arch/Vol_16/Sec_53/Philips_Tech_Review/PTechReview-30-1969-312.pdf`

[78] R. Gouiran: Five major proton synchrotrons, Philips Technical Review, Vol. 30. No. 11/12 (1969) p. 330-365.

A remarkably complete account: 1) The Alternating Gradient Synchrotron at Brookhaven near New York; 2) The CERN Proton Synchrotron at Geneva; 3) The Zero Gradient Synchrotron at Argonne near Chicago; 4) The "Nimrod" at Chilton near Harwell in England; 5) The Princeton -Pennsylvania Accelerator at Princeton (New Jersey). The account technological and physics aspects of the design and construction, includes charged particle beam dynamics.

[79] Ian S.K. Gardner: Ferrite Dominated Cavities, CERN Accelerator School (CAS) - RF Engineering for Particle Accelerators, Oxford 1991, p. 349. Content = Ferrite loaded cavities of the Spallation Neutron Source at the Rutherford Appleton Laboratory (SNS RAL), United Kingdom. The SNS is called ISIS after 1986.

`https://cds.cern.ch/record/400743/files/p349.pdf`

[80] Alexander Schnase: Cavities With a Swing, CAS - CERN Accelerator School : Radio Frequency Engineering, CERN-2005-003, pg. 236-272.

[81] Harald Klingbeil: Ferrite Cavities, CERN Accelerator School (CAS) - RF for Accelerators, Ebeltoft, Denmark June 2010, p. 299. Content = Ferrite loaded cavities at GSI-SIS Germany.

GSI-SIS =

https://cds.cern.ch/record/1411778/files/p299.pdf

[82] Quentin A, Kerns, Gerald S. Tool, and Joseph E. Katz: Ferrite Measurements for Synchrotron RF Accelerating System Design, Proc. 1965 IEEE Particle Accelerator Conference, Washington DC USA pp. 185-189.

Despite the title, the article is mostly about a cavity design methodology.

[83] James E. Griffin and Q.A. Kerns: NAL Main-Ring Cavity Test Results, Proc. 1971 IEEE Particle Accelerator Conference, Chicago IL USA.

[84] Klaus Klopfer *et al*: Measurement of the magnetic material properties for ferrite-loaded cavities, Physical Review Special Topics - Accelerators & Beams Vol. 18, Article 010101 (2015).

[85] K. Klopfer, W. Ackermann, and T. Weiland: Eigenmode Computation for the GSI SIS18 Ferrite Cavity, Proc. IPAC'13, Shanghai, China, May 2013, paper MOPWO006, pp. 894–896.

[86] H. G. Koenig *et al.*: The FAIR-SIS100 Accelerating RF Station, Proc. IPAC'18, Vancouver, Canada, Apr.-May 2018, pp. 2762–2764.

[87] Marina Koledintseva, Takanori Tsutaoka: Gyromagnetic Properties of Ferrites. Chap. 7 in Modern Ferrites: Basic Principles, Processing and Properties, Volume 1, Wiley (2022). See in particular Secs. 7.3.2.1 (Ni-Zn) and 7.3.2.2 (Garnet).

[88] Roger Poirier: Perpendicular Biased Ferrite-Tuned Cavities, Proc. 1993 Particle Accelerator Conf., Washington DC May 1993, pp. 753-757.
A five page review paper.

[89] Ernst Schlömann: Microwave Behavior of Partially Magnetized Ferrites, Journal of Applied Physics, Vol.41 Issue 1, 1970. p 204-214.

[90] J. J. Green and F. Sandy: Microwave characterization of partially magnetized ferrites, IEEE Trans. Micro. Theory Techn. 22, 641 (1974).

[91] P. Gelin: New consistent model for ferrite permeability tensor with arbitrary magnetization state, IEEE Trans. Micro. Theory Techn. 45, 1185 (1997).

[92] Lawrence M. Earley, Henry A. Thiessen, Roger Carlini, James Potter: A High-Q Ferrite-Tuned Cavity, 1983 IEEE Particle Accelerator Conference, Santa Fe, NM, USA, p. 3460.

[93] B.J. Evans *et al*: The 1 MV 114 MHz Electron Accelerating System for the CERN PS, Proc. 1987 IEEE Particle Accelerator Conf., Washington DC USA, p. 1901.

[94] L. Warren Funk *el al*: 52 MHz RF System of HERA, Proc. European Particle Accelerator Conf. Rome Italy 1988, p. 1099.

[95] L. Warren Funk *el al*: The 52 MHz RF System for PETRA-II, ibid, p. 1102.

[96] W. Rod Smythe, T. G. Brophy,R. D. Carlini, C. C. Friedrichs, D. L. Grisham, G. Spalek, and L. C Wilkerson: RF Cavities with Transversely Biased Ferrite Tuning, Proc. 1985 IEEE Particle Accelerator Conf., Vancouver, BC, Canada, p. 2951.

[97] W. Rod Smythe: Reducing Ferrite Tuner Power Loss by Bias Field Rotation, Proc. 1983 IEEE Particle Accelerator Conf., Santa Fe NM USA, p. 2173.

[98] Carl Friedrichs *et al*: Test Results of Los Alamos Ferrite-Tuned Cavity, Proc. 1987 IEEE Particle Accelerator Conf., Washington DC USA, p. 1896.

[99] Roger L. Poirier et al: A Perpendicular AC Biased Ferrite Tuned Cavity for the TRIUMF Kaon Facotry Booster Synchrotron, Proc. 1990 European Particle Accelerator Conf., Nice France, p. 988.

[100] George R. Swain et al: Progress on a Prototype Main Ring RF Cavity, Proc. 1989 IEEE Particle Accelaertor Conf., Chicago IL USA, p. 177.

[101] Roger L. Poirier, T.A. Enegren, I.B. Enchevich: AC Bias Operation of the Perpendicular Biased Ferrite Tuned Cavity for the TRIUMF Kaon Factory Booster Synchrotron, 1991 IEEE Particle Accelaertor Conf., San Francisco CA USA, p. 2943.

[102] Carl Friedrichs & G. Hulsey: The Effects of Temperature and RF Power Level on the Tuning of the Water-Cooled SSC Low-Energy Booster Cavity, Proc. 1993 Particle Accelerator Conf., pp. 803-805.

[103] Yehuda Goren, N.K. Mahale, Linda Walling, Terry Enegren, G. Hulsey: Non-linear Effects in Ferrite Tuned Cavities, PAC 1993.

[104] Marina Koledintseva, Takanori Tsutaoka: Gyromagnetic Properties of Ferrites. Chap. 7 in Ref.[55]. See in particular Secs. 7.3.2.1 (Ni-Zn) and 7.3.2.2 (Garnet).

[105] Takanori Tsutaoka: Frequency dispersion of complex permeability in Mn–Zn and Ni–Zn spinel ferrites and their composite materials. Journal of Applied Physics Vol. 93 (5): pp. 2789–2796. (2003).

[106] Takanori Tsutaoka, Teruhiro Kasagi, Kenichi Hatakeyama: Permeability spectra of yttrium iron garnet and its granular composite materials under dc magnetic field, Journal of Applied Physics, Vol. 110, Issue 5, 053909 (2011).

[107] Christine Vollinger and Fritz Caspers: Accurate Measurement of Ferrite Garnets to be used for Fast-tuned Ferrite Loaded Cavities in the Range of 20-40 MHz, Proc. IPAC'12, New Orleans, LA, USA, May 2012, paper THPPC020, pp. 3317–3319.

[108] C. Vollinger and F. Caspers: Enlargement of Tuning Range in a Ferrite-tuned Cavity through Superposed Orthogonal and Parallel Magnetic Bias, Proc. IPAC'13, Shanghai, China, May 2013, paper WEPFI054, pp. 2812–2814.

[109] J. Eberhardt, F. Caspers, and C. Vollinger: Ferrite Material Characterization in a Static Bias Field for the Design of a Tunable Cavity, Proc. IPAC'14, Dresden, Germany, Jun. 2014, pp. 3890–3892.

[110] J. Eberhardt, F. Caspers, and C. Vollinger: Preliminary Design of a Perpendicular Biased Ferrite Loaded Accelerating Cavity, Proc. IPAC'15, Richmond, VA, USA, May 2015, pp. 3163–3166.

[111] J. Eberhardt, F. Caspers, and C. Vollinger: Ferrite Characterization for the Design of an Accelerating Cavity With Perpendicular Biasing, IEEE Transactions On Nuclear Science, Vol. 63, No. 2, April 2016, pp. 693-698.

[112] Gennady Romanov et al: Perpendicular Biased Ferrite Tuned Cavities for the Fermilab Booster, Proc. Int. Particle Accelerator Conf. (IPAC2014), Dresden Germany, July 2014, p. 3911 - 3913.

[113] R. Madrak, G. Romanov, and I. Terechkine: Permeability of AL800 Garnet Material, FERMILAB-TM-2757-TD (2015).

[114] R. Madrak et al: The FNAL Booster 2nd Harmonic RF Cavity, Proc. 61st ICFA Advanced Beam Dynamics Workshop on High-Intensity and High-Brightness Hadron Beams (HB2018) ; Daejeon Korea, 2018, p. 434-439.
Also FERMILAB-CONF-18-297-AD and arXiv:1808.09513.

[115] G. Rakowsky and A. Tranis: Nonlinear Effects in 'Linear' Ferrites at High RF Fields, IEEE Trans. Nuc. Sci., Vol. NS-16 No. 3 p. 543. (1969).

[116] Shane Koscielniak: Mean-Square Resonator And Relation to the Duffing Resonator, TRIUMF Laboratory report TRI-BN-24-36R.